Test and Theoretical Researcj of Prestressed Concrete Berthing Piles

Xu, Xibin; Nielsen, Mogens Peter

Publication date:
2006

Document Version
Publisher's PDF, also known as Version of record

Department of Civil Engineering DTU

Xu Xibin

Test and Theoretical Research of Prestressed Concrete Berthing Piles

PHD THESIS

BYG • DTU

Xu Xibin

Test and Theoretical Research of Prestressed Concrete Berthing Piles

Ph.d Thesis
BYG · DTU
2005

Contents

Preface

This paper is finished under the guidance of main supervisor Prof. M.P.Nielsen, Technical University of Denmark, and co-supervisor Prof. Wang Zhengling, Chongqing University of China. The author will remember forever that the two supervisors have made painstaking effort in the whole process of the selection of the subject, model tests and the theoretical research as well in the process of completing this paper. The supervisor's meticulous scholarship, spirit of loyal, profound knowledge, self-giving dedication and strictness with the author will benefit me for life. Here, deep-felt respect and heartfelt thanks are given to my supervisors.

During the project time I devoted about 80% of normal working time to the project including the test. The remaining time had to be used to teaching etc. at my university.

The research of this project is financially supported by the Chongqing Science and Technology Commission. Chongqing University has offered great support and assistance to the experiments of the project, and the Department of Structural Engineering and Materials, Technical University of Denmark, has supplied favorable research conditions. Hence, great appreciation is given to all of them.

Special thanks are given to Mrs. Bente Jensen, Technical University of Denmark, for her assistance during the period of time staying in Denmark, and to Per and Carol Monsrud for language support. Finally, I'd like to give my thanks to my wife and my daughter for their encouragement and support.

Xu Xibin

June 20,2005

Notation

A	**Sectional area**
B	**Pile diameter**
$[B]$	**Strain matrix**
C	**Damping coefficient matrix**
C_{ij}	**Damping coefficient**
c_s	**Strain damping coefficient**
$[D]$	**Elasticity matrix**
E'_{1b}	**Tangent modulus in the σ_1 direction**
E'_{2b}	**Tangent modulus in the σ_2 direction**
E_0	**Effective impact energy of the ship**
EI	**Bending rigidity of the pile**
E	**Initial elastic modulus of concrete**
E_c	**Elastic modulus of concrete**
E_0	**Secant modulus of concrete**
E_S	**Calculation soil modulus**
E_S	**Elastic modulus of steel**
F	**Inertial force matrix**
F_D	**Damping force matrix**
F_S	**Elastic force matrix**
F	**Softening degree parameter of the soil**
f_1	**Unit length of inertial force**
f_t	**Uniaxial tensile strength of concrete**
$f_{ji}(t)$	**Inertial force**
$f_{Di}(t)$	**Damping force**
$f_{Si}(t)$	**Elastic restoring force**
$\{F\}^e$	**Nodal force in finite element**
H	**Lateral load**
k	**Horizontal reacting force coefficient of the soil**
K_1	**Elasticity coefficient of the berthing pile**
K_2	**Elasticity coefficient of the fender**
$[K]$	**Stiffness matrix**
$[K_0]$	**Initial stiffness matrix**

[*k*]	**Unit stiffness matrix**
K_{ij}	**Stiffness coefficient**
L_c	**Critical length of the pile**
L	**Penetration depth of the pile**
m	**Frictional angle**
m	**Mass per unit length**
M_0	**Moment**
M	**Mass matrix**
M_{ij}	**Mass coefficient**
P	**Soil resistance force per unit length**
P_u	**Limit resistance of the soil**
P_i(t)	**Disturbing force**
P (t)	**Disturbing force matrix**
Q_0	**Lateral force**
R	**Reaction force**
$\{R\}$	**Load vector**
$\{R_0\}$	**Initial load vector**
$\ddot{u}_i^*$	**Value of acceleration vector**
V_n	**Normal velocity of the ship in berthing**
x	**Depth below soil surface**
x_r	**Reference depth**
y	**Horizontal displacement**
y_1	**Displacement of the pile**
y_2	**Displacement of the fender**
y_c	**Reference displacement**
y_0	**Displacement of the soil surface.**
α	**Constant**
β	**Constant**
Δ	**Area of the triangular unit**
$\{\delta\}$	**Displacement**
$\{\Delta\delta\}$	**Displacement increment**
ρ	**Effective kinetic energy coefficient**
ε	**Strain**
ε_1	**Principal strain**

ε_2	**Principal strain**
ε_c	**Concrete strain**
ε_0	**Concrete strain corresponding to maximum stress**
$\{\varepsilon_0\}$	**Initial strain**
ε_u	**Ultimate strain**
λ	**Constant**
ω	**Angular velocity**
$\{\Delta\sigma\}$	**Stress increment**
$\{\Delta R\}$	**Load increment**
σ_1	**Principal stress**
σ_2	**Principal stress**
σ_{2u}	**Adjusted stress**
$\sigma_{2,ex}$	**Difference between σ_2 and σ_{2u}**
σ_c	**Concrete stress**
$\sigma_{c\max}$	**Maximum stress of concrete**
σ_D	**Damping stress**
σ_K	**Pre-tensile stress in reinforcement**
σ_p	**Proportional limit of steel**
σ_u	**Ultimate strength of the steel**
σ_y	**Yield stress of steel**
$\{\sigma_0\}$	**Initial stress**
φ	**Curvature**
φ_0	**Angular deflection at soil surface**

Resumé

For at reducere virkningen af og forhindre kollisioner mellem en vandbygningskonstruktion og et skib findes i enhver havn forskellige installationer, der har til formål at absorbere de til tider store energier, der optræder, når et skib lægger til kaj. Afhængigt af spændingsniveau og servicekrav må disse installationer besidde en så stor elasticitet, at de kan absorbere den kinetiske energi ved skibsstødet og ligeledes modstå tangentielle kræfter. Samtidigt må de være holdbare og økonomiske.

Fenderpæle er en af de vigtigste installationer i havnekonstruktioner. Når disse benyttes opbygges de direkte foran den konstruktion, der skal beskyttes for stød.

Indtil nu har fenderpæle i Kina og også i andre dele af verden hovedsageligt været udført af stål, mens armeret beton kun har været benyttet sporadisk. Dette skyldes et alt for lille omfang af forsknings- og udviklingsarbejde vedr. armeret betons deformationsegenskaber og dette materiales evne til at absorbere energi.

I denne afhandling er der rapporteret en række forsøg med efterspændte beton fenderpæle. Desuden er der udført en stor mængde beregninger for at studere brugsegenskaberne af forspændte beton fenderpæle. Studiet har fokuseret på de faktorer, som indvirker på brugsegenskaberne af sådanne pæle, såsom betonstyrke, forspændingsniveau, armering, revnedannelse, bæreevne og energiabsorbering.

På basis af dette udviklingsarbejde er det muligt at angive den optimale tværsnitsdimensionering af forspændte beton fenderpæle. Indholdet af afhandlingen er følgende:

1. Opførsel af beton fenderpæle for brugs- og brudlast.
2. Kraft-deformationsegenskaber ved forskellige belastningsniveauer.
3. Revneåbnings- og revnelukningsopførsel for beton fenderpæle.
4. Virkningen af betonstyrken på tøjningsenergien.
5. Effekten af forspænding på tøjningsenergien.
6. Virkningen af bøjlearmering og armeringsarrangement.
7. Sammenhæng mellem energiabsorption, kraft og deformation af fenderpæle med forskellige egenskaber.

Det vises, at forsøgsresultaterne er i god overensstemmelse med de beregnede værdier, hvilket bekræfter, at den valgte forsøgsmetodik og de teoretiske beregningsmetoder har været korrekt valgte. De vigtigste fundne resultater er opsummeret i det følgende:
1. Forsøg ved cyklisk last har vist, at der ved aflastning efter revnedannelse vil ske en fuldstændig lukning af revnerne. En effektiv lukning af revnerne vil reducere

muligheden for korrosion af armeringen, og vil øge duktiliteten af forspændte betonpæle anvendt som skibsværn.
2. Forspændingen har stor indflydelse på deformationskapaciteten i det sene laststadium. For elementer med høj betonstyrke vil den totale udbøjning reduceres, når forspændingen øges, men for elementer med lav betonstyrke er resultatet omvendt. Det foreslås, at forspændingen af pælene bestemmes ved at forudsætte en vis revnemodstand i hhv. byggefasen og anvendelsesperioden under alle omstøndigheder skal de have en relativ stor deformationskapacitet.
3. Inden for det interval af betonstyrker, som har været undersøgt i denne afhandling, er det vist, at energiabsorptionsmuligheden for forspændte betonpæle øges ved en øget betonstyrke. Vi foreslår, at betonstyrken for forspændte betonpæle vælges mellem beton 60 og beton 80. En lav styrke vælges, når forspændingen er stor, og omvendt.
4. Den symmetriske armering med lukkede, rektangulære bøjler giver bedre mulighed for en øget energiabsorption, lavere kraftpåvirkning og lettere fremstilling. Derfor er det den optimale type tværarmering.
5. De forspændte betonpæle skal dimensioneres så forholdet mellem kraftpåvirkning og energiabsorption minimeres. Det er dog ikke tilstrøkkeligt at opnå en optimal energiabsorption, det er ogsa nødvendi gt at opnå en effektiv lukning af revnerne.

Nøgleord: Efterspændt beton, fenderpæle, revnedannelse, deformation, energiabsorption.

Summary

Collision protection facilities in a harbor are mainly used to absorb the huge impact energy when a ship is berthing, thus reducing the impact force and preventing collision between hydraulic structures and the body of the ship. Depending on the stress and the service requirements of the impact prevention facilities, these must have enough elasticity to absorb the kinetic energy of the ship impact and to resist tangential forces. At the same time, they should be wearable and cost-efficient. Berthing piles are one of the major impact-prevention types adopted in port structures. In this method, the piles are arranged directly in front of the structure to undertake impact forces from ships. To this date, the berthing piles in China and overseas are mainly made of steel, and there is little application of prestressed reinforced concrete berthing piles because little research has been conducted on their deformation behavior and energy absorption effects. Based on tests on six post-tensioned concrete berthing piles and a large amount of theoretical computations, we have studied the service performance of prestressed concrete berthing piles. This research work focused on factors that affect the service performance of the prestressed concrete berthing piles, such as concrete strength, pre-tensile stress, sectional reinforcement, cracking characteristics, ultimate bearing capacity and absorption of energy. On the basis of this research, the optimal sectional design of prestressed concrete berthing piles has been obtained. The research contents are as follows:

1. The work performance at service load and ultimate load;
2. The relationship between load and deflection at different loading levels;
3. Crack characteristics and crack closing performance of the berthing piles;
4. Effects of concrete strength on the strain energy of the berthing piles;
5. Effects of pre-tensile forces on the strain energy of the berthing piles
6. Types of stirrups and sectional reinforcement; and
7. The relationship between absorbed energy, reaction force and deformation of the berthing piles using different design parameters.

The actual measured results are consistent with theoretically computed ones, which indicates the correctness of the test scheme and the theoretical computation methods adopted in this paper. The main findings are summarized as follows:

1. The cyclic load tests have shown that when unloading after cracking, the cracks will be fully closed. The good crack closure performance will reduce the steel bar corrosion and greatly help to improve the durability of the prestressed concrete berthing piles.

2. The pre-stress obviously influences the deformation capacity at the later stage of loading. For the members with a high concrete strength, the total deformation ability will be reduced when the pre-stress increases, but for the members with low concrete strength, the result is just the opposite. It is suggested that the pre-stress of the berthing pile should be determined by the premises of guaranteeing a certain cracking resistance during the

period of construction and service; meanwhile, it must have a relatively large deformation capacity.

3. Within the range of concrete strength which has been studied in the thesis, the energy absorption ability of the prestressed concrete berthing piles increases with the concrete strength. We suggest that the concrete strength of the prestressed concrete berthing piles is selected between C60 and C80. A small value of the strength should be used when the pre-stress is high, and vice versa.

4. The symmetric reinforcement of the closed rectangular stirrups may provide large energy absorption, lower reaction force, and easy manufacturing, and therefore it is the optimal transverse reinforcement type.

5. The prestressed concrete berthing piles should be designed to minimize the ratio between reaction force and energy absorption. This is not only good to obtain optimal energy absorption effectiveness, but also to have a good crack closure performance.

Keywords: Post-tensioned concrete, berthing pile, crack, deformation, energy absorption effectiveness

Chapter 1

General Principles

1.1 Introduction

Cargo jetties consist of a berthing head at which the ships are moored in order to load or discharge their cargo, and an approach structure connecting the berthing head to the shore and carrying the road or rail vehicles used to transport the cargo. Where minerals are handled in bulk the approach structure may carry a belt conveyor or an aerial ropeway. In addition to its function in providing a secure mooring for ships, the berthing head carries cargo-handling cranes or special equipment for loading and unloading dry bulk cargo and containers.

Berthing structures or jetties used exclusively for handling crude petroleum and its products are different in layout and equipment from cargo jetties. The tankers using the berths can be very much larger than the cargo vessels. On the other hand, the hose-handling equipment and its associated pipework are likely to be much lighter than the carnage or dry bulk-loading equipment installed on cargo jetties serving large vessels. The approach from the shore to a petroleum loading jetty consists only of a trestle for pipework and an access roadway. Where the deep water required by large tankers commences at a considerable distance from the shore-line, it is the usual practice to provide an island berthing structure connected to the shore by pipelines laid on the sea bed [1][2].

In spite of the considerable differences between the two types of structures, piling is an economical form of construction for cargo jetties as well as for berthing structures and pipe trestles for oil tankers. The berthing head of a cargo jetty is likely to consist of a heavy deck slab designed to carry fixed or traveling cranes and the imposed loading from vehicles and stored cargo. The berthing and mooring forces from the ships using the berths can be absorbed by fenders sited in front of and unconnected to the deck structure (Figure 1.1a), but it is more usual for the fenders to transfer the berthing impact force to the deck and in turn to the rows of supporting piles. The impact forces may be large and because the resistance of a vertical pile to lateral loading is small the deck is supported by a combination of vertical and raking piles (Figure 1.1b). These combinations can also be used in structures of the open trestle type such as a jetty head carrying a coal conveyor.

The piles in the berthing head of a cargo jetty are required to carry the following loads[3].

(1). lateral loads from berthing forces transmitted through fenders;

(2). lateral loads from the pull of mooring ropes;

(3). lateral loads from wave forces on the piles;

(4). current drag on the piles and moored ships;

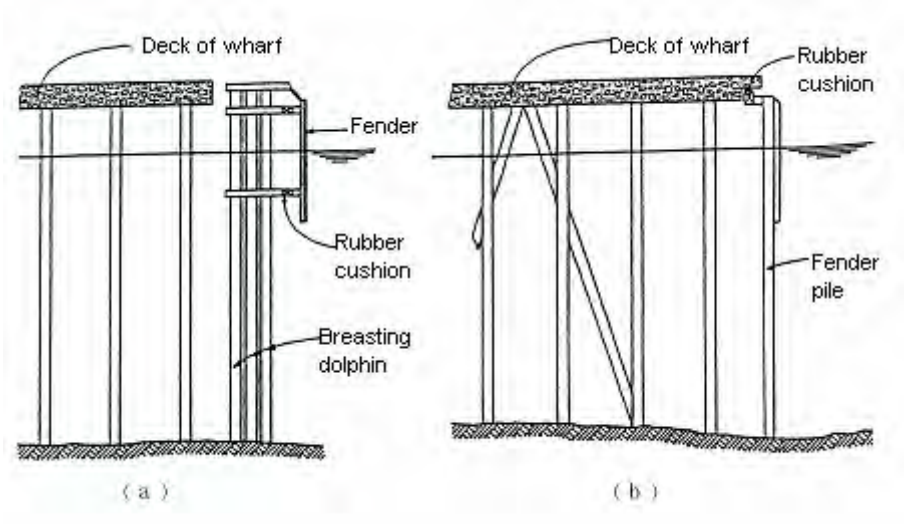

(a) in independent breasting dolphin, (b) attached to main deck structure

Fig. 1.1 Fender piles for cargo jetties:

(5). lateral loads from wind forces on the berthing head, moored ships, stacked cargo and cargo handling facilities;

(6).compressive loads from the dead weight of the structure, cargo handling equipment and from imposed loading on the deck slab;

(7).compressive and uplift forces induced by overturning movements due to loads (1) to (5) above; and

(8).in some parts of the world piles may also have to carry vertical and lateral loads from floating ice, and loading from earthquakes.

The above forces are not necessarily cumulative. Whereas wind, wave and current forces can occur simultaneously and in the same direction, the forces due to berthing impact and mooring rope pull occur in opposite directions. Berthing would not take place at times of maximum wave height, nor would the thrust from ice sheets coincide with the most severe wave action. Where containers are stored on the deck slab the possibility of stacking them in tiers above a nominal permitted height must be considered.

Comparing with the coastal berthing structures, however, the river port structures are more complicated. A large water level range is a main characteristic of river ports, as illustrated by the conditions of the Yangtze River [4],(shown in Figure 1.2). In the lower reaches of the Yangtze River, such as Nanjing Port, the range between high water level and low water level is about 7 meters. In the middle reaches, for example in Wuhan Port, the range is around 15 meters. At Chongqing Port, located in the upper reaches of this river, it is around 33 meters. Consequently, wharves supported on piles are the main structural types in the river ports in China, in which most superstructures are reinforced concrete frames. In addition to higher rigidity and integrity, the mooring facilities can be

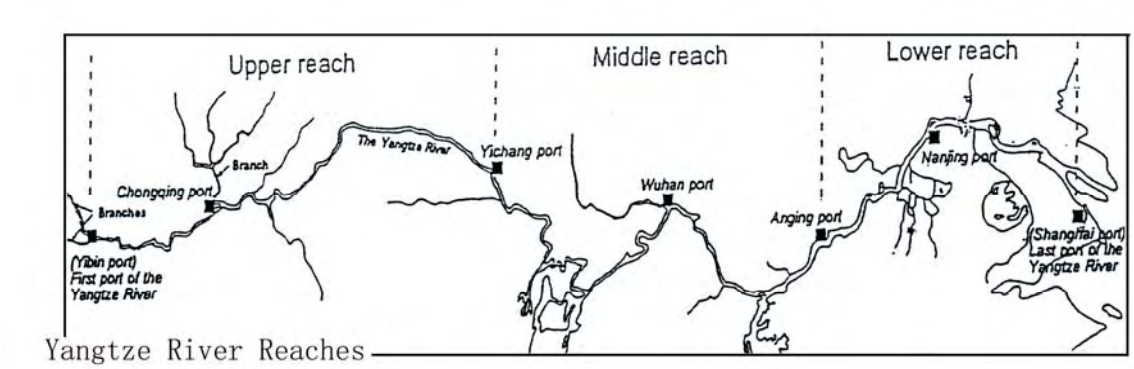

Figure 1.2 Distribution of main ports along the Yangtze River

easily installed in different elevations for reinforced concrete frame wharves, as shown in Figure 1.3, which is very necessary because of the characteristics of small river ships and the large water level range.

The maneuvre of bringing a ship to a berth is so difficult, due to wind, waves, currents and changing of water level, that accidents often occur during berthing. With the increase in the size of ship and bad natural conditions, the berthing maneuvre will be even more difficult. The impact force easily makes the berth structure to be damaged. Therefore, a suitable fender system to absorb the impact energy is very important and necessary.

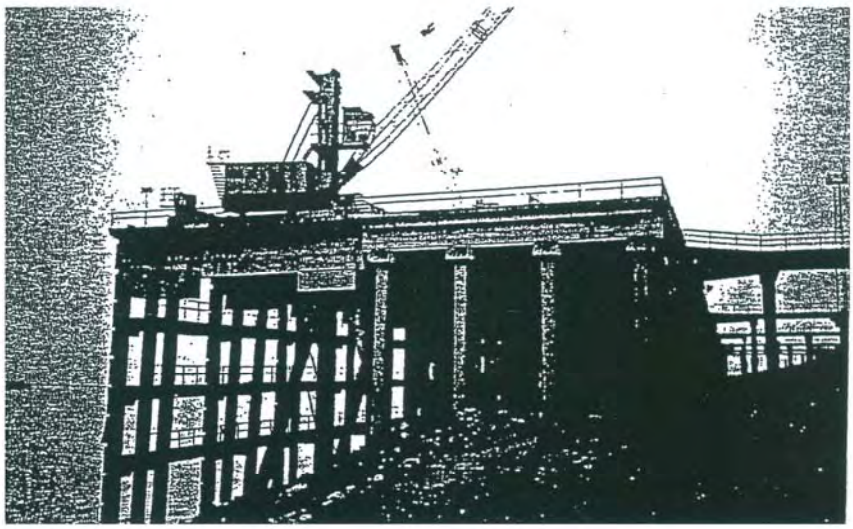

Fig.1.3 Wharf supported on piles of Wuhan Port

1.2 Fender system

The marine fenders provide the necessary interface between the berthing ship and the berth structure, and therefore the principal function of the fender is to transform the

impact load from the berthing ship into reactions which both the ship and berth structure can safely sustain. A properly designed fender system must therefore be able to gently stop a moving or berthing ship without damaging the ship, the berth structure or the fender. When the ship has berthed and been safely moored, the fender system should be able and strong enough to protect the ship and the berth structure from the forces and motions caused by wind, waves, currents, water level changes and the loading or unloading of cargo. The design of fenders should also take into account the importance of the consequences suffered by the ship and the berthing structure in the case of an eventual accident due to insufficient energy absorption capacity.

The correct procedure would be to plan and design the fender and berth structures jointly. The choice of fenders should be dependent on the size of berthing ships and maximum impact energy. After having identified the fender criteria, one can finalize the design of the berth superstructure. The following factors are therefore considered in selecting the fender system [5]:

(1). the fender system must have sufficient energy absorption capacity;

(2). the reaction force from the fender system should not exceed the loading capacity of the berthing system;

(3). the pressure exerted from the fender system should not exceed the ship hull pressure capacity; and

(4). the construction and maintenance costs should be evaluated during the design of both the berth structure and the fender system.

This procedure will lead to a correct structural solution, lower construction costs and lower annual maintenance costs.

Fenders may be divided into two main groups [6]. One is protective fenders, which are supposed to function as an energy absorbing protective pad between the ship and the berth structure available at all times; another one is impact fenders, which in particular are supposed to absorb the impact during the berthing maneuvres. The fenders used widely in practice are wood, rubber and berthing piles.

The wooden fenders may be arranged as shown in Figure 1.4, with horizontal and vertical members. Exposed timber members may be provided with a relatively thin protection of hard wood which may be fastened to the main vertical members by spikes.

Various kinds of rubber fenders are used as protection, as shown in Figure 1.5. Hollow round or square rubber fenders can be hung on the berth structure. Solid rubber members or tubes may also be used on the front side. Old tires may serve the same purpose in small berth structures. They may be hung directly on the berth structure or bound together horizontally or vertically. The fenders mentioned above all have energy absorption diagrams like the rubber fenders in figure 1.6.

Generally, piles are columnar elements in a foundation which have the function of transferring load from the superstructures through weak compressible strata or through water, onto stiffer or more compact and less compressible soils or onto rocks. They may be required to carry uplift loads when used to support tall structures subject to overturning forces from winds or waves. Piles used in marine structures are subjected to lateral loads from the impact of berthing ships. A berthing pile is the main protective or

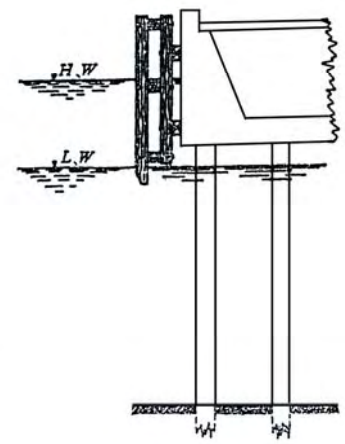

Fig.1.4 Wooden fender

Fig. 1.5 Rubber fender

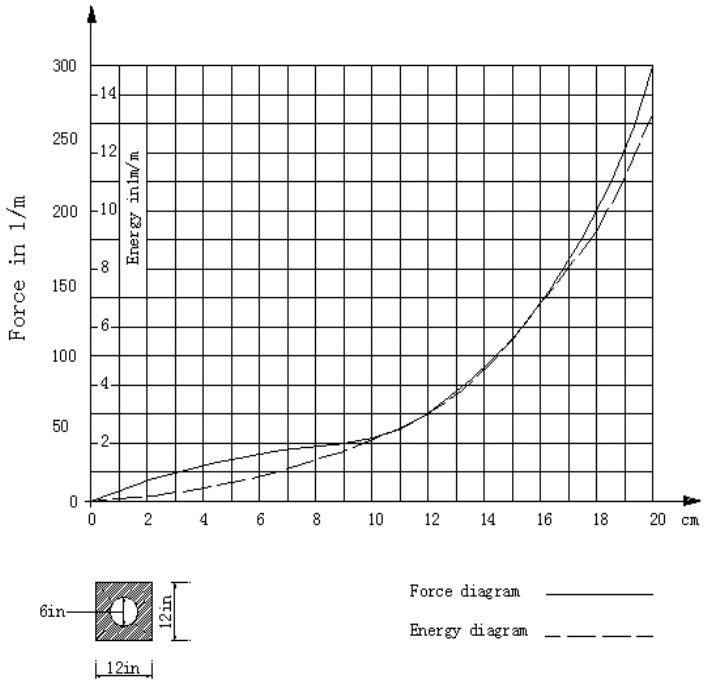

Fig. 1.6 Energy absorption diagrams of rubber fender

impact system used in hydraulic structures. A steel pipe pile or prestressed concrete pile may be used in practice, as shown in Figure 1.7.The piles are arranged in the front of the wharf to directly absorb the energy from an impacting ship. Figure 1.8 shows lateral movement of berthing piles due to impact force of a ship [8]. On the assumption that the velocity of a ship transverse and parallel to the berthing line has been correctly calculated the problem is then to assess the manner in which the energy is absorbed by the berthing piles. Taking the case of a vertical berthing pile acting as a simple cantilever from the point of virtual fixity below the bed, such a pile is able to receive the impact force from

Fig.1.7 Steel berthing pile

the berthing ship. The bending moment which can be applied to a pile is limited by the allowable working stress on the extreme fibers of the material forming the pile for normal berthing impacts, and by the yield stress or failure stress for abnormal berthing velocities. If the capacity of the pile is inadequate, the blow from the ship must be absorbed by more than a single pile. In practice, vertical piles are grouped together and linked at the head and at some intermediate point to form a single berthing dolphin, or they are spaced in rows or “bents” in the berthing head of a jetty structure. In the latter case, the kinetic energy of the ship may be absorbed by a large number of piles. The case where the piles are fixed against rotation by the deck slab of a structure is shown in figure 1.8.

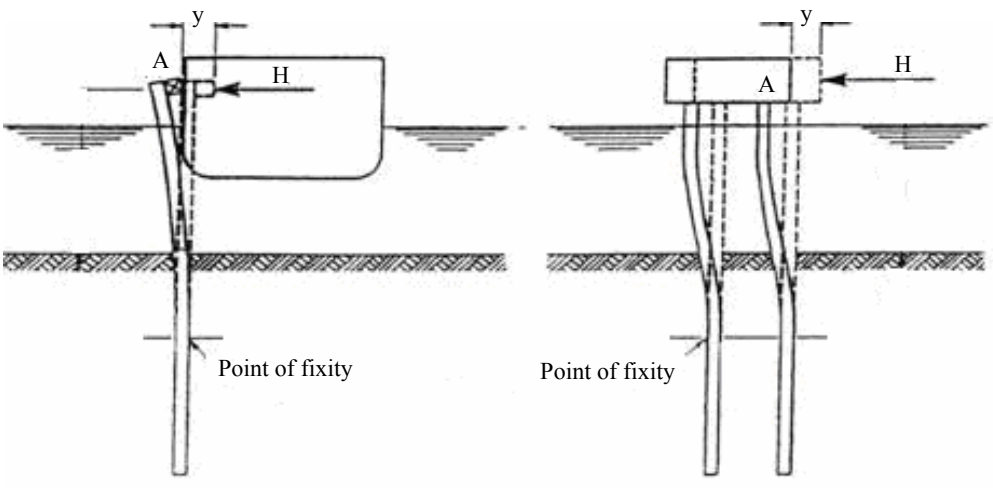

Fig. 1.8 Lateral movement of fender due to impact force from berthing ship

1.3 Properties and calculation method of the berthing pile[9]

1.3.1 Properties of the berthing pile

The berthing pile differs greatly from piles subjected to the action of a horizontal load. It absorbs the impact force of a ship by taking advantage of its elasticity, while the general open type of wharf on piles absorbs the impact force of a ship by utilizing the entire structure. Compared with the piles under the action of a horizontal load, for the berthing pile it is required that (1) high strength material is used to adapt to a large displacement performance; (2) the foundation conditions are good, otherwise the berthing pile will not return to its original position after withstanding the impact force of a ship and its capability of absorbing the impact force by displacement will gradually die away. A treatment of the foundation material should be made in case of unfavorable foundations or the penetration depth of a berthing pile into soil should be increased.

Besides high requirements for the material and foundation, the berthing pile also needs to be made by a proper structural type, that is to say, the pile and fender structure should be fully utilized to absorb the large ship impact kinetic energy while the pile itself carries a relatively small external force.

1.3.2 Calculation method

Based on a study of calculation methods of existing horizontal load piles, the author proposes the following method for calculating internal forces of the berthing pile, which consists of three parts: (1) calculation of effective kinetic energy; (2) setup of the mechanical model of the berthing pile; (3) iterative solution of mechanical response by using the finite difference procedure to the P-y curve.

1. Calculation of effective kinetic energy

In the design of a berthing pile, many horizontal forces, such as wave loads, the impact forces of a ship, earthquake loads, etc. should be taken into consideration. This thesis only deals with the impact force when a ship berths at a jetty, which, for the berthing pile, is a frequently repeated load. The calculation of the forces is based on assumptions such as berthing angle and berthing speed, etc.

Currently, the kinetic energy is employed in general to calculate the impact kinetic energy of a ship. The equation is

$$E_0 = \frac{1}{2} M V_n^2 \rho \tag{1.1}$$

where E_0 is the effective impact energy of the ship; M is the mass of the ship; V_n is the normal velocity of the ship in berthing; ρ is the effective kinetic energy coefficient.

2. Setup of mechanical model

Simplify the energy absorbing structure composed of the ship fender and the pile into a mechanical model of two massless springs in series (Fig. 1.9).

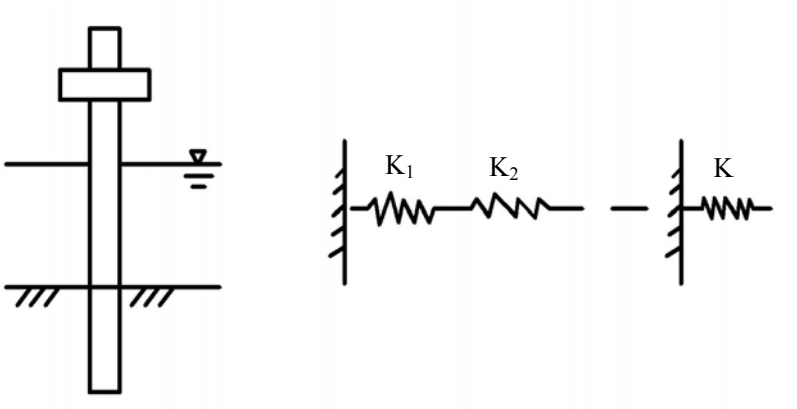

Fig. 1.9 Mechanical model

Suppose K_1 is the elasticity coefficient of the berthing pile, K_2 the elasticity coefficient of the fender. Thus the effective impact energy of the ship is absorbed by two springs. If the displacement of the pile head is y_1 and the displacement of the fender is y_2, then

$$\frac{1}{2}K_1 y_1^2 + \frac{1}{2}K_2 y_2^2 = E_0 \tag{1.2}$$

Assume that the two springs are substituted by a large spring with elasticity coefficient K, thus

$$\frac{1}{2}K_1 y_1^2 + \frac{1}{2}K_2 y_2^2 = \frac{1}{2}K(y_1 + y_2)^2 = \frac{1}{2}Ky^2 = E_0 \tag{1.3}$$

Since $K_1 y_1 = K_2 y_2$, we get by substitution into equation (1.3)

$$K = \frac{K_1 K_2}{K_1 + K_2} \tag{1.4}$$

Generally speaking, equation (1.4) cannot be established easily because a lot of factors influence K_1. K_1 relates to the section type and material of the berthing pile, more importantly to the nature of the soil, and additionally to the impact point of the ship. In addition, the pile driving process also influences the elasticity coefficient of the berthing pile. Hence, it is very difficult to determine the elasticity coefficient of the pile. In calculation, the first step is to estimate the elasticity coefficient of the pile, and then to determine it by repeated iterative calculations.

K_2 is generally given by the producer according to the material of the fender.

3. Calculation of the internal force of the berthing pile by using a *P-y* curve (see Fig.1.10).

The load carried by the berthing pile is a repeating load. A decrease in the maximum resistance of the soil not only results from the repeated disturbance of the soil, but is also caused by another important factor, that is, the soil particles in a certain depth range (interface of pile and soil) are carried away by high speed currents. This is because under the huge impact action of a ship, the displacement of the berthing pile at the soil surface

makes some small cracks between the pile and its surrounding soil. When a certain displacement of the berthing pile occurs under a huge impact force of a ship, the water in the cracks will be squeezed out at very high speed. While the water is being squeezed out, soil particles are introduced, which make the small cracks to extend to a certain depth along the pile. The process will tend towards stability with an increase in the number of repeated loads. Based on the consideration mentioned above, the *P-y* curve chosen as shown in Fig.1.10 is used[9].

In the figure, y is the transverse displacement; y_c is a reference displacement; P_u is the ultimate resistance of the soil; P is the soil resistance per unit length of the pile; F is a parameter to indicate the softening degree of the soil; x is the depth below soil surface and x_r is a reference depth, $x_r = L_c/4$, in which L_c is a critical length of the pile[9].

The differential equation of the pile is

$$EI\frac{d^4y}{dx^4} = -kyB \tag{1.5}$$

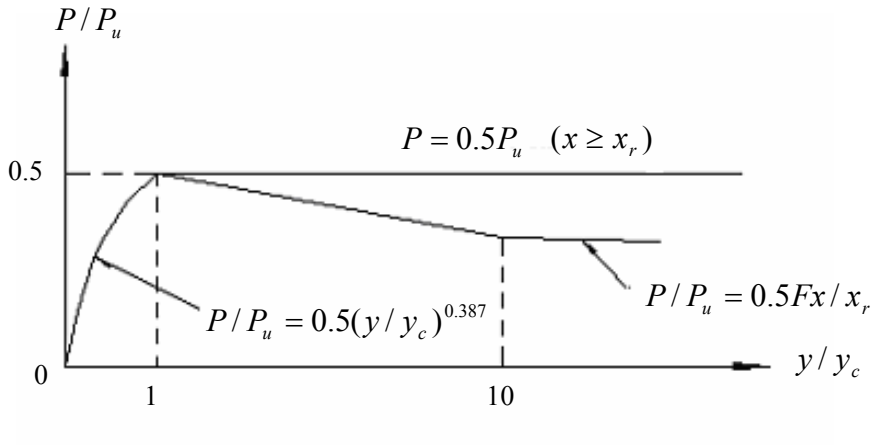

Fig.1.10 P-y curve

Here: k is a horizontal reaction force coefficient of the soil, EI is bending stiffness of the pile and B is diameter of the pile. Equation (1.5) is the basic equation for solving the berthing pile under the action of the horizontal force.

The berthing pile is now subdivided into n lengths (Fig.1.11), and Equation (1.5) is transformed to the following difference equation:

$$EI\{(y_{i+2} - 4y_{i+1} + 6y_i - 4y_{i-1} + y_{i-2})/\alpha^4\} + k_i y_i B = 0$$

Here $\alpha = L/n$, where L is the penetration depth of the pile and n is the number of units along the pile length.

The above equation is rewritten as follows:

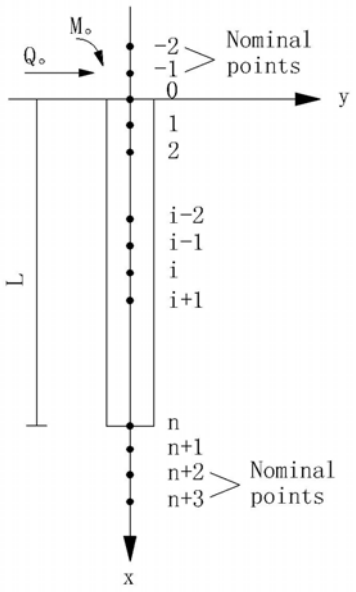

Fig.1.11 Subdivision of the pile

$$y_{i+2} - 4y_{i+1} + (6 + A_i)y_i - 4y_{i-1} + y_{i-2} = 0 \tag{1.6}$$

where $A_i = B \cdot k_i/EI \cdot \alpha^4$

Boundary conditions:

(a) The pile top

When the top of the pile is acted upon by a lateral force Q_0 and a moment M_0, the boundary conditions are

$$Q = Q_0 \qquad y_2 - 2y_1 + 2y_{-1} - y_{-2} = \frac{2\alpha^3}{EI} Q_0$$

$$M = M_0 \qquad y_1 - 2y_0 + y_{-1} = \alpha^2 M_0 / EI$$

When the top of the pile is fixed,

Rotation = 0 $\qquad y_{-1} - y_1 = 0$

Deflection = 0 $\qquad y_0 = 0$

(b) The pile bottom

If the pile is a long elastic pile (common in engineering), the bending moment at the bottom of the pile is very small and can be ignored. Then,

$$M = M_n = 0 \qquad y_{n+1} - 2y_n + y_{n-1} = 0$$

At the same time, the shear at the bottom of the pile is also very small and may also be ignored. Then

$$Q = Q_n = 0 \qquad y_{n+2} - 2y_{n+1} + 2y_{n-1} - y_{n-2} = 0$$

Other boundary conditions, such as a fixed end or a hinge at pile toe, may be treated in similar way. In this way, the pile body is divided into n units and n+1 points, therefore n+1 difference equations (1.6) can be formulated. Considering the two nominal points at the pile top and the pile bottom, respectively, four boundary equations can be obtained, so we have n+5 equations to determine n+5 unknowns y_i.

The solution of the difference equations makes it possible to calculate the stiffness coefficient introduced above.

4. Method of this thesis

(1) Based on the above analysis, we can have

$$K = \frac{K_1 K_2}{K_1 + K_2}$$

and from the following relationships

$$(y_1+y_2)^2 = 2E_0/K$$

and $y_1K_1 = y_2K_2$, we obtain

$$y_1 = \sqrt{\frac{2E_0K_2}{K_1(K_1+K_2)}}$$

After the energy is absorbed by the berthing pile and the fender system, the impact force against the pile is

$$H = K_1y_1 = \sqrt{\frac{2E_0K_1K_2}{K_1+K_2}} = \sqrt{2E_0K} \tag{1.7}$$

So, the phenomenon that the berthing pile absorbs effective kinetic energy may be transformed to the phenomenon that a single pile is under the action of a repeating load $\sqrt{2E_0K}$.

(2) Iterative solution of the internal force and displacement of the berthing pile by using the finite difference procedure based on the cyclic load curve (*P-y* curve).

(3) Find the displacement of the impact point according to the following equation:

$$y = \frac{h^3H}{3EI} + \varphi_0 h + y_0 \tag{1.8}$$

Here φ_0 is the angular deflection at the soil surface, and y_0 is the displacement at the soil surface.

(4) Substitute the supposed pile elasticity coefficient K_1 into Equations (1.4) and (1.7) to solve for *y*, then substitute the calculated *y* (the displacement of impact point of berthing pile) into $y_1 = \sqrt{\frac{2E_0K_2}{K_1(K_1+K_2)}}$ to calculate the elasticity coefficient K_1 of the berthing pile.

If the calculated elasticity coefficient K_1 equals to the supposed elasticity coefficient K_1, the supposed pile elasticity coefficient K_1 is correct; otherwise the pile elasticity coefficient K_1 should be supposed again. Repeat the above process until the supposed elasticity coefficient equals the calculated elasticity coefficient. After determination of the elasticity coefficient K_1, the impact force and the internal force, as well as the displacement of the berthing pile, may be calculated.

1.4 Research contents

There are many kinds of piles. The selection of pile type depends on the following three principal factors: the location and type of the structure, the ground conditions, and durability [10][11]. Considering the first factor, a solid precast or prestressed concrete pile can be used in shallow water, but in deep water a solid pile becomes too heavy to handle and either a steel tubular pile or a tubular precast concrete pile is used. The second factor, the ground conditions, influences both the material forming of the pile and the method of installation. The factor of durability affects the choice of materials. Although timber piles are inexpensive, they are susceptible to decay. For the same reason, steel piles used in a hydraulic structure must be protected against corrosion by cathodic means if a long life is required. Prestressed concrete piles do not suffer corrosion in saline water below the "splash zone", and rich well-compacted concrete can withstand attack from quite high concentrations of sulphates in soils and water. Up to now, however, steel piles have been widely used because they have a good resilience, high resistance to buckling and bending forces, and because there are very few of studies on the performance of prestressed concrete berthing piles[12]. Due to the advantages of lower costs, good durability, simple manufacture and easy construction, it is significant to study the strain energy and absorbing effectiveness of prestressed concrete berthing piles. This research work focused on the factors to affect service performance of prestressed concrete berthing piles, such as concrete strength, pre-tensile stress, sectional reinforcement, cracking characteristics, ultimate bearing capacity and absorption of energy. On the basis of the research mentioned above, the optimal sectional design of a prestressed concrete berthing pile will be obtained. The research contents are as follows:

(1) the work performance at service load and ultimate load;

(2) the relationship between load and deflection at different loading levels;

(3) crack characteristics and crack closing performance;

(4) effects of concrete strength on the strain energy;

(5) effects of pre-tensile forces on the strain energy;

(6) types of stirrups and sectional reinforcement; and

(7) the relationships between absorption energy, reaction force and deformation of the berthing piles using different design parameters.

The purpose of this research is to provide an experimental and theoretical basis for practical use in engineering. Since in China there are 5,700 rivers each with a drainage area larger than 100 square kilometers and with a combined total length of 430,000 kilometers, the port constructions have proceeded at a good pace in recent years, especially a rapid development of coordination of river-and-ocean research. Doubtlessly, the results of this paper will have vast prospects for practical utilization.

References

[1] "Handbook for design of sea harbors", volume 2, The first design institute of navigation engineering, The Ministry of Communications, China, The people's Communications Publishing House, 1998

[2] Cheng Wanjia, "Hydraulic structures", The people's Communications Publishing House, 2000

[3] Wang Dongya and Li Mingqao, "Port layout and design in theory and practice", Waterway Engineering, 1999.10

[4] Xu Xibin, "Research on structural types of wharf supported on piles", Journal of Port and Waterway Engineering, June 2000

[5] P. Bruun, "Port Engineering", Translated by The First Design Institute of Navigation Engineering, The Ministry of Communications, China, The people's Communications Publishing House, 1996

[6] Carl A.Thoresen, "Port design guidelines and recommendations", Tapir, 1988

[7] Edited by Tianjin University et al, "Large offshore design and construction", Jiaotong Press, 2001

[8] Translated by Zhu Shijie, "Pile design and theory", The People's Communications Publishing House, 1986

[9].Zhou Chuner, "Properties and Calculation Method of the Berthing Pile", Journal of Port and Waterway Engineering, June 2001

[10].W.G.K.Fleming.A.J.Weltman, M.F.Randolph and W.K.Elson, "Piling Engineering", 2nd edtion,Blackie Glasgow and London, Halsted press, an Imprint of John Wiley and Son, Inc. 1992

[11]. "Code of the pile engineering", The Ministry of Communications, China, The People's Communications Publishing House, 1997

[12]. Jiang Xizhu and Lu Weiyu，"New Wharf Structural Types"，People's Publishing Press, Beijing China,1999

Chapter 2

Test

2.1 Design and manufacture of specimens

Extensive researches have been undertaken on the resistance of piles to lateral loading, which are described in references [1] and [2]. The difference from the ordinary vertical piles subjected to lateral loads emerges from the fact that the problems related to the berthing pile are not only its ultimate capacity, but also its deformation capacity. Thus, the performance of the prestressed concrete berthing pile at the service loads is an important design consideration. If sections are proportioned by strength requirements alone, there is a danger that although the degree of safety against collapse will be adequate, the performance of the structure at the service loads may be unsatisfactory[3][4]. For example, at the service loads the deflections of the members may be excessively large, or the cracking of the concrete may be unacceptably great. Therefore, the berthing pile should be designed with reference to several states, the most important being strength at ultimate load, deflection at service loads, strain energy and cracking performance at service loads. The aim in the design should be to ensure an adequate margin of safety against collapse and the best performance of energy absorption.

Thus, to produce a satisfactory design, it must be ascertained that the magnitude of deflection and the extent of cracking at the service loads lie within reasonable limiting values.

This chapter deals with service load behavior through experiments. In order to do tests on the prestressed concrete berthing pile with the optimal absorbing energy effectiveness, six specimens using different parameters were designed as in Table 2.1, and the steel reinforcement of the specimens is shown in Figure 2.1.

Table 2.1 Design parameters

No	Type of Reinforcement	Section dimension	Stranded cable	Concrete strength	Pre-tensile stress	Remarks
1		27.5×27.5cm	Eight （7Φ5）	C60	$\sigma_K=0.5\sigma_u$	Symmetry
2	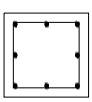	27.5×27.5cm	Eight （7Φ5）	C60	$\sigma_K=0.7\sigma_u$	Symmetry

3		27.5×27.5cm	Eight （7Φ5）	C80	$\sigma_K=0.5\sigma_u$	Symmetry
4		27.5×27.5cm	Nine （7Φ5）	C60	$\sigma_K=0.5\sigma_u$	Symmetry
5		27.5×27.5cm	Eight （7Φ5）	C60	$\sigma_K=0.5\sigma_u$	Symmetry
6		27.5×27.5cm	Eight （7Φ5）	C60	$\sigma_K=0.5\sigma_u$	No symmetry

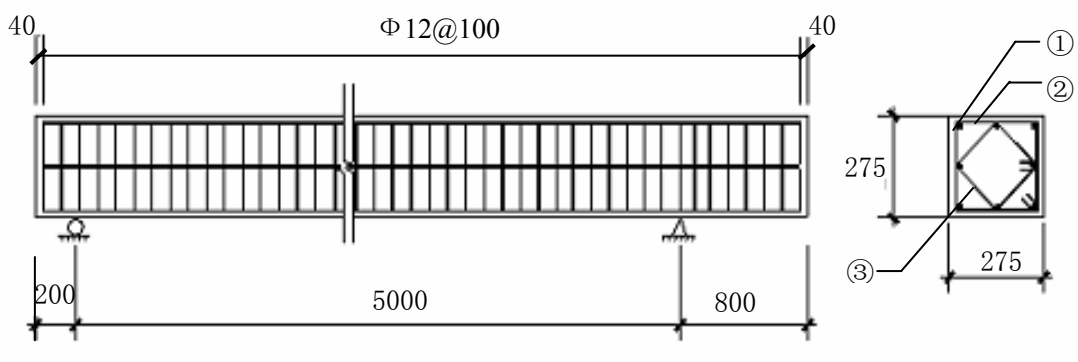

①-Stranded cable (7Φ5); ②-Basic stirrup (Φ12@100);
③-Additional stirrup (Φ12@100)

Figure 2.1 Steel reinforcement and measurements of the specimen (unit: mm)

In practice, the tensile and compressive stresses exist in a section of the berthing pile during the period of construction. At service time, there are forces from a ship acting on the berthing pile. These forces may be impact forces and mooring forces or pressure from the ship[5]. The purpose of the stranded cables arranged symmetrically is to satisfy the force performance of the berthing pile. An anchorage of type P produced by the OVM company of China is used at the two ends of the specimens. An anchored block is arranged at two ends respectively to make the pressure well-distributed (as shown in Figure 2.2). In addition, in order to prevent shear failure in the concrete, an additional stirrup is increased to enhance the shear resistance capacity.

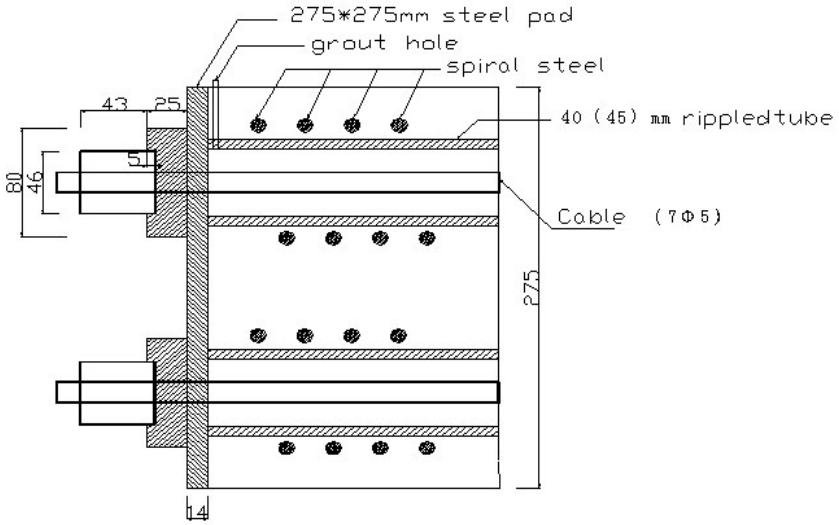

Fig. 2. 2 Anchorage equipment

The concrete strength of the specimen is designed as C60 and C80. When the concrete strength reaches 70% of the designed value, the cables are tensioned, in which the tension is simultaneously controlled by the tensile force and the deformation of the cable. The grouting follows immediately after the tensile work. Figure 2.3 shows the process of the cable to be tensioned and grouted.

Fig.2.3 The process of tensioning and grouting

2.2 Performances of Materials

2.2.1 Stress-Strain Relation of Concrete

The stress-strain relation of concrete is one of important properties for the performance

of prestressed concrete berthing piles. The stress-strain relations for both uniaxial compression and uniaxial tension exhibit a maximum value when the stress σ is depicted as a function of strain ε. The maximum values are the compressive strength and tensile strength, respectively. The compressive strength is often considered the most important property of concrete because other properties, including durability, are more or less closely related to the compressive strength. For berthing piles, deflection and cracking are also closely associated to the stress-strain relation of concrete.

When performing non-linear analysis of concrete structures, the stress-strain curve is one of the factors that shall be determined at first. However, it is not so easy to determine the stress-strain relation of concrete because it depends on many factors, such as loading velocity and sizes and shapes of components[13].

At present, the stress-strain curve of concrete is usually taken into account to analyze and calculate prestressed concrete structures. Regarding the shape of the curve, many proposals of stress-strain curves exist, in which the ascending branches of the curves are very different[3][17]. In the following table 2.2, different suggestions have been given.

Table 2.2 Equations of ascending branch in the concrete stress-strain curve

Authors	Concrete stress	No. of equations	Remarks
Saenz	$E\varepsilon[1+(3E_0/E-2)(\varepsilon/\varepsilon_0)+(1-2E_0/E)(\varepsilon/\varepsilon_0)^2]$	(2-1)	When $E/E_0=2$, it turns into (2-3)
Saenz	$E\varepsilon/[1+(E/E_0-2)(\varepsilon/\varepsilon_0)+(\varepsilon/\varepsilon_0)^2]$	(2-2)	When $E/E_0=2$, it turns into (2-5)
Hognestad	$E\varepsilon(1-\varepsilon/2\varepsilon_0)$	(2-3)	$E/E_0=2$
Torroja	$0.43E\varepsilon_0[(1-(1-\varepsilon/\varepsilon_0)^{7/3}]$	(2-4)	$E/E_0=7/3$
Krishman	$E\varepsilon[(1-\varepsilon/\varepsilon_0)^2]$	(2-5)	$E/E_0=2$
Tulin & Gerstle	$E\varepsilon[(1-\varepsilon/\varepsilon_0)^n]$	(2-6)	$E/E_0=n$
Baumann	$E\varepsilon\ [(1-(1-E_0/E)(\varepsilon/\varepsilon_0)]$	(2-7)	When $E/E_0=2$, it turns into (2-3)
Popovics	$(n-1)E\varepsilon[(n-1+(\varepsilon/\varepsilon_0)^n]$	(2-8)	$E/E_0=n/(n-1)$
Liebenberg	$E\varepsilon[(1-\varepsilon/\varepsilon_0)^n/(n+1)]$	(2-9)	$E/E_0=1+1/n$
Shah &Winter	$E\varepsilon(E_0/E)[(E\varepsilon-2)/(E\varepsilon_0-2)]^m$	(2-10)	

Smith& Young	$E\varepsilon e-\varepsilon/\varepsilon_0$	(2-11)	$E/E_0=e$
Young	$2E\varepsilon_0/\pi(\sin[(\pi/2((\varepsilon/\varepsilon_0)]$	(2-12)	$E/E_0=\pi/2$
Bach	$C_1\varepsilon^n$	(2-13)	$E/E_0=\infty$
Sturman	$C_2\varepsilon(1+C_3\varepsilon^{n-1})$	(2-14)	$E/E_0=n/(n-1)$
Ritter	$C_4(1-e^{-\varepsilon})$	(2-15)	
Alexander	$C_5\varepsilon/[(\varepsilon+C_6)^2C_7]-C_8\varepsilon$	(2-16)	
Kriz & Lee	$\{[C_9\varepsilon+C_{10})^2C_{11}\varepsilon^2]/4-C_{12}\varepsilon-(C_9\varepsilon+C_{10})/2\}^{1/2}$	(2-17)	

In this table 2.2, E is the initial modulus of elasticity of concrete and E_0 is the secant modulus for $\varepsilon = \varepsilon_0$, the strain at the peak value. The table gives the right hand side of the stress-strain curve $\sigma = f(\varepsilon)$.

In non-linear analysis of prestressed concrete berthing piles in this thesis, a combined stress-strain curve is used, in which the ascending branch is a second-degree parabola and the descending branch is a straight line, as shown in Fig.2.4.

Ascending branch $$\sigma_c=\sigma_{c\max}[2\frac{\varepsilon_c}{\varepsilon_0}-(\frac{\varepsilon_c}{\varepsilon_0})^2] \qquad 0\le\varepsilon_c\le\varepsilon_0 \qquad (2\text{-}3)$$

Descending branch $$\sigma_c=\sigma_{c\max}=[1-0.15\frac{\varepsilon_c-\varepsilon_0}{\varepsilon_u-\varepsilon_0}] \qquad \varepsilon_0<\varepsilon_c\le\varepsilon_u \qquad (2\text{-}18)$$

Here

σ_c - concrete stress

ε_c - concrete strain

$\sigma_{c\max}$ - maximum stress of concrete, i.e., the compressive strength.

ε_0 - strain corresponding to maximum stress of concrete, let $\varepsilon_0=0.002$

ε_u - ultimate compressive strain of concrete, let $\varepsilon_u=0.0035$. This value depends on the concrete strength; therefore, its variation should be considered in future research on this subject.

In hydraulic structures in China, the concrete strength grade is indicated by a capital letter of *C*. The strength is obtained by cubes with side length of 20cm and at the age of 28 days. Normally, the temperature should be from 15-20^{0}C and the relative humidity should be larger than 90%.

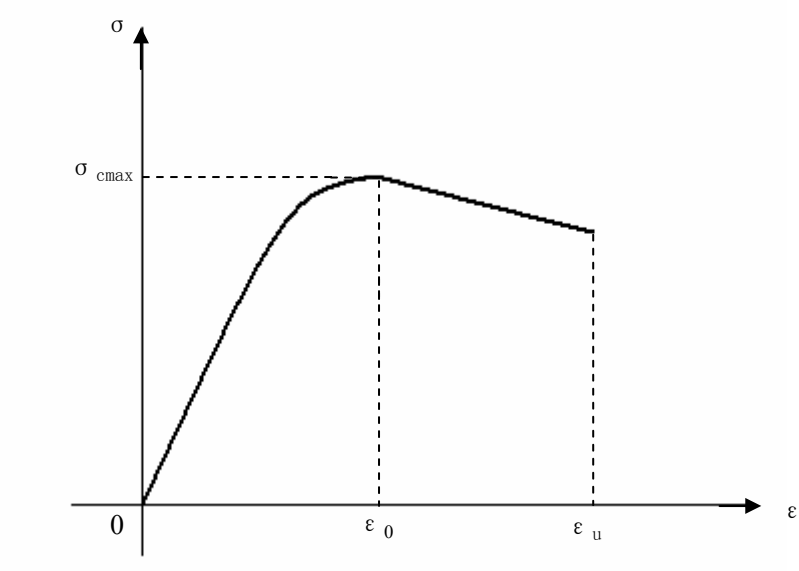

Figure 2.4 Stress-strain relation of concrete

For each specimen, there are nine group cubes cast and cured under the same conditions as the specimen. Before test is started, the cubes are measured to determine compressive strength of the concrete. The measured compressive strengths and modulus of elasticity of concrete in the present test are shown in Table 2.3

Table 2.3 Measured compressive strengths and modulus of elasticity of concrete

Specimen	No.1	No.2	No.3	No.4	No.5	No.6
compressive strength(MPa)	50.49	49.72	71.63	52.44	51.37	49.25
modulus of elasticity $E\times10^{-4}$(MPa)	3.36	3.34	4.0	3.42	3.39	3.32

2.2.2 Material Properties of Reinforcement

Stranded cable of 7Φ5 is adopted in the present prestressed concrete berthing piles, and the measured stress-strain curve of the stranded cable is shown in Fig. 2.5.

With increment of load, the steel shows gradual yielding, but the curve continues to rise monotonically until fracture. The actual measured elastic modulus E_s = 214,000MPa, proportional limit σ_p = 1,240 MPa, and ultimate strength σ_u = 1860MPa, ultimate strain ε_u = 1.36%

For the non-prestressed reinforcement used in the berthing pile, the elastic modulus *E*

= 210,000MPa, yielding limit $\sigma_y = 240$ MPa, ultimate strength σ_u = 380MPa and the elongation percentage is 28%.

2.3 Installation of specimens

The work performance of the prestressed concrete berthing pile is analogous to the performance of a single vertical pile subjected to lateral load, as shown in Figure 2.6[6]. The ultimate resistance of a vertical pile to a lateral load and the deflection of the pile as the load builds up to its ultimate value are complex matters involving interaction between

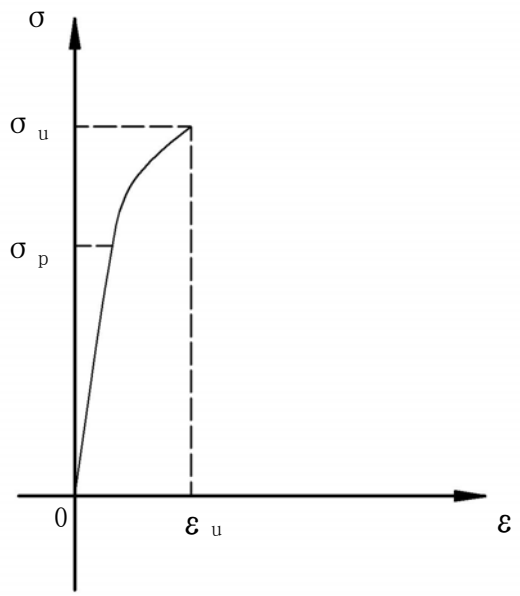

Figure 2.5 Stress-strain relation of stranded cable

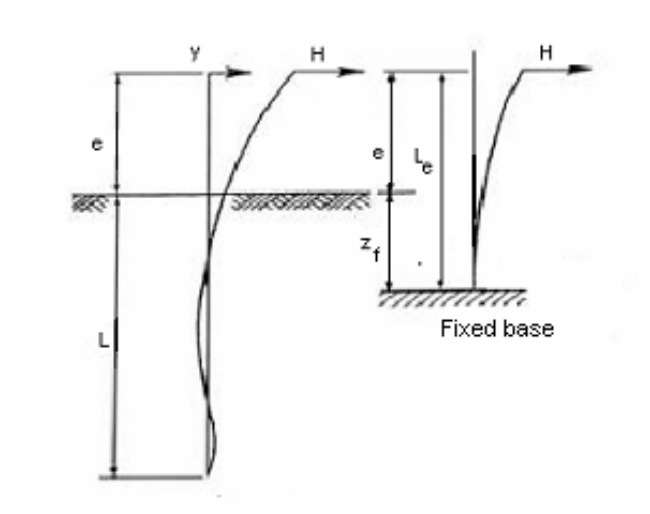

(a) (b)

(a) partly embedded pile (b) equivalent fixed base pile

Figure 2.6 Bending of the pile

the pile and the soil, which deforms partially elastically and partially plastically. Quite extensive research has been undertaken on the resistance of piles to lateral loading, but this research has not yielded any simple design method which can be universally applied to any soil or type of pile[7][8].

In analysis, it may be necessary to determine the bending moments, shearing forces and deformed shape of a pile over its full depth at a selected working load. Because the berthing pile is an energy absorbing member resisting the berthing impact force of ships, it is necessary to calculate the bending moments, shearing forces and the deflection of laterally-loaded pile. In fact, the prestressed concrete berthing pile is elastically fixed in soil, as shown in Figure 2.6(b), and the position of the fixing point depends on the soil conditions, section dimensions, connecting characteristics of the two ends and free length of the pile[9][10]. Usually, the lateral loading tests are made by pulling a pair of piles together, or jacking them apart. Where the lateral loads on piles are of a repetitive character, as in wave loading or traffic loads on a bridge, it is desirable to make cyclic loading tests. This involves alternately pushing and pulling of a pair of piles, using a rig of the type as shown in Figure 2.7(b). Instead of a pair of piles a single pile can be pushed or pulled against a thrust block (Figure 2.7a). Where pushing methods are used restraining devices should be provided to ensure that the jack and strut assembly does not buckle during the application of a load[11].

According to the practical usage of the berthing piles, they are arranged in front of a wharf to directly absorb the energy by an impacting ship. Normally, the free length of the berthing pile is much larger than that of an ordinary pile subjected to lateral loads. Considering current conditions and the available equipment in the laboratory, the specimens are installed horizontally with a fixed and a simple support, respectively, at the two ends. The fixed end is simulated by a special jack based on compatibility analysis, as shown in Figure 2.8, which makes its deformations and internal forces be the same as for a real fixed support.

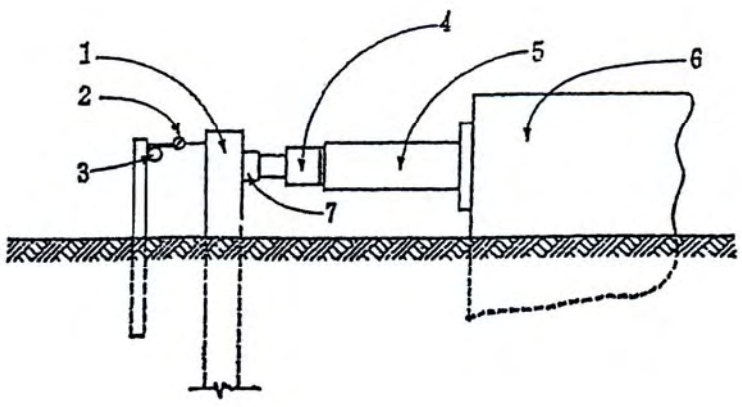

(a) Testing rig for pushing and pull lateral loading test on a single pile
1 – sleeve; 2 – tie rod; 3 – hydraulic jack; 4 – load cell; 5 – dial gauge; 6 – dial gauge support; 7 – tubular strut;

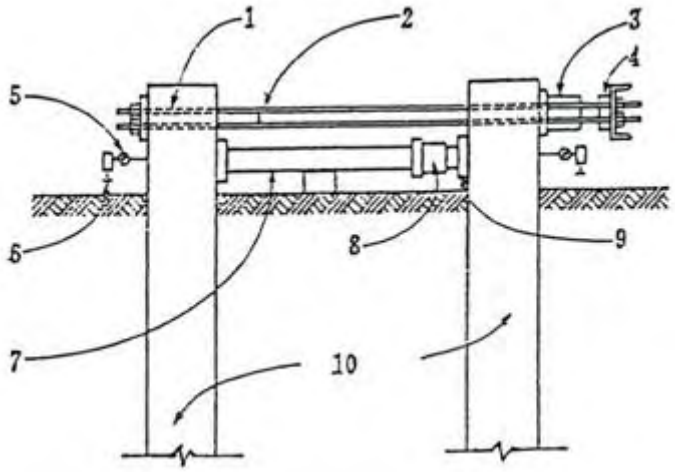

(b) Testing fir for lateral loading test on a pair of piles
1 - test pile; 2 – dial gauge; 3 – support; 4 – hydraulic jack; 5 – strut;
6 – concrete thrust block; 7 – load cell; 8 – jack; 9 – bearing pad; 10 – test piles

Figure 2.7 Lateral loading test

There is a loading sensor under the jack. The force of the jack is controlled by the loading sensor. The deflection of the specimen is measured at the middle span by deflection meter. An inclination meter is installed at the fixed end, which is used to control the condition of no-rotational angle at the simulated fixed end, as shown in Figures 2.8 and 2.9.

2.4 Loading scheme

The occurrence of cracks in reinforced concrete structures is inevitable because of the low tensile strength of concrete. The tensile resistance of concrete is normally neglected in design. Structures designed with low steel stresses at the service load serve their intended function with very limited cracking. In many cases no cracking is visible at all because many members are not subjected to their design service load and the concrete has some tensile strength. However, with high service load steel stresses, particularly as a result of the use of high-strength steel, some cracking must be expected at the service load. In hydraulic structures, cracking will greatly weaken integral rigidity and durability of the specimens，and therefore, there are special restrictions for cracking. Especially, it is hoped that the cracking produced by an occasional load should be closed when the load is removed [12].

To probe into the service performance, i.e. the strain energy and the crack closing behavior of the prestressed concrete berthing piles, the test scheme is designed as three cycles of loading. The first cycle is to gradually load the specimen until cracking is produced, and then the load is gradually removed. In the second cycle, there are several loading steps larger than the first cracking load. Finally, gradual loading is performed until the specimen fails. Figure 2.8 and Figure 2.9 show the installation and the

arrangement of test equipment of the specimen, respectively.

In each round of loading cycle, the operating process is as follows: ① Before the first loading cycle begins, the data collection system collects data, and initial balance is made; ② The mid-span jack is loaded to a given load value according to designed loading grade; ③ At the end of the beam another jack is used to simulate a fixed-end condition. ④ When the fixed-end condition is met, collection of data is carried out; ⑤After data collection is finished, next stage of loading is carried out. Other procedures are the same as ②～⑤.

The principles of selecting and arranging measuring points are: First, with the premise of meeting the objects of the tests, it is advisable to use a small number of measuring points so that measurement of key test points can be conducted. Secondly, the test points should represent the behavior well. The actual measuring points are arranged that the steel strain gauges are placed in the prestressing bars at the range of middle span and at the simulated fixed end, and the concrete strain gauges are positioned in tensile and compression faces of middle span and fixed end, respectively.

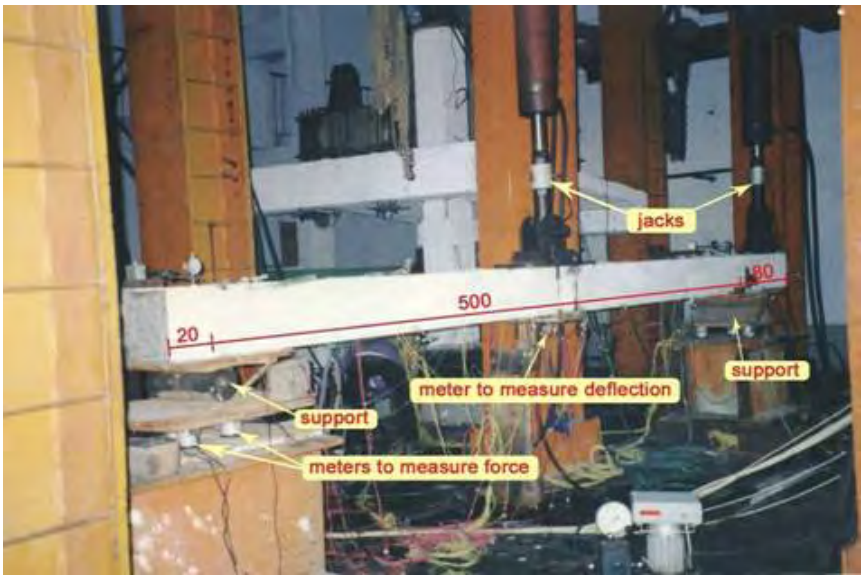

Fig.2.8 Installation of the specimens

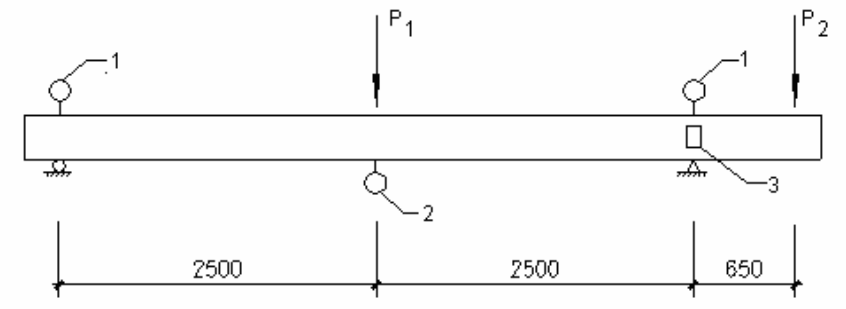

(P_1 is the jack in span, P_2 is the jack to simulate fixed end condition,

1 and 2 are deflection meters and 3 is an inclination meter。Unit: mm)

Fig.2.9 Arrangement of test equipment of the specimen

2.5 Test results

2.5.1 Load - deflection relationships

The relationship between load and deflection is a very important service performance of the berthing pile. The magnitude of absorption energy depends on the deflection at loading. Therefore, sufficient deflection to be produced at service loads is required. But deflections may need to be limited to prevent the structural behavior from being different from that assumed in the design. Examples in this category are deflections causing instability; deflections causing a change in the stress system and deflections causing dynamic effects that increase stresses. When possible, the effects of deflections on the structural behavior should be included in the design of the element.

Figures 2.10(a) to (f) are, respectively, the load-deflection curves of specimens from No.1 to No.6 under the conditions of the three cyclic loadings. The characteristics are described as follows:

1. With increasing of loading, the deflection is gradually increased. Before cracking, a linear relationship exists between load and deflection, which shows that the specimen is in a linear elastic state before cracking. However, after a crack appears, the slope of the curve is evidently decreased, which will weaken the integral rigidity of the specimen. As soon as a crack occurs, the loading is stopped. With the removal of the load, the specimen recovers along the original curve. When loaded again, the specimen follows almost the same path up to the curve, as shown in Figure 2.10.

2. By varying the amount of compressive prestress, the number and width of the cracks can be desirably limited, and consequently the deflection of the member may be controlled. The choice of a suitable amount of prestress is governed by a variety of factors, such as the nature of the loading, the ratio of live to dead load, the frequency of occurrence of the full load, and the presence of corrosive agents[13]. Normally, with the increasing of the pre-tensile force, the ultimate deflection of the member will be decreased because the rigidity of the member is increased with the increasing of the pre-tensile force. Also, should heavily prestressed members be overloaded and fail, they may do so in a brittle way, rather than gradually as do members with a smaller amount of prestress. This is important from the point of view of safety, because sudden failure without warning is dangerous, and gives no opportunity for corrective measures to be taken. Comparing with the specimens no.1 and no.2, however, a larger pre-tensile force may improve the service performance of the berthing pile, which is different from an ordinary prestressed concrete member with a low concrete strength. Both the ultimate load and deflection are increased with the increase in pre-tensile force, as shown in Figure 2.10(b). Considering the service requirements and working environment of the berthing pile, a suitable increasing of the pre-tensile force is possible with no change to its service performance.

3. Specimen no.3 has a higher concrete strength. Usually, high-strength concrete has a higher elastic modulus than low-strength concrete, so that any loss of prestressing force due to elastic shortening of the concrete is reduced. Creep losses, which are roughly proportional to elastic losses, are lower as well. High bearing stresses in the vicinity of tendon anchorages for post-tensioned members are more easily accommodated, and the size of expensive anchorage hardware may be reduced. Further higher bond strength results in a reduction in the development length required to transfer the prestressing force from the cable to the concrete. In addition, concrete of higher compressive strength also has a higher tensile strength, so that the formation of flexural and diagonal tension cracks is delayed. The test curve of Figure 2.10(c) shows the advantages of the high strength

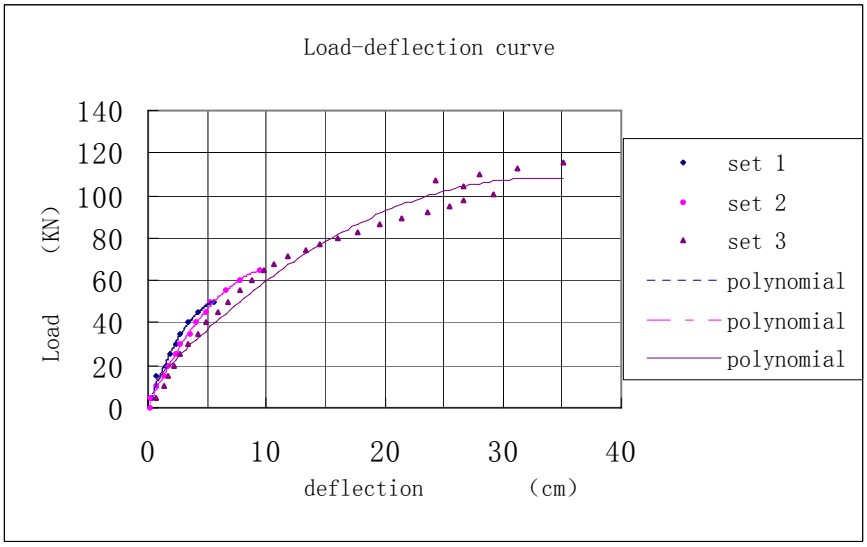

(a) Specimen no.1

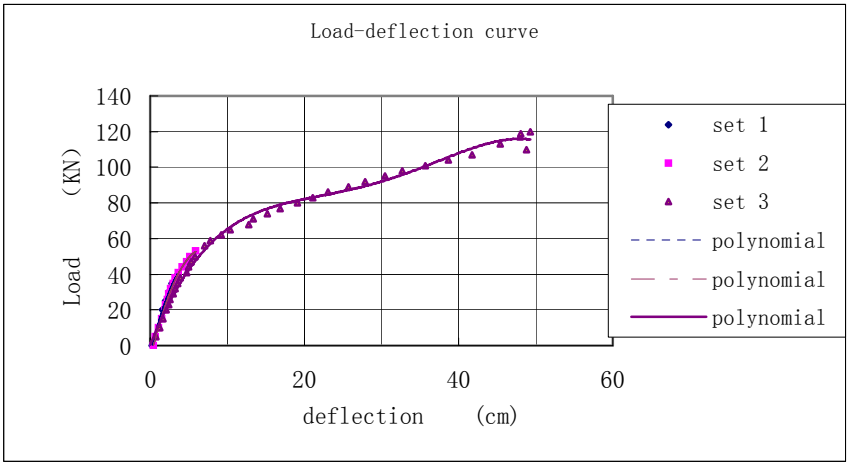

(b) Specimen no.2

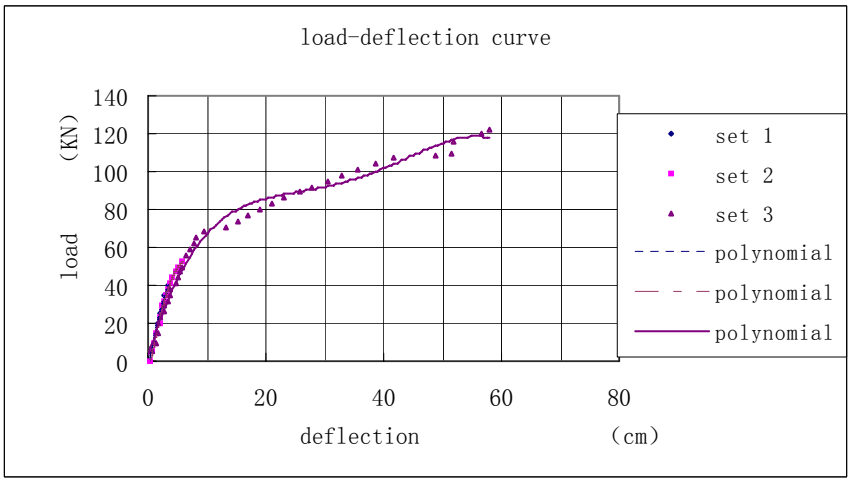

(c) Specimen no.3

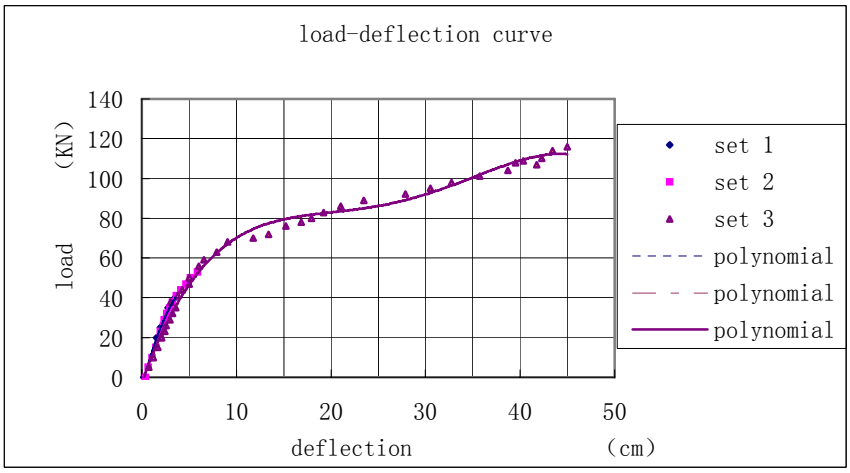

(d) Specimen no.4

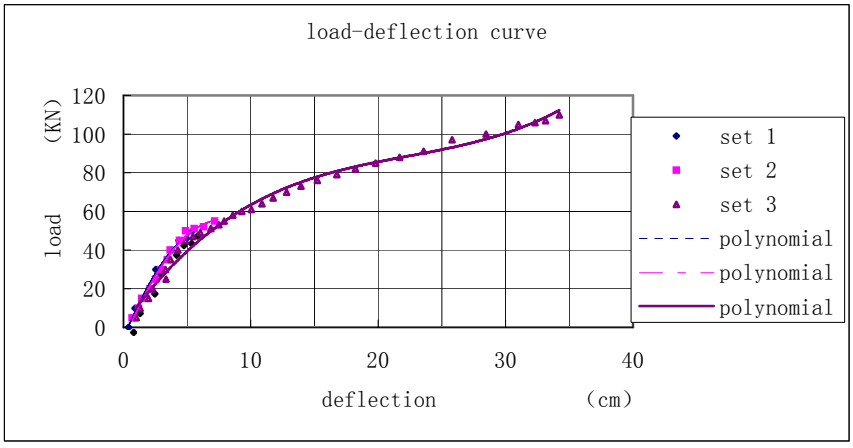

(e) Specimen no.5

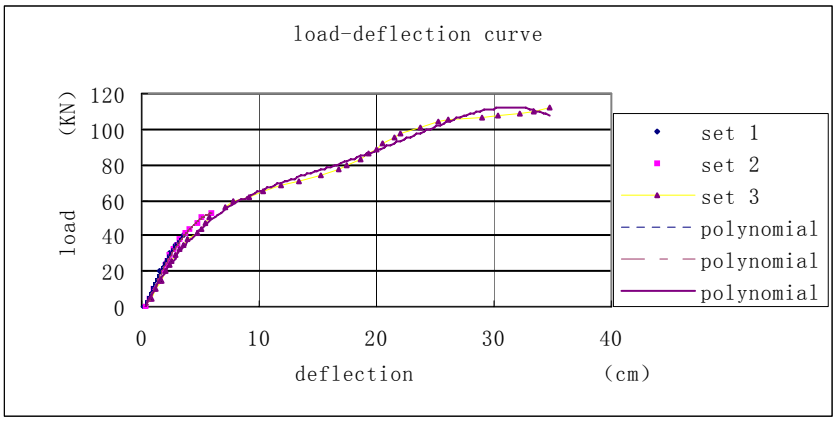

(f) Specimen no.6

Figure 2.10 Load-deflection curves

（set 1- first cycle, set 2 – second cycle, set 3 – third cycle）

materials. They not only give a higher cracking load, but also the largest deflection under the ultimate loading state. It has been shown, after comparing with the test results, that the absorbing energy of the specimen is enlarged with increasing of concrete strength. Meanwhile, the slope of the curve of specimen no.3 is the largest in all specimens, which means that the integral rigidity of the specimen is changed with the strength of the concrete.

4. Figures 2.10(a) and (e) show, respectively, test relationships of load and deflection under the conditions of closed rectangular stirrups and spirals. In practice, concrete is usually confined by transverse reinforcement, commonly in the form of closely spaced steel spirals or hoops. In this case, at low levels of compressive stress, the transverse reinforcement is hardly stressed and the behavior of the concrete is unaffected by the reinforcement. The concrete becomes confined when at stresses approaching the uniaxial strength the transverse strains becomes very high because of progressive internal cracking and the concrete dilatates against the transverse reinforcement, which then applies a confining reaction to the concrete. Thus, the transverse reinforcement provides passive confinement. Tests by many investigators have shown that confinement by transverse reinforcement can considerably improve the stress-strain characteristics of concrete at high strains. Figure 2.11 shows stress-strain curves obtained from three sets of concrete cylinders confined by circular spirals[14]. Each set was for a specific unconfined strength of concrete. The increase in strength and ductility with content of confining steel is very significant. Tests have demonstrated that circular spirals are much more effective than rectangular or square hoops. The reason is that circular spirals attains an axial hoop tension and provides a continuous confining pressure around the circumference, which at large transverse strains approximates fluid confinement. As a rule, however, square hoops can apply only confining reactions near the corners of the hoops because the pressure of the concrete against the sides of the hoops tends to bend the sides outwards. Therefore, a considerable portion of the concrete cross section may

be unconfined. Because of internal arching between the corners, the concrete is confined effectively only in the corners and the central region of the section. However, the results of the tests are different from the tests mentioned above. It can be seen from Figure 2.10(a) and Figure 2.10(e) that the cracking loads, ultimate loads and ultimate deflections of the specimen with rectangular stirrups are higher than for those with circular spirals. This is because the prestressed concrete berthing pile is subjected to a horizontal impact force from a berthing ship, instead of an axial compressive load, and before failure of the specimens, large transverse concrete strains are not produced. The failure of the specimens is a result of the onset of concrete spalling. Therefore, the advantages of the circular spirals have not appeared.

In practice, however, care must be taken concerning the ratio of the transverse bar diameter to the unsupported length in the case of rectangular stirrups or hoops, because a larger bar diameter leads to more effective confinement. Transverse bars of small diameter will act merely as ties between the corners because the flexural stiffness of the hoop bar is small and the hoops bow outward rather than effectively confining concrete

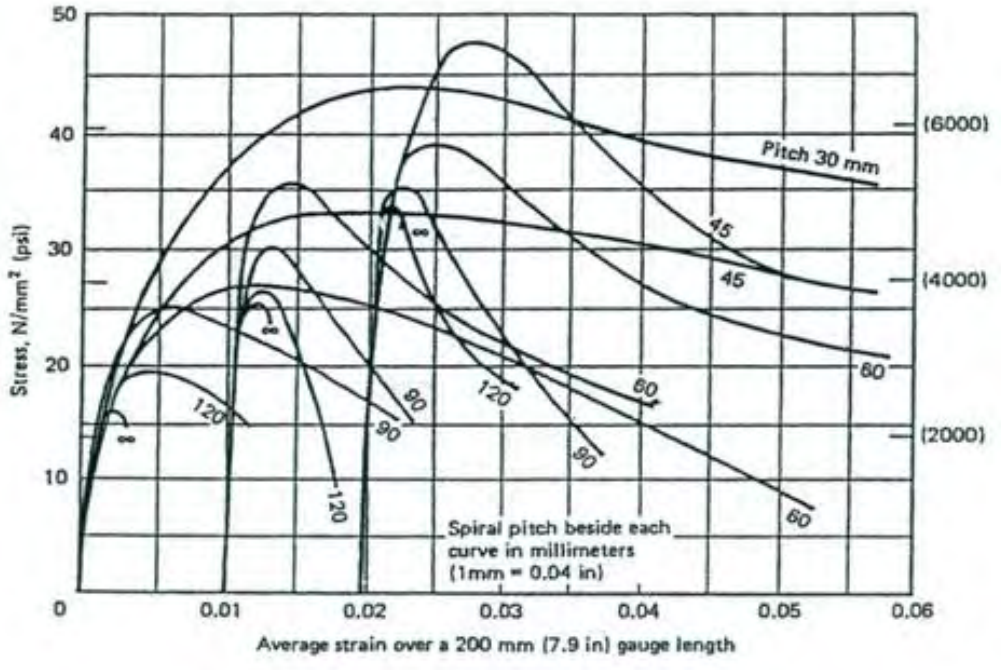

Fig.2.11 Stress-strain curve for concrete cylinders 150mm diameter by 300mm height, confined by circular spirals from 6.5mm diameter mild steel bar.

in the regions between the corners. With a large transverse bar diameter to unsupported length ratio, the area of concrete effectively confined will be large due to the greater flexural stiffness of the hoop side. Thus, it is very important to pay attention to this ratio.

5. A load-deflection curve of non-symmetric reinforcement is shown in Figure 2.10(f). The occurrence of cracks is delayed, and the increase of the cracking load is larger than that of the ultimate load so that the ratio of cracking load to ultimate load is decreased.

Meanwhile, the ultimate deflection is smaller than that of the specimen with symmetric reinforcement. Thus, non-symmetric reinforcement can not result in a satisfactory effectiveness of the absorption energy.

6. Regardless of the amount of prestressing force applied, the amount of steel must be such as to provide adequate flexural strength when the member is overloaded, so that the desired factor of safety is obtained. All specimens designed in table 2.1 satisfy the requirements of the minimum reinforcement ratio[15][16]. This is necessary because if the reinforcement ratio is very small, the calculated flexural strength of a reinforced concrete section becomes less than the bending moment required to crack the section, and on cracking, failure is sudden and brittle. When the steel content of the section is small, the steel will reach the yield strength before the concrete reaches its maximum capacity. However, if the specimen is over reinforced, the concrete may reach its maximum capacity before the steel yields. With the increase in the sectional steel, as shown in Figure 2.10(d), the steel can not provide higher flexural strength as expected, and the ratio of cracking load to ultimate load is decreased with the increase of sectional steel content.

2.5.2 Cracking

The consideration of durability of the berthing piles is a very important factor in the design, and the durability is closely related to cracks. The causes of cracking in concrete are numerous, and cracking will result in corrosion so that the durability of the pile may be decreased. Therefore, the factors to be taken in consideration are the thickness and permeability of the cover concrete, the width, shape, and length of cracks, the period of time the cracks are open, and finally the corrosive nature of the environment. Thus, the effect of cracking is one of the main subjects of research. Test cracking results prove the following characteristics:

1. The first crack is generated at a loading point in the middle span. It is a flexural crack, and with an increase in loading it develops in the direction perpendicular to the neutral axis. The cracking of concrete is accompanied by an instantaneous increase in steel stress, as the tensile force formerly carried by the concrete is transferred to the steel. In the region of high shear force, significant principal tensile stresses are generated at approximately 45^{o} to the axis of the member. These result in inclined cracks. With few exceptions these inclined cracks are extensions of flexural cracks, as shown in Figure 2.12.

2. Because of different design parameters, there are substantial differences in the cracking characteristics of all specimens, including the number of cracks, crack distribution and width. Table 2.4 gives the crack number, width and distribution, respectively. A sufficient number of cracks have been produced with the increase of loading, and the test results show that the cracks are distributed over a relatively large region, which illustrates good bond performance due to good quality of grouting. Since

there is a large contact area between steel and concrete in Specimen 4, therefore, in this specimen there is a relative large bond force, which results in more cracks with smaller width. This special case indicates that a reasonable increase in the ratio of reinforcement can improve cracking behavior. Figure 2.12 shows the typical characteristic of cracks in the middle span.

（a）Cracks in span

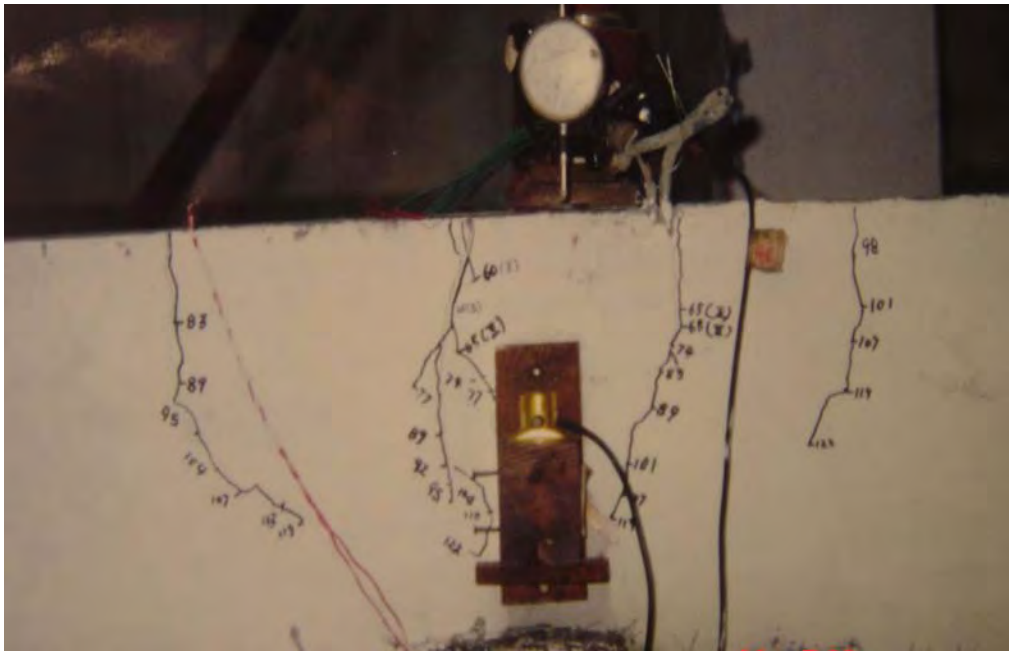

(b) Cracks at fixed end support

Fig. 2.12　Distribution of cracks

Table 2.4 The distribution of cracks

Contents \ Specimen		No.1	No.2	No.3	No.4	No.5	No.6
Crack number	In span	13	12	10	23	12	21
	Support	8	6	4	6	7	6
Distribution of cracks in span		210cm	203.8cm	201cm	208cm	204cm	205cm
Average spacing of cracks	In span	16.4cm	18.5cm	22.2cm	9.5cm	15.5cm	10.7cm
	Support	14.9cm	13.3cm	21.0cm	15.3cm	15.5cm	14.8cm

3. Parts of the test relationships between the load and the crack width are shown in Figure 2.13. Because high concrete strengths are used, the specimen no.3 shows relatively large cracking load and a small crack width when the first crack appears. With an increase in load, meanwhile, the rate of the cracking is much lower than that of the other specimens. It can be seen from Figure 2.13 that at the same loading level, the crack width of No.3 is the smallest of all specimens. The characteristics mentioned above indicate that the materials of high strength used in design of prestressed concrete berthing piles may improve the cracking performance, which is very useful for practical purposes.

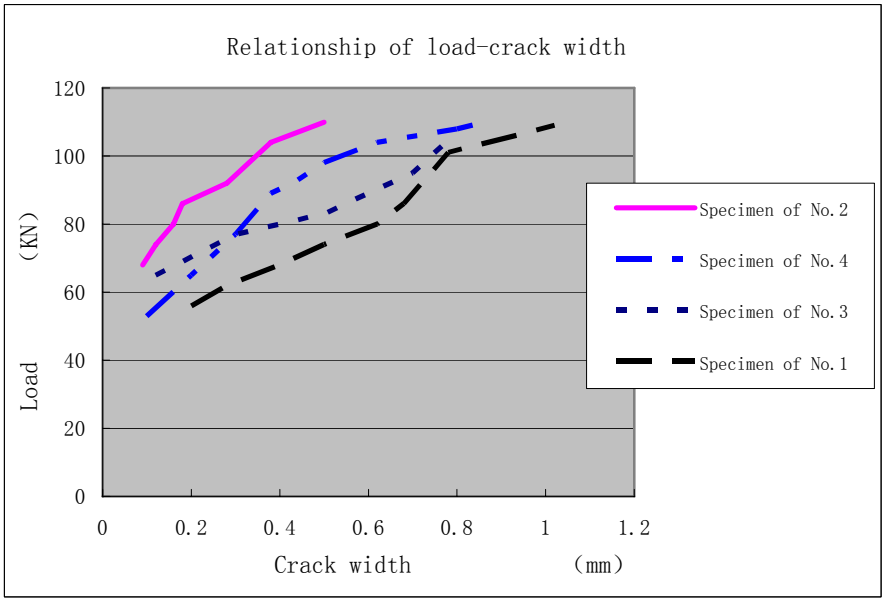

Fig. 2.13 Relationship of load-crack width

2.5.3 Crack closing performance

The loading of a prestressed concrete member will in general produce an increase in stress in the steel. As long as the member remains uncracked, the increase is so small that it is usually neglected in design. However, cracking of the concrete is accompanied by an instantaneous increase in steel stress, as the tensile force formerly carried by the concrete is transferred to the steel. After the yield stress of the steel is reached, the steel elongates disproportionately, but carries increasing stress due to the shape of its stress-strain curve, and the stress vs. load curve continues upward with a gradually reducing slope. At failure, the steel stress may be equal to the tensile strength, but is usually somewhat below, depending on many factors.

The prestressed concrete berthing piles are arranged in front of the wharf, that is to say, they are in an environment of water and subjected to the impact force from the berthing ship. To meet the service requirements, the piles should have good capacity of cracking resistance and the ability of cracks to be closed.

In practical usage of the piles, the tensile stress and possible cracking may be allowed at maximum service load, and it is recognized that maximum service load may only be infrequently applied. A very important point is that cracks may occur occasionally, when the maximum load is applied, but they will be closed completely when the load is removed. The occasional cracking may be considered a small price for the improvements in performance and economy that are obtained.

In the process of test, the first cyclic loading is applied until the first crack takes place. While gradually removing the load, the load-deflection curve returns to zero along the original path, and the crack is completely closed. The same process exists in the second cycle, which shows that the specially designed specimens have a good performance of crack closure. This performance is important for hydraulic structures, because it is very useful in avoiding corrosion problems due to cracking produced by an occasional load, and to effectively increase the integral rigidity and durability of the prestressed concrete berthing pile. Relatively speaking, the performance of specimens no.2 and no.3 is better than that of the rest of the specimens.

2.5.4 Relationship between load and steel stress

Figure 2.14 is a typical load-strain curve of the prestreesed cables in the center of a span. It shows that the loading of the prestressed concrete member generally produces an increase in steel stress. As long as the member remains uncracked, the increase is so small that it is usually neglected in design. However, cracking of the concrete is accompanied by an instantaneous increase in steel stress, as the tensile force formerly carried by the concrete is transferred to the steel. At the second loading cycle, there is the same performance to be produced. The sudden increase in steel stress is accompanied by new cracks generated. During the later period of loading, the load-strain curve of the steel shows a non-linear relationship so that the increasing of the strain is faster than that

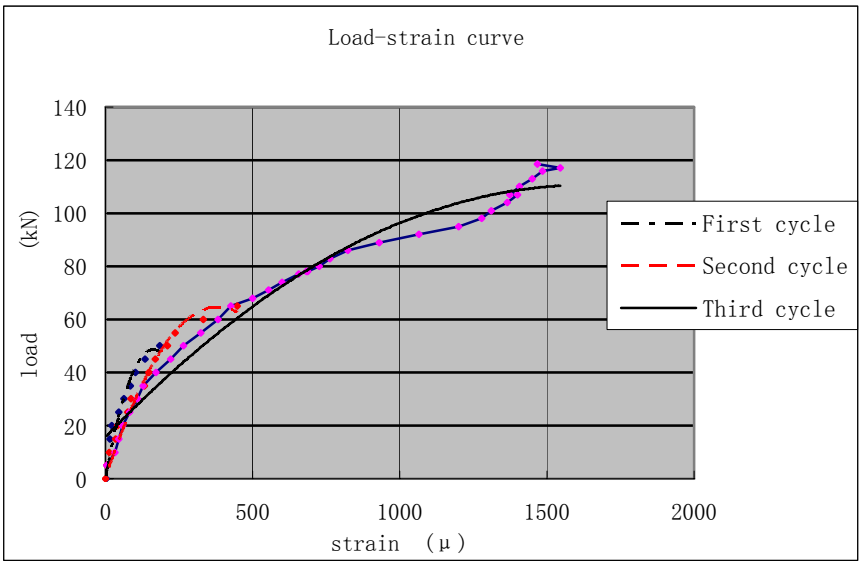

Fig. 2.14 Typical load-strain curve of steel

of the load. But the stress does not reach the ultimate strength before the member fails. All tests of the specimens show that the concrete reaches its maximum capacity before the steel yields, and the failures are generated by the concrete spalling away (as shown in Figure 2.15), which is a marked characteristic of the failure of prestressed concrete berthing piles. Hence, from the view to give full play to the function of high strength steel, the sectional steel content of the prestressed concrete berthing pile may be controlled by the minimum reinforcement ratio.

Fig. 2.15 Typical failure characteristic

2.5.5 Summary of test results

Table 2.5 gives a summary of test results, including those based on laboratory work, consisting of cracking loads, ultimate loads, cracking moments, ultimate moments and ultimate deflection, as well as deformation energy. The loads in this table come from the jack at the middle span. According to the results, the preliminary conclusions can be given as follows:

1. Even though specimens with different design parameters lead to different test results, all results from the tests have shown that prestressed concrete piles with high strength materials may be utilized as protective equipment between a berthing ship and a berthing

Table 2.5 Summary of test results

Specimens / Contents	Specimen of No.1	Specimen of No.2	Specimen of No.3	Specimen of No.4	Specimen of No.5	Specimen of No.6
Cracking loads（kN）	56	68	65	53	51	59
Ultimate loads（kN）	115	120	122	116	110	112
Cracking moments（kN·m）	32.61	39.60	37.86	30.87	29.70	34.36
Ultimate moments（kN·m）	92.97	97.66	96.91	93.96	89.10	95.58
Ultimate deflections (cm)	35.44	49.28	58.02	44.98	34.23	34.70
Ultimate deformation energy (N·m)	2 567	3 645	4 171	3 354	2 389	2 603

structure, and a satisfactory energy absorption may be produced at the action of service loads. If they are used together with other fender equipment, a more economic and safe fender system will be obtained.

2. Because of the special working environment of the berthing pile, the cracking will result in corrosion which weakens its integral rigidity. The good crack closure performance shown in testing is important for hydraulic structures and is very useful in avoiding corrosion problems due to cracking produced by occasional loads. Hence, it can

increase the integral rigidity and durability of the prestressed concrete berthing piles.

3. The confinement by transverse reinforcement can improve the stress-strain characteristics of concrete at high strains. Because it is not possible to produce large concrete transverse strains for the prestressed concrete berthing pile, therefore, rectangular or square hoops should be used because of the advantages of lower costs and easy construction.

4. From the point of view of increasing the capacity of resistance to cracking, the higher the tensile force or the concrete strength, the better the capacity of resistance to cracking. However, the deformation capacity of the prestressed concrete berthing piles is remarkably affected by the pre-tensile force and the concrete strength. For the berthing piles with high concrete strength, the pre-tensile force is properly increased so as not to change the service performance. Comparatively, the service performance of the specimens with high concrete strength and large pre-tensile stress is better than that of other specimens.

References

[1]. “Code of the pile engineering”, The Ministry of Communications, China, The People’s Communications Publishing House, 1997

[2].W.G.K.Fleming.A.J.Weltman, M.F.Randolph and W.K.Elson, “Piling Engineering”,2nd edtion,Blackie Glasgow and London, Halsted press, an Imprint of John Wiley and Son, Inc. 1992

[3]. R.Park and T.Paulay, “Reinforced concrete structures”, A Wiley-interscience publication, John Wiley and Sons, New York., London, Sydny,. Toronto, 1975

[4]. He Hai University, “Hydraulic reinforced concrete”, 3rd edition, The People’s Communications Publishing House, 1996

[5]. “Handbook for design of sea harbors”, volume 2, The First Design Institute of Navigation Engineering, The Ministry of Communications, China, The People’s Communications Publishing House, 1998

[6]. Carl A.Thoresen, “Port design guidelines and recommendations”, Tapir, 1988

[7]. Xu Xibin, “The research on strain energy of prestressed concrete berthing piles”, Journal of Chongqing Jiaotong University, Vol.15 no.4, 2003

[8]. Ruan Qinan, Zhang Hongjien and Kong hue, “Design of pile foundation”, Industrial Publishing House, China, 1999

[9]. Per Bruun, Port Engineering, 4th edition, Gulf Publishing Company,USA,1989

[10] Wang Binghuang，Code of Pile and Foundation in Port Engineering（JTJ254—98）， People Jiaotong Publish House, Beijing China，1998

[11]. M.J.Tomlinson, “Pile design and construction practice”, 4th edition, E & FN SPON, An Imprint of Chapman and Hall, 1994.

[12]. Lu Shusheng，Modern Prestressed Concrete Theory and Practice, China Railway Publishing House，Beijing China，2000

[13]. Arthur H.Nilson, “Design of Prestressed Concrete”, John Wiley and Sons, New York, Santa Babara, Chicheester, Brisbane, Toronto, 1978

[14]. Translated by Qing Wenyu et al, “Reinforced concrete structures”, Chongqing University Publishing Press, 1985
[15]. “Code of reinforced concrete”, The Ministry of Communications, China, The People’s Communications Publishing House, 1997
[16]. Xu Xibin and Tu Zhongren, “Researches on the behaviors of post-tensioned prestressed concrete vertical piles subjected to impact force from ship”, Journal of Chongqing Jianzhu University, 2001.3
[17]. Chao Juyi, “Concrete stress-strain relationship”, Journal of Sichuan Jianzhu Scientific Research, Vol.15 no.4, 2002

Chapter 3

General theoretical calculation methods

3.1 Non-linear whole process analysis method

In the actual application of prestressed concrete berthing piles, when the stress of a reinforced steel bar goes beyond the proportional limit, the stress-strain relationship will be non-linear, and the stress-strain relationship of the concrete will also be non-linear. Thus relevant elements in the stiffness matrix shall be continuously adjusted according to the variation of the stress field in theoretical analysis. For concrete, when the tensile stress (tensile strain) exceeds the tensile strength limitation (tensile strain limitation) and causes cracks, this will cause another non-linear relationship, which belongs to a material non-linear problem. In addition, when there are large displacements of the members in the process of loading, which causes the load-deflection to become non-linear, we have a geometric non-linear question[1][2].

Factors such as creep strain, contraction, temperature and load history, etc. are not considered in the theoretical analysis in this paper.

The calculation method for non-linear questions can be classified into three categories: incremental method, iteration method and mixed method.

The incremental method divides load into many small increments, and one load increment is applied each time. At level one load increment, we may assume the stiffness matrix to be a constant. However, for other load increments, the stiffness matrix may have different values, corresponding to the stress-strain relationship. The iteration method has all loads applied during each iteration process, but the displacements and strains are gradually changed to adjust to the non-linear stress-strain relationship. The mixed method adopts both the incremental and the iteration methods, and divides the load into load increments with fewer increment levels, and also carries out iteration calculations for each level of load increment[3].

3.1.1 Incremental method

From the above we can see that, when using the incremental method to analyze non-linear problems of prestressed concrete berthing piles, the load is subdivided into many load increments, which may be equal or different. However, one level of load increment is treated at one time. In a specific load increment, we assume that the stiffness matrix $[K]$ is a constant, while the stiffness matrix may have different values for different load increments. For every level of load increment $\{\Delta R\}$, we may obtain one corresponding displacement increment $\{\Delta\delta\}$, which then may be added up to get the displacement $\{\delta\}$.

Therefore, the incremental method solves a series of linear problems in order to approach the solution of non-linear problems. Thus actually a polygon is used to replace the non-linear curves[4].

Dividing the load into *n* levels of increments, the total load is

$$\{R\} = \sum_{j=1}^{n} \{\Delta R_j\}$$

When applying the i^{th} level load increment, the load is

$$\{R_i\} = \sum_{j=1}^{i} \{\Delta R_j\} \tag{3.1}$$

Each level of load increment will generate a displacement increment $\{\Delta\delta_j\}$ and a stress increment $\{\Delta\sigma_j\}$; thus, after applying the i^{th} level of load increments, the displacement and stresses are, respectively

$$\{\delta_i\} = \sum_{j=1}^{i} \{\Delta\delta_i\} \tag{3.2}$$

$$\{\sigma_i\} = \sum_{j=1}^{i} \{\Delta\sigma_j\} \tag{3.3}$$

There are three methods used to calculate the displacement increment $\{\Delta\delta_i\}$ and the stress increment $\{\Delta\sigma_i\}$ from the load increment $\{\Delta R_i\}$.

(1) Initial point stiffness method

In Figure 3.1, we assume that we have obtained the stress $\{\sigma_{i-1}\}$ after the *i-1*th level of load increment, then according to $\{\sigma_{i-1}\}$ and the stress strain relationship, we can determine the elasticity matrix $[D_{i-1}]$ after the *i-1*th level load increment, and thus to calculate corresponding stiffness matrix $[K_{i-1}]$. Assume the stiffness matrix at the i^{th} level of the load increment was kept unchanged and approximately assumed equal to $[K_{i-1}]$, then

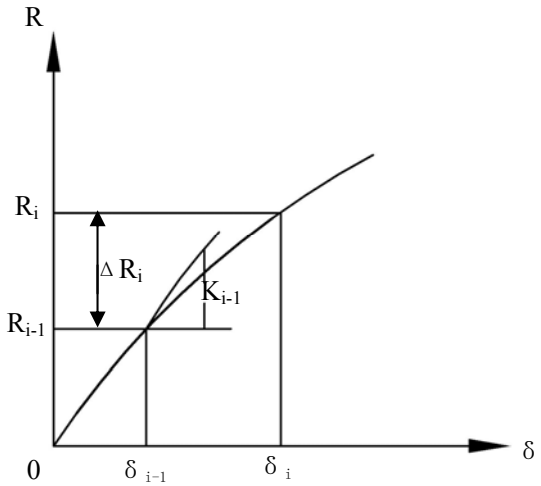

Fig. 3.1 Initial point stiffness method

the displacement increment $\{\Delta\delta_i\}$ of the i^{th} level of load increment could be calculated by following equation:

$$[K_{i-1}]\{\Delta\delta_i\} = \{\Delta R_i\}; (i = 1,2,3\cdots\cdots n) \tag{3.4}$$

where $[K_{i-1}] = [K_{i-1}(\{\delta_{i-1}\})]$

That is to say that the stiffness matrix at the former level of load increment is adopted at the latter level of load increment calculation.

Equations (3.1)-(3.4) are basic equations for the incremental method. The initial stiffness matrix $[K_0]$ can be calculated and determined according to such parameters as the initial elasticity modulus of the stress-strain relationship.

(2) Average stiffness method

The initial stiffness method calculation is relatively simple but the accuracy is not so high. In order to improve the accuracy, the average stiffness method may be adopted. Thus in the calculation for each level we calculate temporary values of $\{\Delta\delta_i'\}$ and $\{\delta_i'\}$ on the basis of $[K_{i-1}]$ using equation (3.4). Then we calculate the stiffness matrix $[K_i]$ at the end of the i^{th} level according to the temporary displacement $\{\delta_i'\}$ and the stress-strain relationship; thus, we may calculate the average stiffness matrix for the i^{th} level as follows:

$$[\overline{K_i}] = \frac{1}{2}([K_{i-1}] + [K_i]) \tag{3.5}$$

The displacement increment for the i^{th} level may then be calculated according to the following equation:

$$[\overline{K_i}]\{\Delta\delta_i\} = \{\Delta R_i\} \tag{3.6}$$

(3) Center point stiffness method

In order to reduce the required memory of the computer, it is feasible to adopt the center point stiffness method. As shown in Fig. 3.2, we first apply half the load increment, i.e, $\{\Delta R_i\}/2$, using the stiffness matrix $[K_{i-1}]$ at the end of the i-1^{th} level, and then we calculate the temporary displacement increment $\{\Delta\delta_{i-\frac{1}{2}}\}$ as follows:

$$[K_{i-1}]\{\Delta\delta'_{i-\frac{1}{2}}\} = \frac{1}{2}\{\Delta R_i\} \tag{3.7}$$

The center point displacement is

$$\{\delta'_{i-\frac{1}{2}}\} = \{\delta_{i-1}\} + \{\Delta\delta'_{i-\frac{1}{2}}\} \tag{3.8}$$

Using the displacement $\{\delta'_{i-\frac{1}{2}}\}$ and the stress-strain relationship we may obtain the center point stiffness matrix $[K_{i-\frac{1}{2}}]$, and therefore the i^{th} level displacement increment $\{\Delta\delta_i\}$ can

be calculated according to the following equation:

$$[K_{i-\frac{1}{2}}]\{\Delta\delta_i\} = \{\Delta R_i\} \tag{3.9}$$

Figure 3.2 also shows the difference between the initial point stiffness method and the center point stiffness method. $[\delta_i]$ in the figure is the displacement calculated with the stiffness matrix $[K_{i-\frac{1}{2}}]$ according to the center point stiffness method; $[\delta_i']$ is the displacement calculated with the stiffness matrix $[K_{i-1}]$ according to the initial point stiffness method. Obviously the accuracy of $[\delta_i']$ is lower than that of $[\delta_i]$. Can we then obtain the same accuracy as the center point stiffness method by halving the load increment? Not exactly. $[\delta_i'']$ in the figure indicates the displacement obtained from the initial point stiffness method by halving the load increment. The calculation has been conducted by the stiffness matrix $[K_{i-\frac{1}{2}}]$. However, due to different initial points, the center point stiffness method uses point *A* as the initial point and the initial point method uses *B* as the initial point, which will improve the accuracy slightly, but still not as well as the center point stiffness method, and the calculation time is almost the same.

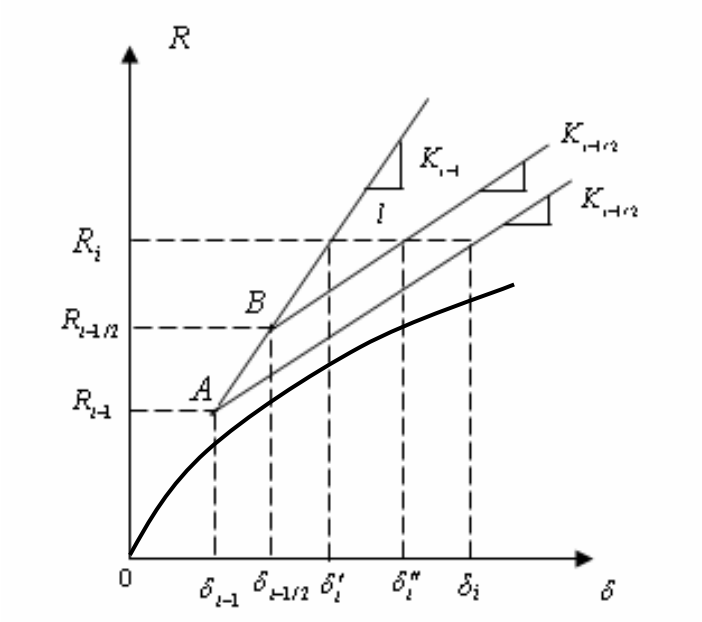

Fig.3.2 Center point stiffness method

3.1.2 Iteration method

When the iteration method is used to solve non-linear problems for prestressed concrete berthing piles, we apply all loads at once and gradually adjust the displacement to meet the requirements of the fundamental equation[5]. There are three calculation methods, i.e., the variable stiffness method, initial stress method and initial strain method:

(1) Variable stiffness method

The concrete non-linear stress-strain relationship can be written as:

$$\{\sigma\} = [D]\{\varepsilon\} \tag{3.10}$$

where the elasticity matrix $[D]$ is not a constant but a function of the strain $\{\varepsilon\}$ and also a function of the displacement $\{\delta\}$, i.e.,

$$[D] = [D(\{\varepsilon\})] = [D\{\delta\}] \tag{3.11}$$

Therefore, the stiffness matrix $[K\{\delta\}]$ is also a function of the displacement $\{\delta\}$.

For non-linear problems, it is required to solve the following non-linear sets of equations:

$$[K(\{\delta\})]\{\delta\} - \{R\} = 0 \tag{3.12}$$

One simple iteration method to solve the above non-linear equation is at first to set the displacement $\{\delta_0\} = \{0\}$. Then from the stress-strain relationship we can get $[K_0] = [K(\{\delta_0\})]$, and further we may obtain the following first order solution for the displacement:

$$\{\delta_1\} = [K_0]^{-1}\{R\}$$

Using $\{\delta_1\}$, we may obtain the secant stiffness matrix $[K_1] = [K(\{\delta_1\})]$, and then we may find the second order solution for the displacement:

$$\{\delta_2\} = [K_1]^{-1}\{R\}$$

Repeating the above steps, an approximate value of the displacement is found using the following equation:

$$\{\delta_n\} = [K_{n-1}]^{-1}\{R\} \tag{3.13}$$

This procedure is used until $\{\delta_n\}$ and $\{\delta_{n-1}\}$ are sufficiently close (refer to Fig 3.3). The characteristics of this calculation method are: All loads $\{R\}$ are applied at each iteration, and all matrices $[K_1]$, $[K_2]$... $[K_{n-1}]$ are secant stiffness matrices.

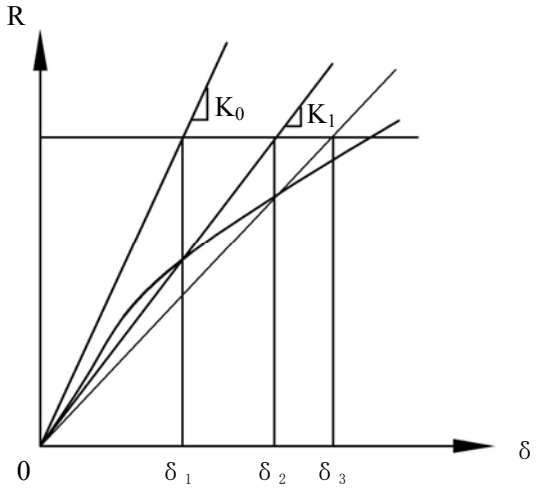

Fig.3.3 Secant stiffness method

The major disadvantage of the variable stiffness method is that the stiffness matrix must be re-calculated and new sets of equations set up for every displacement adjustment. Obviously it is not economical to do this by the direct method. A more effective iteration method is to use the same stiffness matrix for all calculations at every displacement adjustment. But the unbalanced force should be constantly adjusted to obtain a more accurate displacement solution. This is called the initial stress method or the initial strain method.

(2) Initial stress method

Assume that the non-linear stress-strain relationship of the material is

$$\{\sigma\} = f(\{\varepsilon\}) \tag{3.14}$$

The tangent elasticity matrix is $[D_0]$ (Figure 3.4). If calculated according to the linear stress-strain relationship, the elastic stress is

$$\{\sigma_e\} = [D_0]\{\varepsilon\} \tag{3.15}$$

We now introduce the initial stress $\{\sigma_0\}$ in the stress-strain relationship, which makes the stress calculated by the linear relationship equal to the non-linear stress calculated according to Equation (3.14), i.e.

$$\{\sigma\} = [D_0]\{\varepsilon\} - \{\sigma_0\} \tag{3.16}$$

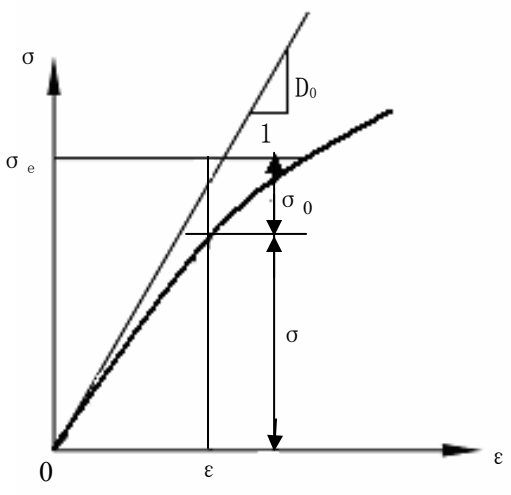

Fig.3.4 Initial stress method

From the above three equations we may see that the initial stress $\{\sigma_0\}$ may be calculated according to the following equations:

$$\{\sigma_0\} = [D_0]\{\varepsilon\} - f(\{\varepsilon\}) = \{\sigma_e\} - \{\sigma\} \tag{3.17}$$

We can then obtain the nodal loads $\{R\}^e_{\sigma_0}$ generated from the initial stress, as follows

$$\{R\}^e_{\sigma_0} = \iint [B]^T \{\sigma_0\} t dx\ dy \tag{3.18}$$

We then add up the nodal loads of the relevant elements around the actual node to get the total nodal load for the initial stress:

$$\{R\}_{\sigma_0} = \sum_e \{R\}^e_{\sigma_0} = \sum_e \iint [B]^T \{\sigma_0\} t dx\, dy \tag{3.19}$$

The calculation steps for analyzing the non-linear problems with the initial stress method are: firstly, use the initial load $\{R_0\}$ and the stiffness matrix $[K_0]$ to calculate the first order solution for the displacement $\{\delta_1\}$;

$$\{\delta_1\} = [K_0]^{-1}\{R_0\} \tag{3.20}$$

From $\{\delta_1\}$ we obtain the stress $\{\varepsilon_1\}$ and then we calculate the initial stress using Equation (3.17):

$$\{\sigma_0\}_1 = [D]\{\varepsilon_1\} - f(\{\varepsilon_1\}) \tag{3.21}$$

And finally the nodal loads by using Equation (3.19) is

$$\{R_{\sigma_0}\}_1 = \sum_e \iint [B]^T \{\sigma_0\}_1 t dx\, dy \tag{3.22}$$

Now we can carry out an adjustment to the displacement, and calculate the first order solution for the displacement increment $\{\Delta\delta_1\}$ with the following equation:

$$\{\Delta\delta_1\} = [K_0]^{-1}\{R_{\sigma_0}\}_1 \tag{3.23}$$

Then a second order solution can be calculated according to following equation:

$$\{\delta_2\} = \{\delta_1\} + \{\Delta\delta_1\} \tag{3.24}$$

From $\{\delta_2\}$ we can get the strain $\{\varepsilon_2\}$ and the stress $\{\sigma_2\} = f(\{\varepsilon_2\})$, then we may calculate the second initial stress $\{\sigma_0\}_2$ by Equation (3.17), the nodal loads generated by the second initial stress by Equation (3.22), and then the second displacement increment $\{\Delta\delta_2\}$.We repeat the above steps until the value of $\{\Delta\delta_n\}$ is very small.

From the above, the equations for the n^{th} calculation are as follows:

$$\{\sigma_0\}_n = [D_0]\{\varepsilon_n\} - f(\{\varepsilon_n\}) \tag{3.25}$$

$$\{R_{\sigma_0}\}_n = \sum_e \iint [B]^T \{\sigma_0\}_n t dx dy \tag{3.26}$$

$$\{\Delta\delta_n\} = [K_0]^{-1}\{R_{\sigma_0}\} \tag{3.27}$$

$$\{\delta_{n+1}\} = \{\delta_n\} + \{\Delta\delta_n\} \tag{3.28}$$

$$\{\varepsilon_{n+1}\} = [B]\{\delta_{n+1}\} \tag{3.29}$$

$$\{\sigma_{n+1}\} = f(\{\delta_{n+1}\}) \tag{3.30}$$

From this we can see that when carrying out the iterations with the initial stress, the initial stress $\{\sigma_0\}_n$ is determined by the difference between the actual stress $\{\sigma_n\}$ and the elastic stress $[D_0]\{\varepsilon_n\}$, then another adjustment is made to make the displacement

further approach the true value. The iteration process is shown as in Fig 3.5. $\{R_{\sigma_0}\}_n$ is the unbalanced force of a node, which can be used to evaluate the error in the calculation process. Since the same stiffness matrix is adopted in every calculation, thus, when using the direct method we only need to decompose the stiffness matrix once, and we can conduct simple back substitution in all calculations later, which is relatively simple. If the non-linearity of the stress-strain relationship is not too strong, the stiffness matrix can be changed after the first calculation, and in all later calculations, $[K_1]$ can be used to replace $[K_0]$ to speed-up the convergence rate of the calculation.

(3) Initial strain method

The stress of certain problems, such as creep，can not be expressed by strain as in Equation (3.14). Instead, the stress can be used to express the strain or the strain increments

$$\{\varepsilon\} = f(\{\sigma\}) \tag{3.31}$$

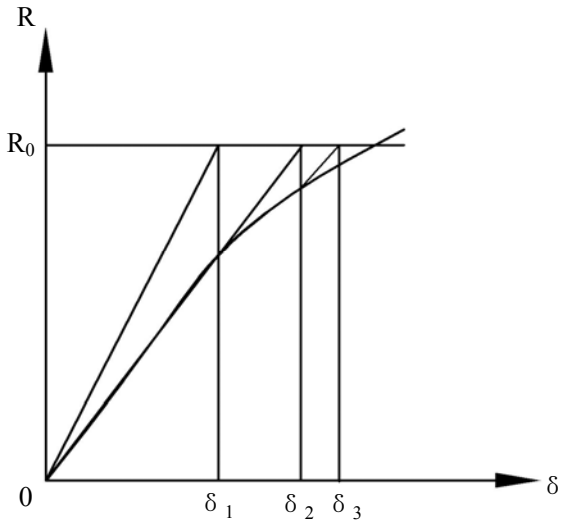

Fig. 3.5 Initial stress method iteration calculation

The elasticity stress-strain relationship is

$$\{\varepsilon_e\} = [D]^{-1}\{\sigma\} \tag{3.32}$$

We now introduce an initial strain $\{\varepsilon_0\}$ in the stress-strain relationship (Fig. 3.6). This makes the strain calculated by the linear relationship equal to the non-linear strain calculated by equation (3.31). Thus

$$\{\varepsilon\} = [D]^{-1}\{\sigma\} + \{\varepsilon_0\} \tag{3.33}$$

From the above equations we find that the initial strain $\{\varepsilon_0\}$ can be calculated according to the following equation:

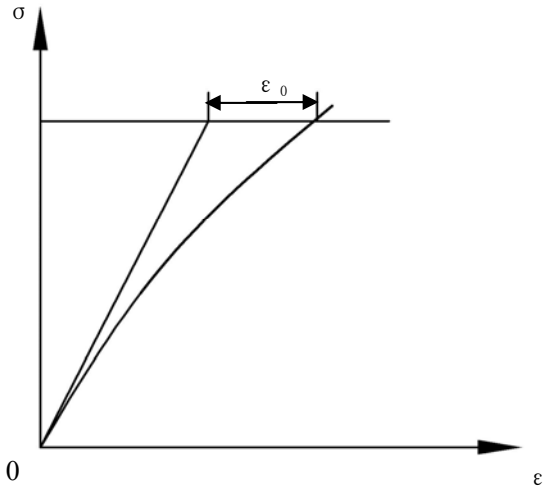

Fig.3.6 Initial strain method

$$\{\varepsilon_0\} = \{\varepsilon\} - [D]^{-1}\{\sigma\} = f(\{\sigma\}) - [D]^{-1}\{\sigma\} \tag{3.34}$$

The nodal load from the initial strain is

$$\{R_{\varepsilon_0}\}^e = \iint [B]^T [D]\{\varepsilon_0\} t dx dy \tag{3.35}$$

If we integrate the elements around the node, we can obtain the nodal load generated by the initial strain:

$$\{R_{s_0}\} = \sum_e \iint [B]^T [D]\{\varepsilon_0\} t dx dy \tag{3.36}$$

The calculation procedure of analyzing non-linear problem with the initial strain method is similar to the initial stress method, that is, a first order of solution for the displacement is calculated with the initial load $\{R_0\}$ and stiffness matrix $[K_0]$:

$$\{\delta_1\} = [K_0]^{-1}\{R_0\} \tag{3.37}$$

Then the stress $\{\sigma_1\}$ is calculated with $\{\delta_1\}$. The initial strain $\{\varepsilon_0\}$ is calculated with Equation (3.34) as well as the nodal load $\{R_{s_0}\}_1$ generated by the initial strain is calculated with Equation (3.36). Then the displacement is adjusted and the first order of the displacement increment is calculated according to the following equation:

$$\{\Delta\delta_1\} = [K_0]^{-1}\{R_{s_0}\}_1 \tag{3.38}$$

We repeat the above calculation until the value of $\{\Delta\delta_n\}$ is sufficiently small.

3.1.3 Mixed method

As shown in Fig. 3.7, we simultaneously apply the incremental method and iteration method to divide the load increment into several increments with smaller values, and then carry out iteration calculations for each level of the load increment.

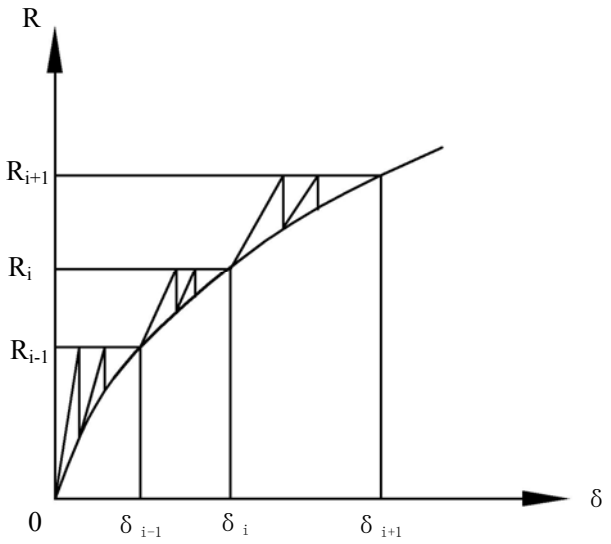

Fig.3.7 Mixed method

In all the above calculation methods, the advantages of the incremental method are the wide application range, large versatility and ability to provide the whole process of the load-displacement variation. The disadvantages are that this method takes more computing time than that of the iteration method, and we have no idea how much the difference is between the approximate solution and the true solution. The iteration method has relatively less calculation effort compared to the incremental method and is able to control calculation accuracy; however, it is unable to give the whole process of load-displacement and is limited in certain application ranges. For instance, when deformation characteristics of the material are related to the load-applying process (loading and unloading isomerism), dynamic questions, etc., the iteration method can not be used. The mixed method has the advantages of both the incremental method and the iteration method. For a calculation of every load increment, the degree of approximation can be estimated by using iteration, which gives a better accuracy but larger calculation effort. After a comprehensive consideration of the characteristics of all the above calculation methods, this thesis has adopted the incremental method to calculate the non-linear whole process for pre-stressed concrete berthing piles.

3.1.4 Treatment after cracking or other damage of concrete element[3].

During the non-linear whole process of analytical computation, phenomena such as cracking due to tension or failure from pressure may occur in a concrete element. The following two conditions should be first formulated before solving these two problems:

(1) criterion of cracking or failure;

(2) determination of the concrete performance after cracking or failure.

Secondly, we have to conduct a non-linear computation after cracking. The closer the above conditions are processed to the actual performance of the material, the closer the results of the computation to the actual stress.

1. Treatment of tensile cracks in a concrete element

The concrete will crack when the principal tensile stress or the principal tensile strain applied to the concrete unit reaches the cracking condition. After cracking, we assume that no tensile force can be transferred in the direction that is perpendicular to the crack direction (i.e.we do not consider the descending branch of the tensile stress-strain curve), thus the related process can be performed. The cases of unidirectional tensile and unidirectional compression and bi-directional tension are given below.

(1) Unidirectional tension and unidirectional compression

When the maximum principal tensile stress σ_1 or the principal tensile strain ε_1 in the element does not reach the cracking conditions, no processing is required except for an adjustment to the stiffness matrix [K] according to the stress increment.

When the maximum principal tensile stress σ_1 or the principal tensile strain ε_1 in the element reaches cracking conditions, the processing is as follows:

Adjust σ_1 to zero along the σ_1 direction of cracking. Since the stress in the element is unbalanced, we need to convert the unbalanced stress into nodal forces, which will be redistributed again in the structure to obtain a new balance. These forces can be added together with the next load increment level for computation.

In the direction of σ_2, the element is normally in unidirectional compressed state after σ_1 is adjusted to zero, which is different from the situation before cracking, where one direction is under tension and one under compression, thus the compressive stress should be relatively adjusted. That is to say, the compressive strain ε_2 is taken as the original value, but the stress is evaluated by the uniaxial stress-strain relational expression, which is here taken to be:

$$\sigma_{2u} = \frac{E_0 \varepsilon_2}{1 + \left[\frac{E_0}{E_\varepsilon} - 1\right]\frac{\varepsilon_2}{\varepsilon_c} + \left(\frac{\varepsilon_2}{\varepsilon_c}\right)^2} \tag{3.39}$$

The difference $\sigma_{2,ex}$ between the original stress σ_2 and the adjusted stress σ_{2u} is converted into nodal forces for redistribution.

$$\sigma_{2,ex} = \sigma_2 - \sigma_{2u}$$

Here, we take the triangular element (Fig.3.8) as an example to illustrate the computation method for the force conversion.

(a) Convert the excess stress of the two parts to the x, y-system of coordinates;

$$\begin{Bmatrix}\sigma_x\\ \sigma_y\\ \tau_{xy}\end{Bmatrix}=\begin{bmatrix}c^2 & s^2\\ s^2 & c^2\\ sc & -sc\end{bmatrix}\begin{Bmatrix}\sigma_1\\ \\ \sigma_2\end{Bmatrix}_{ex} \tag{3.40}$$

where c and s indicate cosθ and sinθ, respectively,

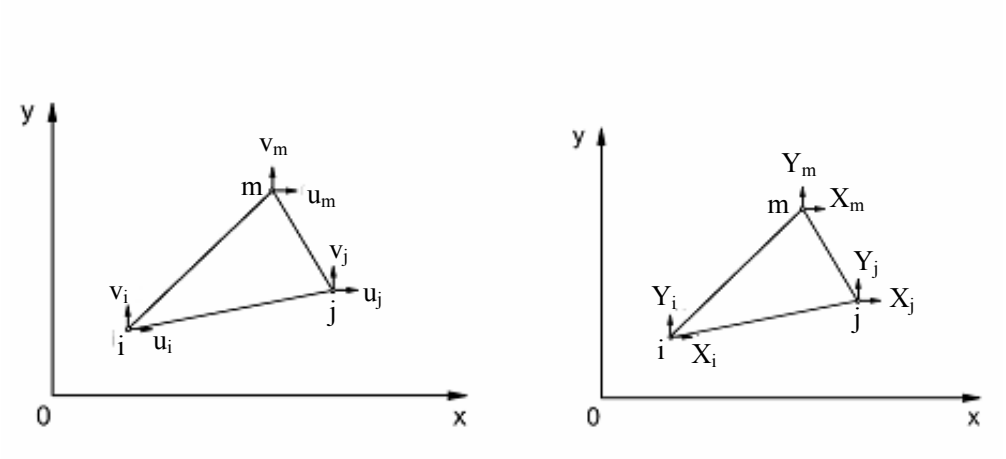

(a) Nodal displacements (b) Nodal forces

Fig.3.8 Nodal displacements and forces

$$\sigma_{1,ex}=\sigma_1$$

$$\sigma_{2,ex}=\sigma_2-\sigma_{2u}$$

(b) Compute the nodal forces:

$$\{F\}^e=[K]\{\delta\}^e=[B]^T[D][B]t\Delta\{\delta\}^e=[B]^T\{\delta\}t\Delta \tag{3.41}$$

in which

$$[K]=[B]^T[D][B]t\Delta$$

$$\{\delta\}=[D][B]\{\delta\}^e$$

Here Δ is the area of the triangle *i,j,m* (Fig.3.8); *t* is thickness of the element.

(c) Convert the remainder major stress in the *x, y*-system to be superimposed with the stress caused by the lower level load increment, where the partial stress in the element is converted into the nodal forces,

$$\begin{Bmatrix}\sigma_x\\ \sigma_y\\ \tau_{xy}\end{Bmatrix}=\begin{bmatrix}c^2 & s^2\\ s^2 & c^2\\ sc & -sc\end{bmatrix}\begin{Bmatrix}0\\ \\ \sigma_{2u}\end{Bmatrix} \tag{3.42}$$

(d) At this time, the tangent modulus in the σ_1 direction is $E_{1b}^{'}=0$, which indicates that no more tension is borne in this direction. The tangent modulus $E_{2b}^{'}$ in the σ_2 direction

is computed according to the uniaxial stress-strain formula. We use values $E_{1b}^{'}$ and $E_{2b}^{'}$ to substitute $[D^{'}]$ in the elastic-plastic stress-strain increment and in the strain increment formula to evaluate the element stiffness matrix [K] during the computation of the next level of load increment.

(2) Bi-directional tension

(a) If the maximum principal tensile stress σ_1 or the maximum principal strain ε_1 does not reach cracking conditions, no special process is necessary except to adjust the stiffness matrix [K].

(b) If the maximum principal tensile stress σ_1 or the maximum principal tensile strain ε_1 reaches the cracking conditions, set σ_1=0, and convert σ_1 into nodal forces, and then the excess stress is

$$\{\sigma\}_{ex} = \begin{Bmatrix} \sigma_{1,ex} \\ \sigma_{2,ex} \end{Bmatrix} = \begin{Bmatrix} \sigma_1 \\ 0 \end{Bmatrix}$$

Substitute into equation (3.41) to calculate the nodal forces. The stress remaining in the element is zero in the σ_1 direction, and the original stress value is kept unchanged in the σ_2 direction:

$$\{\sigma\} = \begin{Bmatrix} \sigma_1 \\ \sigma_2 \end{Bmatrix} = \begin{Bmatrix} 0 \\ \sigma_2 \end{Bmatrix}$$

Substitute into equation (3.42) to evaluate the stress value that has been converted into the x, y-system. When evaluating the element stiffness matrix, use $E_{1b}^{'} = 0$ to substitute matrix $[D^{'}]$ for adjustment.

(c) If the σ_2 stress reaches the cracking condition later, also convert the σ_2 into the nodal forces, and then the excess stress is

$$\{\sigma\}_{ex} = \begin{Bmatrix} \sigma_{1,ex} \\ \sigma_{2,ex} \end{Bmatrix} = \begin{Bmatrix} 0 \\ \sigma_2 \end{Bmatrix}$$

which can be substituted into equation(3.41) to obtain the nodal forces. The stress in the element is zero. $E_{1b}^{'} = E_{2b}^{'} = 0$, i.e., the element stiffness matrix [K] = [0].

(d) If σ_1 and σ_2 reach the cracking condition simultaneously, the excess stress is

$$\{\sigma\}_{ex} = \begin{Bmatrix} \sigma_{1,ex} \\ \sigma_{2,ex} \end{Bmatrix} = \begin{Bmatrix} \sigma_1 \\ \sigma_2 \end{Bmatrix}$$

which can be substituted into equation (3.41) to obtain the nodal forces. The element stress is zero. $E_{1b}^{'} = E_{2b}^{'} = 0$. [K] = [0].

2. Treatment of the element after compression damage

(1) Bi-directional compressed element

If both the maximum principal stress σ_2 or the maximum principal strain ε_1 do not reach the cracking condition, no special treatment is necessary (except to adjust [k]) .

When both the maximum principal stress σ_2 and the maximum principal strain ε_1 reach the cracking condition, this element is regarded as completely damaged and can carry no further external force. Here, we convert all stresses into the nodal forces, which will be redistributed within the whole component, then the excess stress is

$$\{\sigma\}_{ex} = \begin{Bmatrix} \sigma_{1,ex} \\ \sigma_{2,ex} \end{Bmatrix} = \begin{Bmatrix} \sigma_1 \\ \sigma_2 \end{Bmatrix}$$

which is substituted into equation (3.41) to obtain the nodal forces. All stresses in the unit are zero. $E_{1b}^{'} = E_{2b}^{'} = 0$, [K] = [0].

(2) Unidirectional tensile and unidirectional compression

Generally, a crack in this element occurs first in the tensile direction, then this element is considered to be completely damaged and not able to sustain any external force. Convert the stress in the element into the nodal forces for redistribution and the excess stress of the element is

$$\{\sigma\}_{ex} = \begin{Bmatrix} \sigma_{1,ex} \\ \sigma_{2,ex} \end{Bmatrix} = \begin{Bmatrix} 0 \\ \sigma_2 \end{Bmatrix}$$

which is substituted into equation (3.41) to obtain the nodal forces. All stresses in the element are zero. $E_{1b}^{'} = E_{2b}^{'} = 0$, [K] =[0].

3.2 Structural dynamics analysis method

3.2.1 General description

Structural dynamics is the science that studies dynamic properties of a structural system and the dynamic response analysis principles and methods under dynamic load. The target is to provide a solid theoretical foundation for improving the safety and reliability of an engineering structural system in a dynamic environment.

In the 18th century, dynamic mechanisms were widely applied in different engineering structures and had impelled the generation of structural dynamics. In the 19th century, steam engines were used in propulsion system of ships, assisting in the development in size and speed, but also causing vibration problems. In 1892, A. A. Yerrow presented a calculation method to reduce ship vibrations due to the unbalanced forces of steam engines[6]. In 1979, a British scholar, R. E. Bishop presented a water-ship elasticity theory

based on fluid-solid coupling, using modal analysis technology, and this method has been used as an effective tool in calculating impact vibrations and the systematic vibration response of large marine structures.

Development in the aerospace and aviation industry has pushed forward the non-linear dynamic calculation theory, since here, the recovery force of a system is a non-linear function of the special location of the system, and the damping force is a non-linear function of the system's movement or vibrating velocity; thus, only a very few low-dimensional non-linear vibration equations provide analytic solutions and most equations only provide approximate solutions. For high-dimensional problems, a numerical calculation method [7][8] is most often used, such as the Runge-Kutta method, Wilson θ method or the Newmark β method, etc..

Since the 1960's, the development of the theory of calculation based upon the finite element method has enabled us to carry out dynamic analysis of large and complicated structural systems which contain thousands of degrees of freedom, such as the vibrations of deep-sea drilling platforms and non-linear vibration responses in the aerospace and aviation industry, etc..

Structural dynamics deal with a variety of subjects. For our specific research purpose, only relevant theories related to the berthing pile calculation are introduced in following text. First we will introduce a general vibration equation for a multiple degrees of freedom system; secondly, we will illustrate two solutions for the berthing pile vibration response as a multiple-step parameter system: the direct method (partial differential equation) and the natural mode of the vibration method, and finally we give a brief introduction to the principles of the calculation method adopted.

3.2.2 General form of vibration equation in a system with multiple degrees of freedom

There are two ways of setting up a systematic displacement equation for a multiple degrees of freedom system: the dynamic balance method based upon d'Alembert's principle and the Lagrange method based upon the energy principle. In the following derivation, a direct balance principle in the dynamic balance method is adopted. According to d'Alembert's principle, the system is subjected to four forces, i.e. disturbing force, inertial force, damping force and elastic restoring force. Their stress components should be balanced for every generalized coordinate of the system[9][10]. According to this relationship, the inertial force will be applied on every generalized coordinate, which will convert the original dynamic problem to a static problem in analytical form; thus, we can list the balance equation of force by using statics, and this method is called the direct balance method.

For the i^{th} generalized coordinate, the above mentioned four forces are, respectively, $P_i(t), f_{Ii}(t), f_{Di}(t)$ and $f_{Si}(t)$, and then the dynamic equation is

$$f_{Ii} + f_{Di} + f_{Si} = P_i(t) \qquad (i = 1,2,....n)$$

where $P_i(t)$ is the disturbing force related to the i^{th} generalized coordinate; $f_{Ii}(t)$ is the inertial force related to the i^{th} generalized coordinate; $f_{Di}(t)$ is the damping force related to

the i^{th} generalized coordinate; $f_{Si}(t)$ is the elastic restoring force related to the i^{th} generalized coordinate.

For the n^{th} degrees of freedom structural system, the balance relationship of force can be expressed as

$$F_I + F_D + F_S = P(t) \tag{3.43}$$

where F_I is the inertial force matrix; F_D is the damping force matrix; F_S is the elastic force matrix and $P(t)$ is the disturbing force matrix.

The elastic restoring force matrix of a vibrating system is proportional to the vibrating displacement. Assume the displacement vector of the system is

$$x = [x_1 \quad x_2 \quad x_3 \quad \dots \quad x_n]^T \tag{3.44}$$

Then

$$F_S = K x \tag{3.45}$$

where K is the stiffness matrix of the structure, a matrix of form $n \times n$, and its elements K_{ij} are called the stiffness coefficients. K_{ij} is defined as the elastic restoring force generated at the i^{th} coordinate when the unit displacement occurs at the j^{th} coordinate (other displacements are all zero). Assume the damping of the system to be viscous or to be simplified as an equivalent viscous damping; then the damping is proportional to the velocity $\dot{x}$, i.e.

$$F_D = C \dot{x} \tag{3.46}$$

where C is the damping coefficient matrix, its elements C_{ij} are the damping coefficients, and are defined when a unit velocity occurs at the j^{th} coordinate the damping force C_{ij} is generated at the i^{th} coordinate. $\dot{x}$ indicates the generalized vibrating velocity matrix, i.e. $\dot{x} = [\dot{x}_1 \quad \dot{x}_2 \quad \dots \quad \dot{x}_n]^T$.

The inertial force is proportional to the acceleration vector $\ddot{x}$, i.e.

$$F_I = M \ddot{x} \tag{3.47}$$

where M is the mass matrix, its elements M_{ij} are called the mass coefficients and are defined as the inertial force generated at the i^{th} coordinate when a unit acceleration occurs at the j^{th} coordinate; $\ddot{x}$ is the generalized acceleration matrix $\ddot{x} = [\ddot{x}_1 \quad \ddot{x}_2 \quad \dots \quad \ddot{x}_n]^T$.

Substitute equations (3.45)~ (3.47) into equation (3.43) to obtain the general form of the vibration equation for a n- degrees of freedom system, i.e.

$$M \ddot{x} + C \dot{x} + Kx = P(t) \tag{3.48}$$

3.2.3 Vibration of continuous system

The vibration response analysis obtained from vibration equation (3.48) is only an approximate solution for the dynamic response of an actual structural system, because in fact an actual structure has a distributed mass which means that it is a continuous system.

The prestressed concrete berthing pile is such a system. To describe any transient position of an elastic system, infinite generalized coordinates are needed and this is called the infinite degree of freedom system. Currently, there are two ways to solve the vibration problem of an infinite degree of freedom system: one is to set up a partial differential equation for the elastic system to obtain an accurate solution for vibration, and the other is to adopt the approximate method to convert the infinite degrees of freedom system into the finite degrees of freedom system, and then obtain the solution according to the multiple degrees of freedom method.

3.2.3.1 Direct method (partial differential equation)

Consider the beam shown in Fig. 3.9 (a), assume that the bending stiffness is EI , and that the mass per unit length, denoted by m is constant. The vertical load and vertical displacement are continuous functions of the coordinate and time, denoted by $p(x,t)$ and $y(x,t)$, respectively. For a convenient derivation, consider first the simplest condition and assume that both ends are simply supported. In general the solution will of course depend on the boundary conditions.

Take a beam element dx at a point in a distance of x from the left support, and draw out the forces acting on the beam element, including the inertial force and disturbing force, as shown in Fig. 3.9(b). According to d'Alembert's principle, the beam element is in a dynamic balanced state. By expressing the balance equation of the vertical force of an element *dx*, we get

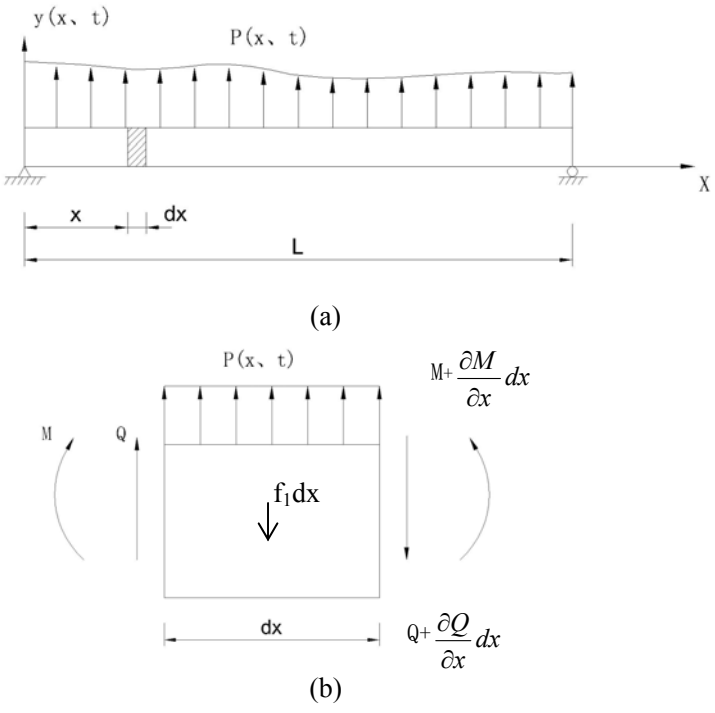

Fig. 3.9 Direct method

$$Q + pdx - (Q + \frac{\partial Q}{\partial x}dx) - f_1 dx = 0 \tag{3.49}$$

Here f_1 is the inertial force per unit length, and the total inertial force on the element is

$$f_1 dx = mdx\frac{\partial^2 y}{\partial t^2} \tag{3.50}$$

According to well-known mechanics, the relationship between the bending moment and the shear force is $Q = \frac{\partial M}{\partial x}$, which can be substituted into equation (3.49). Hence, we obtain

$$\frac{\partial^2 M}{\partial x^2} + m\frac{\partial^2 y}{\partial t^2} = p(x,t) \tag{3.51}$$

Then the relationship between the bending moment and the curvature should be taken into consideration. Thus the vibration equation in the simplest situation considering only the bending is

$$\frac{\partial^2}{\partial x^2}(EI\frac{\partial^2 y}{\partial x^2}) + m\frac{\partial^2 y}{\partial t^2} = p(x,t) \tag{3.52}$$

The berthing pile bears the resistance from the external damping force generated by the surrounding environment, for instance, the vibration displacement of the submersed pile body suffers from water damping stress, the vibration process of the buried pile body suffers resistance from the soil around the pile body, and in the mean time, all layers of fibers on a section of the pile deform repeatedly with certain velocity, and cause internal damping stress distributed along sectional height. When setting up the vibration equation in theory, the effects on the dynamic response from external/internal damping stress to the pile body should be considered.

The external damping force is proportional to the vibration speed, i.e. $f_D = c(x)\frac{\partial y}{\partial t}$

When this is added into equation (3.52) we obtain

$$\frac{\partial^2}{\partial x^2}(EI\frac{\partial^2 y}{\partial x^2}) + m\frac{\partial^2 y}{\partial t^2} + c\frac{\partial y}{\partial t} = p(x,t) \tag{3.53}$$

The damping stress σ_D related to the internal damping stress is correlated to the strain velocity of the material, and this damping stress is

$$\sigma_D = c_S\frac{\partial \varepsilon}{\partial t} \tag{3.54}$$

Here c_S is a strain damping coefficient; ε is the strain in the beam at any point. Assume that this stress has a linear variation along the section, then this damping stress leads to a damping bending moment

$$M_D = \int_A \sigma_D z dA = c_S I(x)\frac{\partial^2 y}{\partial x\ \partial t} \tag{3.55}$$

Here z is the distance between any point on the section and the neutral axis; A indicates the sectional area.

Thus, in theory, the bending vibration equation is

$$\frac{\partial^2}{\partial x^2}(EI\frac{\partial^2 y}{\partial x^2}+c_S I\frac{\partial^2 y}{\partial x\partial t})+m\frac{\partial^2 y}{\partial t^2}+c\frac{\partial y}{\partial t}=p(x,t) \tag{3.56}$$

For equation (3.56), it is necessary to carry out a correction regarding load properties applied to the prestressed concrete berthing pile. In the actual structure, the service load on the pile is a low-speed impact load, which can be expressed by a transient pulse under impact load. The structural maximum response can be reached in a very short time. Prior to this, the external damping of the structure does not absorb enough vibration energy; therefore, when calculating the impact load from a ship, the influence of the external damping can be omitted. Among the internal damping influence factors, the mass damping has little influence on the calculation. However, the influence of the material damping on the final calculated result must not be omitted. From the above, the bending vibration equation of the berthing pile, considering the damping factors and load properties, is

$$\frac{\partial^2}{\partial x^2}(EI\frac{\partial^2 y}{\partial x^2}+c_S I\frac{\partial^2 y}{\partial x\partial t})+m\frac{\partial^2 y}{\partial t^2}=p(x,t) \tag{3.57}$$

This partial differential equation can be solved under the simple boundary conditions to get the dynamic response.

3.2.3.2 Response solution method based upon natural mode of vibration method [11]

For non-damping vibration in a multiple degrees of freedom system, the acting force vector and damping vector in equation (3.48) can be eliminated to obtain matrix equation

$$M\ddot{x}+Kx=0 \tag{3.58}$$

Thus for the free vibration, we can get solutions for (3.58) in the following form:

$$x_j=e_j\sin(\omega t+\alpha) \qquad j=1,2,3\cdots,\ n \tag{3.59}$$

Here ω is an unknown fixed frequency and e_i is the vibration amplitude at an arbitrary point. When substituting (3.59) into (3.58), notice that $\sin(\omega t+\alpha)$ is common for all teams and that, for a particular solution, it must not be zero at all times, therefore

$$(K-M\omega^2)e=0 \tag{3.60}$$

To obtain other solution than $e=0$, the determinant of the matrix coefficient for e must be zero, i.e.

$$\det\left|K-M\omega^2\right|=0 \tag{3.61}$$

By solving the set of equations given in equation (3.61), we obtain n positive real roots of ω^2.

Assume that the characteristic value and the characteristic vectors have been determined. Then for any two different modes, expressed by a lower index r or s, the solution can be written as:

$$K_r e = M\omega_r^2 {}_r e \tag{3.62}$$

and
$$K_s e = M\omega_s^2 {}_s e \tag{3.63}$$

The transposed equation of (3.62) is

$$(K_r e)^T = \omega_r^2 (M_r e)^T$$

or
$${}_r e^T K = \omega_r^2 {}_r e^T M \tag{3.64}$$

Notice that ω_r^2 is a symmetric matrix. If ${}_s e$ is multiplied after equation (3.64) and ${}_r e^T$ is multiplied before equation (3.63), we obtain

$${}_r e^T K_s e = \omega_r^2 {}_r e^T M_s e$$

and
$${}_r e^T K_s e = \omega_s^2 {}_r e^T M_s e$$

Subtract the above two equations and get:

$$(\omega_s^2 - \omega_r^2)_r e^T M_s e = 0$$

Since for different modes we have $\omega_s \neq \omega_r$, thus we get the quadratic condition

$${}_r e^T M_s e = 0 \tag{3.65}$$

Or written in full length

$$\begin{bmatrix} {}_r e_1 & {}_r e_2 & \cdots & {}_r e_n \end{bmatrix} \begin{bmatrix} m_{11} & m_{12} & \cdots & m_{1n} \\ m_{21} & m_{22} & \cdots & m_{2n} \\ \cdots & \cdots & \cdots & \cdots \\ m_{n1} & m_{n2} & \cdots & m_{nn} \end{bmatrix} \begin{bmatrix} {}_s e_1 \\ {}_s e_2 \\ \cdots \\ {}_s e_n \end{bmatrix} = 0$$

For a diagonal mass matrix, i.e., when $m_{ij} = 0$ for $i \neq j$, the above equation is converted into

$${}_r e_1 m_{11s} e_1 + {}_r e_2 m_{22s} e_2 + \cdots + {}_r e_n m_{nns} e_n = 0$$

Introducing the vector

$${}_r z = (\frac{1}{a_r})_r e \tag{3.66}$$

where a_r is a scalar, we find
$${}_r z^T M_r z = 1 \tag{3.67}$$

If the vector ${}_r z$ is normalized vector, we may define a matrix Z, in which the r^{th} column

is the vector ${}_r z$, thus

$$Z = \begin{bmatrix} {}_1z_1 & {}_2z_1 & \cdots & {}_nz_1 \\ {}_1z_2 & {}_2z_2 & \cdots & {}_nz_2 \\ \cdots & \cdots & \cdots & \cdots \\ {}_1z_n & {}_2z_n & \cdots & {}_nz_n \end{bmatrix} \tag{3.68}$$

After rewriting equation (3.60) may be written

$$KZ = MZ\Omega \tag{3.69}$$

Here Ω is diagonal:

$$\Omega = \begin{bmatrix} \omega_1^2 & 0 & \cdots & 0 \\ 0 & \omega_2^2 & \cdots & 0 \\ \cdots & \cdots & \cdots & \cdots \\ 0 & 0 & \cdots & \omega_N^2 \end{bmatrix} \tag{3.70}$$

From equations (3.65), (3.68) and (3.69), we get

$$Z^T MZ = I \tag{3.71}$$

After multiplying equation (3.69) with Z^T, and using equation (3.71), we obtain

$$Z^T KZ = \Omega \tag{3.72}$$

Then we introduce the transformation equation

$$x = Zq \tag{3.73}$$

This coordinate transformation transform from x to the master coordinate q. Substituting into the non-damping free vibration equation (3.58), we get

$$MZ\ddot{q} + KZq = 0 \tag{3.74}$$

Multiplying equation (3.74) with Z^T, and using equation (3.71) and (3.72), we obtain

$$\ddot{q} + \Omega q = 0 \tag{3.75}$$

Equation (3.75) renders *n* non-coupled equations of the form

$$\ddot{q}_r + \omega_r^2 q_r = 0 \qquad r = 1,2,3,...n \tag{3.76}$$

The solutions of these equations are

$$q_r = A_r \sin \omega_r t + B_r \cos \omega_r t \tag{3.77}$$

Here the coefficients A and B are determined by the initial conditions, and the complete solution for non-damping free vibration x_j of the multiple degrees of freedom system under given initial conditions, is

$$x_j = \sum_{r=1}^{n} {}_r z_j (A_r \sin \omega_r t + B_r \cos \omega_r t) \qquad j = 1,2,3....,n \tag{3.78}$$

To take into account the influence of damping and external forces in the actual general system the adoption of the coordinate transformation (3.73) in the general equation (3.48)

$$M\ddot{x}+C\dot{x}+Kx=P(t)$$

by multiplication with Z^T must lead to non-coupled equations. Thus it is obvious that the Z^TCZ must be diagonal. However, this condition can not be met in general, and we have to give the damping matrix a restricting condition. It may be assumed that the damping matrix is a linear combination of the mass matrix and the stiffness matrix, i.e.

$$C=\lambda_m M+\lambda_k K \tag{3.79}$$

where λ_m,λ_k are two constants.

For an actual structure, small damping in an elastic structure can be expressed in an approximate way, and in this case it is usual and reasonable to assume that C is proportional to K.

Substitute (3.79) into equation (3.48), multiply the equation obtained with Z^T, consider (3.71) and (3.72) at the same time, and obtain

$$\ddot{q}+\lambda_m\dot{q}+\lambda_k\Omega\dot{q}+\Omega q=Z^TP(t) \tag{3.80}$$

This represents n non-coupled equations as follows:

$$\ddot{q}_r+(\lambda_m+\lambda_k\omega_r^2)\dot{q}+\omega_r^2q_r=\sum_{j=1}^{n}{}_rz_jP_j(t)\qquad r=1,2,3,...,n \tag{3.81}$$

Assuming the all initial conditions are zero, then by using the Duhamel integral, the solution of equation (3.81) may be written:

$$q_r=\frac{1}{\omega_r^1}\int_0^t f_r(\tau)\exp[-\gamma_r\omega_r(t-\tau)]\sin\omega_r^1(t-\tau)d\tau \tag{3.82}$$

where $\omega_r^1=\omega_r(1-\gamma_r^2)^{\frac{1}{2}}$, $2\gamma_r\omega_r=\lambda_m+\lambda_k\omega_r^2$ and $f_r(t)=\sum_{j=1}^{n}{}_rz_jP_j(t)$

Using finally the coordinate transformation (3.73), assuming $P_j(0)=0$ and using integration by parts to equation (3.82), we get

$$q_r=\frac{{}_rz_jP_j(t)}{\omega_r^2}-\frac{{}_rz_j}{\omega_r^2}\int_0^t\dot{P}_j(\tau)\exp[-\gamma_r\omega_r(t-\tau)][\cos\omega_r^1(t-\tau)+\frac{\gamma_r\omega_r}{\omega_r^1}\sin\omega_r^1(t-\tau)]d\tau \tag{3.83}$$

$$x_s=\sum_{r=1}^{n}{}_rz_sq_r \tag{3.84}$$

Expression (3.84) is the analytical solution for the response of a multiple degrees of freedom system under transient load.

3.2.3.3 Numerical analysis method for dynamics

Among the variety of numerical analysis methods for dynamics, the most often used algorithms are the central difference method, the Newmark-β method, and the Wilson-θ method [12][13]. Since the Newmark-β method is normally the one used in finite element programs, only this method is introduced in the following.

For easy description, we rewrite the basic equation of motion (3.48) with the unknown displacement u in the form;

$$M\ddot{u} + C\dot{u} + Ku = P(t) \tag{3.85}$$

According to the Lagrange mean value theorem, we express the velocity vector at $t + \Delta t$ as

$$\dot{u}_{i+1} = \dot{u}_i + \ddot{u}_i^* \, \Delta t$$

Here $\ddot{u}_i^*$ is a value of the acceleration vector $\ddot{u}$ located at a certain point within the time segment $(t, \Delta t)$ .The Newmark-β method assumes approximately $\ddot{u}_i^* = (1-\delta)\ddot{u}_i + \delta\ddot{u}_{i+1}$, and then the velocity at the time $t + \Delta t$ is

$$\dot{u}_{i+1} = \dot{u}_i + (1-\delta)\ddot{u}_i \Delta t + \delta\ddot{u}_{i+1}\Delta t \tag{3.86}$$

The displacement at time t+ Δ t is in the Newmark-β method written as

$$u_{i+1} = u_i + \dot{u}_i \Delta t + [(\frac{1}{2} - \beta)\ddot{u}_i + \beta\ddot{u}_{i+1}]\Delta t^2 \tag{3.87}$$

In the equations, δ, β are parameters related to precision and stability. When δ >1/2, algorithm damping and artificial attenuation of vibration amplitudes are produced. When δ <1/2, negative damping is generated, the vibration amplitude gradually increases during the calculation process. Usually we use the critical value δ =1/2. The values δ =1/2, $\beta = 0$ is the central difference method; $\beta = 1/4$ is the average acceleration method; $\beta = 1/6$ gives the linear acceleration method.

The equation of motion which must be satisfied at tine step $t + \Delta t$, (i+1), is

$$M\ddot{u}_{i+1} + C\dot{u}_{i+1} + Ku_{i+1} = P(t)_{i+1} \tag{3.88}$$

First we use equation (3.87) to get $\ddot{u}_{i+1}$, expressed by u_{i+1}

$$\ddot{u}_{i+1} = \frac{1}{\beta\Delta t^2}(u_{i+1} - u_i) - \frac{1}{\beta\Delta t}\dot{u}_i - (\frac{1}{2\beta} - 1)\ddot{u}_i \tag{3.89}$$

Substituting this into (3.86), we get

$$\dot{u}_{i+1} = \frac{\delta}{\beta\Delta t}(u_{i+1} - u_i) + (1 - \frac{\delta}{\beta})\dot{u}_i + (1 - \frac{\delta}{2\beta})\ddot{u}_i\Delta t \tag{3.90}$$

Substituting (3.89)and (3.90) into (3.85), we obtain

$$K^* u_{i+1} = P_{i+1}^* \tag{3.91}$$

Here $K^* = K + \frac{1}{\beta\Delta t^2}M + \frac{\delta}{\beta\Delta t}C$

$$P_{i+1}^{*} = P_{i+1} + M\left[\frac{1}{\beta\Delta t^{2}}u_i + \frac{1}{\beta\Delta t}\dot{u}_i + (\frac{1}{2\beta} - 1)\ddot{u}_i\right] + C\left[\frac{\delta}{\beta\Delta t}u_i + (\frac{\delta}{\beta} - 1)\dot{u}_i + \frac{\Delta t}{2}(\frac{\delta}{\beta} - 2)\ddot{u}_i\right]$$

Solving equation (3.91), we get u_{i+1}, and according to (3.89) and (3.90), we get $\dot{u}_{i+1}$ and $\ddot{u}_{i+1}$.

We have now finished the review of the dynamical solution methods.

Direct use of the partial differential equation is often difficult because of difficulties in providing correct boundary conditions. For instance, for the berthing pile the treatment of the part of the pile in soil will be very time consuming. Further the knowledge about the damping coefficients is still in a preliminary stage. Thus it requires further work to apply this method in the solution of an actual engineering problem. Although the method based upon the natural mode of vibration has given an analytical equation for studying the dynamic characteristics of a berthing pile, after simplification, the berthing pile system still has enormous degrees of freedom. We need to sort out a better and more effective method to reduce calculation scale and improve calculation efficiency, which can be better realized by using the numerical analysis method. Thus, this thesis will adopt the finite element method to conduct a dynamical calculation of the prestressed concrete berthing pile.

References

[1]. Zhang Shuhue and Li Dazhong, “Method of non-linear analysis used in prestressed concrete structures”, The People’s Communications Publishing House, 2000.

[2]. Wang Longkuan, “Finite element non-linear analysis”, Chongqing University Publishing House, 2001.

[3]. Zhu Beilong and Dong Zhengxian, “Non-linear analysis of reinforced concrete”, Tongji University Publishing House, 1984.

[4]. Dong Changjue, Rong Xuewen and Pen Shuhua, “Some problems of incremental method in non-linear analysis”, Journal of Chongqing Jiaotong University, 2001.5.

[5]. Xue Guanxing and Kong Rong, “Research on numerial calculation method of prestressed concrete structures”, Journal of Civil Engineering, 2000.3.

[6]. Tang Yougan and Wang Long, “Higher dynamical mechanicals”, Tianjing University Publishing House, 2002.

[7]. R. W. Clough and J. Penzien, “Dynamics of Structures”, McGraw-Hill, New York.,1993.

[8]. M. Paz. “Structural dynamics theory and computation”, Litton Educational Publishing, Inc.1979.

[9]. Li Bingkuen, “Dynamical analysis on reinforced concrete structures for applied dynamical loads”, Journal of Wuhan University, 1999.5.

[10]. Cheng Bingwu and Huang Zhengling, “A numerical model of dynamical calculation”, Journal of Chongqing Jiaotong University, 2002.8.

[11]. G. B. Warburton and H. M. Sons, “The Dynamical Behaviour of Structures”. Robert Maxwell, M.

C. 1996.
[12]. Gong Raonan and Wang Shoutao, “Method of non-linear finite element in structural analysis”, Journal of Shanghai Jiaotong University, 2000.3.
[13]. Zhou Jingxiang, “Structural dynamical mechanicals”, Ha Erbing University Publishing House, 1998.

Chapter 4

Theoretical analysis and computation of the berthing piles

4.1 Basic assumptions

The following basic assumptions are the ones normally used in practice. They lead to a simple calculation method which may be used before doing the more refined theoretical calculations of the prestressed concrete berthing piles:

(1) plane sections before bending remain plane after bending;.

(2) the tensile strength of the concrete may be neglected;

(3) the stress-strain curve of the concrete, and thus the definition of the magnitude and the distribution of compressive stresses are known;

(4) the variable effects related to time may be neglected.

The first assumption, Bernoulli's principle, implies that the longitudinal strain in the concrete and the steel at the various points across a section is proportional to the distance from the neutral axis [1]. A large number of tests on reinforced concrete members have indicated that this assumption is nearly correct at all stages of loading up to flexural failure, provided a good bond exists between concrete and steel [2][3]. Certainly, it is accurate in the compression zone of the concrete. A crack in the tension zone of the concrete implies that some slip has occurred between the steel reinforcement and the surrounding concrete, and this means that the assumption is not completely applicable to the concrete in the neighborhood of the crack [4]. However, if the concrete strain is measured over a gauge length that includes several cracks, it is found that Bernoulli's principle applies to this average tensile strain.

The second assumption is nearly exact. Any tensile stress that exists in the concrete just below the neutral axis is small and has a small lever arm.

Since the strains in the compressed concrete are proportional to the distance from the neutral axis, the section reaches its flexural strength (maximum moment of resistance) when the total compressive force in the concrete multiplied by the internal lever arm is a maximum. Therefore, the third assumption is necessary to assess the true behavior of the section.

4.2 Non-linear whole process analysis and computation steps

4.2.1 For every level of load increment:

(1) Calculate the stress increment and total stress value according to the calculated element stiffness matrix based on the former level of load increment.

(2) Check each element for cracks, compressive damage, yield and so on. For the elements with cracks or damage, it is necessary to adjust their total stress value and their stiffness matrix and convert their excess total stress value into nodal forces.

(3) Obtain the new stress increment and nodal forces with the adjusted stiffness matrix, and then get the new total stress value.

(4) Repeat steps (2) and (3) until no new crack appears or the element is crushed.

The next stage is to enter the next level load increment until the whole component is cracked or damaged.

4.2.2 Specific steps

The specific steps are associated with the detailed approach to be used, for instance:

(1) Basic conditions and mode

(a) A triangular element is used for concrete.
(b) The fracturing or cracking condition is determined under biaxial concrete stress.
(c) After the concrete is cracked, the vertical cracks no longer transfers tension.
(d) The stress-strain relationship under biaxial concrete stress is used.
(e) A linear element is used for the compression reinforcing steel bar and the steel hoops, and a triangular element is used for the tensile reinforcing steel bars. A ideal elasticity-plasticity stress-strain relation is adopted.
(f) A coupling element that simulates adhesive forces is adopted.

(2) Calculating steps

(a) Adding the first-stage load increment, the calculating step of linear analysis is used to obtain the stress increment of each element, $\Delta\sigma_x$, $\Delta\sigma_y$, $\Delta\tau_{xy}$.

In the calculation, the original tangent modulus $E = E_0$ is used for the concrete elasticity modulus, and the usual elasticity value is adopted for the reinforcing steel bars.

Then, the stresses of various elements under the action of the total load value may be found.

Concrete elements: σ_x, σ_y, τ_{xy},

σ_1, σ_2, θ,

Reinforcing steel bars: σ_s.

Coupling elements taking care of bond: σ_h, σ_v.

(b) For each concrete element, three stress states, i.e. compression-compression, tensile-compression and tensile- tensile, are verified and treated separately.
(c) The treatment of each reinforcing steel bar element.
(d) The treatment of each coupling element.
(e) Following steps (b) – (d), the nodal forces $\{F\}^e$ is obtained by transforming the

excess stress, and after adjusting the stiffness matrix [*K*] of each element, the stress increment of each element is found.

Concrete elements: $\Delta\sigma_x$, $\Delta\sigma_y$, $\Delta\tau_{xy}$.

Reinforcing steel bar: $\Delta\sigma_s$.

Coupling elements: $\Delta\sigma_h$, $\Delta\sigma_v$.

Then, the total stress under the action of the total load has been obtained.

Concrete elements: $\sigma_x = \sigma_x + \Delta\sigma_x$, $\sigma_y = \sigma_y + \Delta\sigma_y$, $\tau_{xy} = \tau_{xy} + \Delta\tau_{xy}$.

σ_1, σ_2, θ.

Reinforcing steel bar elements: $\sigma_s = \sigma_s + \Delta\sigma_s$.

Coupling elements: $\sigma_h = \sigma_h + \Delta\sigma_h$, $\sigma_v = \sigma_v + \Delta\sigma_v$.

(f) Repeat steps (b) – (e) until no further cracked or fractured element exists.
(g) Recalculate the stiffness matrix of each element.
(h) Add one more stage of load increment, and with the value [*K*] of step (g), use a linear analysis method to find the stress increment of each element.

Concrete elements: $\Delta\sigma_x$, $\Delta\sigma_y$, $\Delta\tau_{xy}$.

Reinforcing steel element: $\Delta\sigma_s$.

Coupling elements: $\Delta\sigma_h$, $\Delta\sigma_v$.

Then, the total stress under the action of the total load has been obtained.

Concrete elements: $\sigma_x = \sigma_x + \Delta\sigma_x$, $\sigma_y = \sigma_y + \Delta\sigma_y$, $\tau_{xy} = \tau_{xy} + \Delta\tau_{xy}$.

σ_1, σ_2.

Reinforcing steel element: $\sigma_s = \sigma_s + \Delta\sigma_s$

Coupling elements: $\sigma_h = \sigma_h + \Delta\sigma_h$, $\sigma_v = \sigma_v + \Delta\sigma_v$

(i) Repeat steps (b) – (f).
(j) Recalculate the stiffness matrix of each element.
(k) Repeat step (h), step (i) is however used to find the stiffness matrix.
(l) Repeat step (i).
(m) Repeat step (j).
(n) Repeat steps (k) – (m) until the stiffness matrix becomes singular, or the displacement greatly increases.

In order to reduce calculation time, at each level of load increment the stiffness matrix may not be changed, and then the stiffness matrix due to the adjustment of the upper-level load increment calculation is obtained. For cracked or crushed elements, the repeated calculation method can be adopted, i.e. convert the excess total stress value into a nodal force, which is used as an external force to solve a new stress increment and a new total stress value. Then convert the new total stress excess value into a new nodal force, and repeat until the nodal force from the conversion is less than a certain limit value which can be neglected [5]. Then adjust the stiffness matrix and enter the next load increment level. A calculation diagram is shown in Fig. 4.1.

4.3 Dynamical numerical computation model for the berthing pile

When conducting dynamic computations for prestressed concrete berthing piles, the computation model consists of the following three modules:

(1) pre-processing module;

(2) computation module;

(3) post-processing module.

4.3.1 Pre-processing module

The pre-processing module is the key to the whole computation and is related to the accuracy and reliability of the results. The pre-processing module consists of: definition of element type, real parameters and material properties; a setup computation module, which includes a setup geometric module and a setup element module; Element grid partitioning.

1. Element type definition

When choosing an element type for the computation module in this problem, we may consider the specimen to be composed by different materials, e.g. corrugated pipes and their internal mortar, stranded cables and concrete, etc. We choose a solid element (Solid 65) as the computation element type, which is shortly explained by the following problem features: Solid 65 is an eight-node element and each node has three degrees of freedom when it is used for concrete material. The most important feature is that it can simulate a non-linear material, which allows cracking under tensile stress and crushing under compressing; in addition, it allows plastic deformation and creep. This element is usually used in a 3-D solid model with or without steel bars, and can also be applied in geological rock problems and for composite materials such as fiberglass, etc. In the actual model, materials such as the corrugated pipes and stranded cables will be defined as rebars in Solid 65.

The parameters adopted in the element are fixed on the basis of data obtained from actual material performance tests.

2. Material properties definition

Before defining the material properties, the non-linearity of the material must be considered. The material non-linearity can be divided into two types: the first is elastoplasticity, which does not depend on time. Its feature is that the material deformation takes place immediately after a load is applied, but also no further deformation will occur with time. The second is viscosity, which does depend on time. The feature is that the material will not only deform immediately when a load is applied, but the deformation continues over time[6]

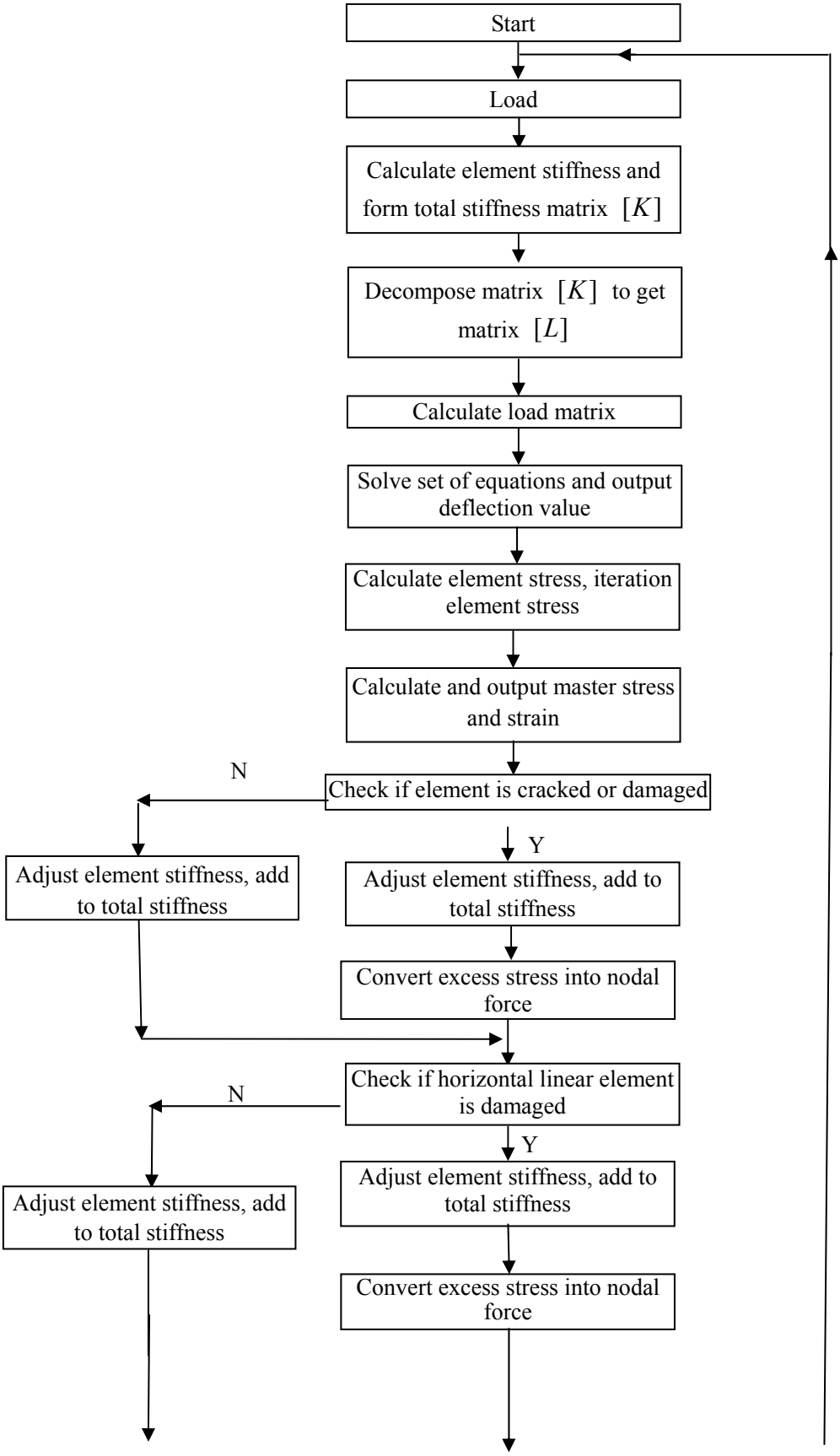
Start
Load
Calculate element stiffness and form total stiffness matrix $[K]$
Decompose matrix $[K]$ to get matrix $[L]$
Calculate load matrix
Solve set of equations and output deflection value
Calculate element stress, iteration element stress
Calculate and output master stress and strain
Check if element is cracked or damaged
N
Y
Adjust element stiffness, add to total stiffness
Adjust element stiffness, add to total stiffness
Convert excess stress into nodal force
Check if horizontal linear element is damaged
N
Y
Adjust element stiffness, add to total stiffness
Adjust element stiffness, add to total stiffness
Convert excess stress into nodal force

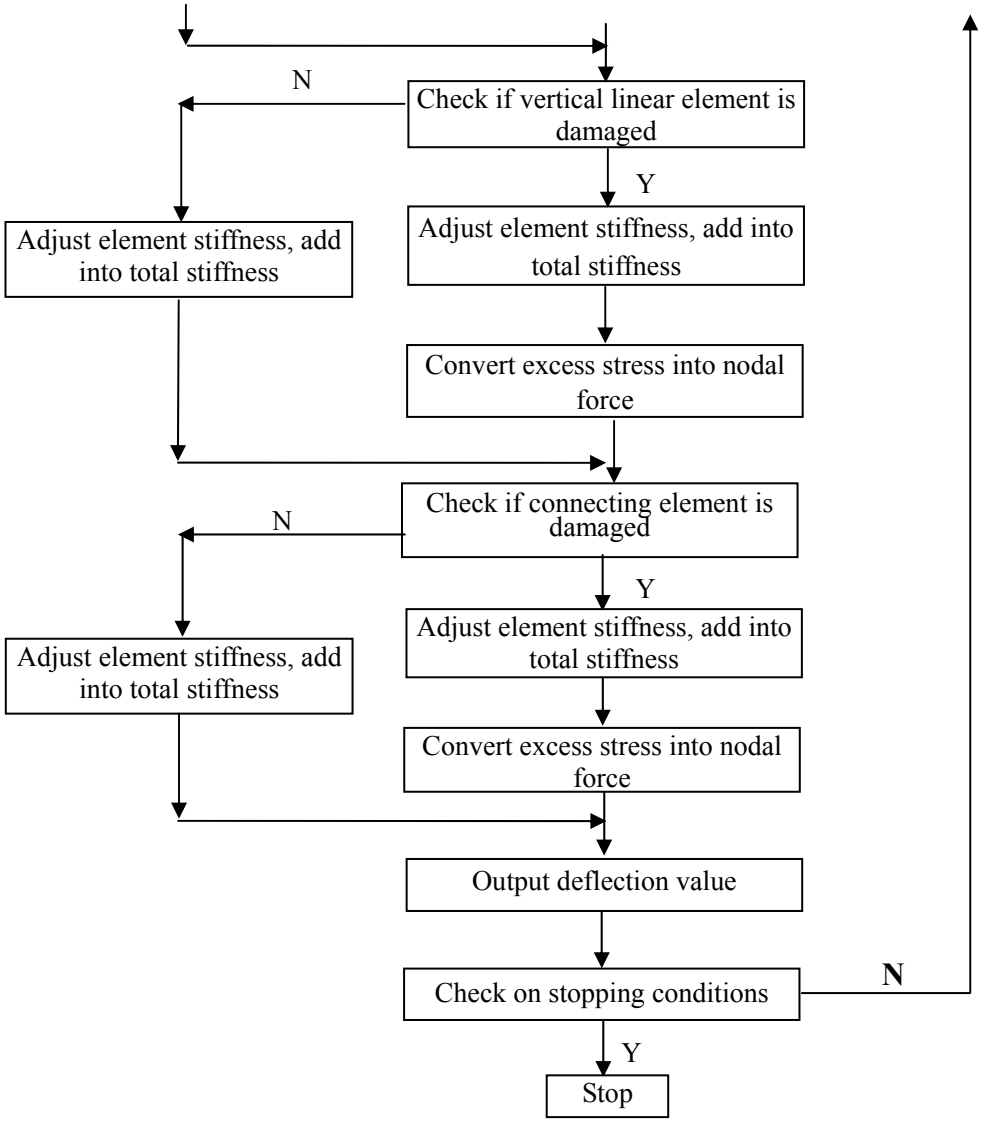

Figure. 4.1 The calculation procedure

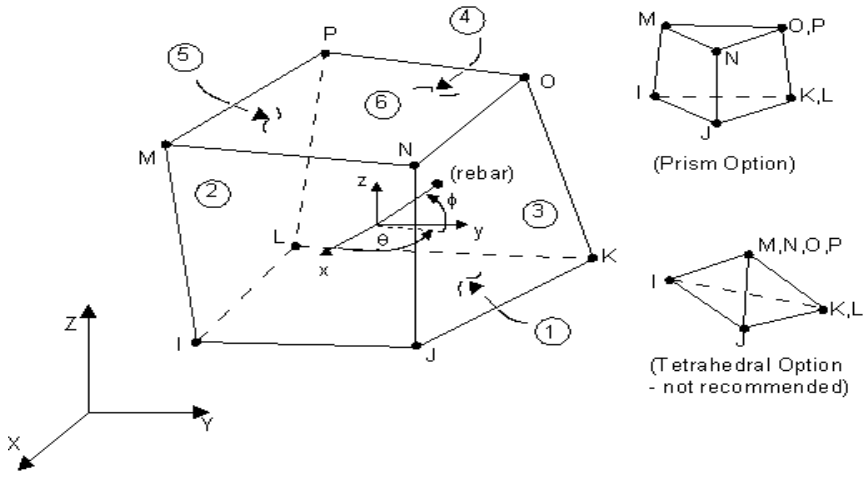

Figure 4.2 Solid 65 unit schematic diagram

The most important type of problem is considered to be the material non-linearity of the present model. The material is assumed isotropic. When defining the material properties, the major parameters are the uniaxial compressive strength and uniaxial tensile strength. The uniaxial compressive strength is taken as 60MPa, and since there are no actually measured data for the uniaxial tensile strength, it is computed according to the formula [7]:

$$f_t = 0.23 \ f_u^{\frac{2}{3}} \quad (f_u \text{ in MPa}) \tag{4.1}$$

3. Unit grid proportioning

When proportioning the element sectional grid, the shape is made as similar as possible so as to save time.

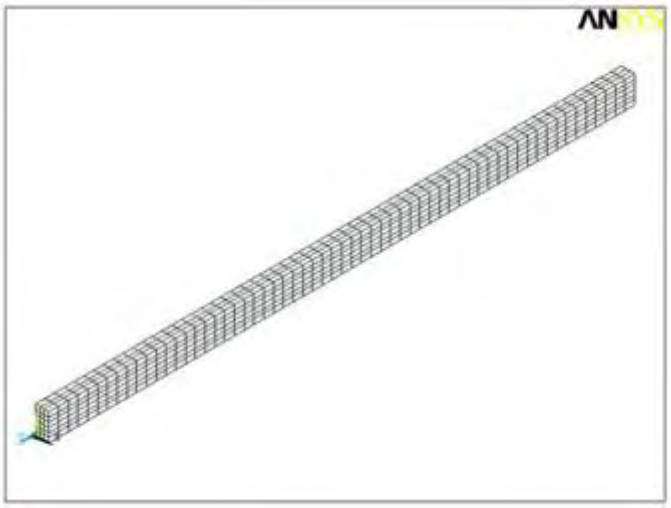

Figure 4.3 Schematic diagram for solid element grid of specimen of no.1

In order to make full use of computer resources, the symmetry command is used during grid portioning, that is, portioning grid for half of the test samples and after then using the grid “reflection” command to generate a grid for the whole section.

After completing the grid partitioning for the sectional element, use the “sweep” command to partition the whole solid grid, and the result is shown in Figure 4.3.

4.3.2 Computing module

The computing module takes care of the restrictions and applies load before completion of the pre-processing module. In this paper, we adopt the finite element method to conduct the dynamic analysis for the prestressed concrete berthing pile.

4.3.2.1. Load mode simulation

1. Motion of ship

The motion of a ship on the water surface can be specified at any instant by the velocity of translation, u, of the center of gravity and by the angular velocity, ω. In the

case $\omega = 0$, all points of the ship will move with the same velocity, and the motion is a simple translation (Figure 4.4). In the case $u = 0$, the velocity of each point of the ship is proportional to the distance from the center of rotation and the motion is a simple rotation (Figure 4.5).

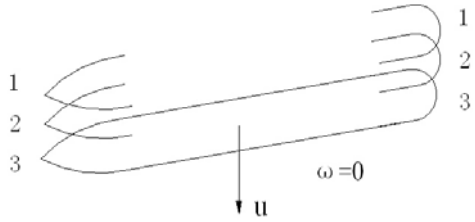

Figure 4.4. Simple translation of a ship

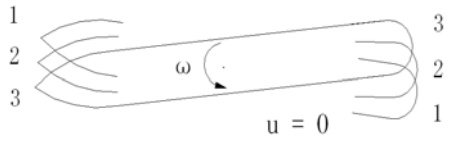

Figure 4.5 Simple rotation of a ship

The motion of a ship on the water surface can alternatively be specified at any instant as a rotation around a point, not necessarily on the ship, the so-called "instantaneous center of rotation". The position of the instantaneous center is usually changing from instant to instant. In simple translation, the instantaneous center of the ship can be considered to be at infinity; in simple rotation, the center is normally coinciding with the center of gravity [9][10].

For the purpose of studying the motion of a ship on the water surface under the action of forces applied to it due to the action of tugboats, ropes, wind or currents, it is necessary to consider the mass m of the ship concentrated at two points at a distance k from her center of gravity.

The distance k is called the radius of gyration and the product $mk^2 = J$ the moment of inertia of the ship (Figure 4.6).

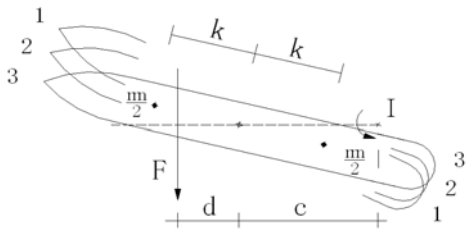

Figure 4.6. Rotation around the instantaneous center

If a force or a system of forces, whose resultant does not pass through the center of gravity, is applied to a ship, the instantaneous center I will be at a line perpendicular to the force and passing through the center of gravity at a distance on the far side of the center of gravity to the center, i.e., see Fig. 4.6,

$$c = k^2 / d \qquad (4.2)$$

where d is the distance from the resultant of the system of forces to the center of gravity (Figure 4.6). The position of the instantaneous center does not depend on the intensity of the forces, but only on their position.

If the resultant of the forces acting on the ship is normal to the center line of the ship,

the instantaneous center *I* will also be on the center line (Figure 4.7). If the resultant, besides being normal to the center line, is applied at one of the points in which we have concentrated half of the mass of the ship, the instantaneous center will be coinciding with the other point, because in this case *c* becomes equal to *d* (Figure 4.8). Equation (4.2) shows that wherever *d* is smaller than *k*, *c* becomes larger than *k* (Figure 4.7), and vice versa (Figure 4.9). These considerations can be of use when choosing the position of forces to be applied to a ship to make it approach a berthing structure in the most convenient way.

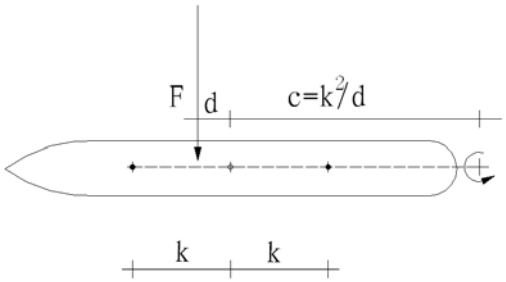

Figure 4.7. Rotation under a force applied near the center of gravity.

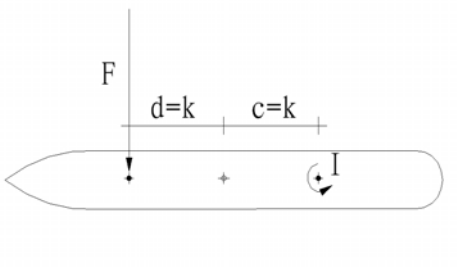

Figure 4.8 Rotation under a force applied at a distance k from the center of gravity.

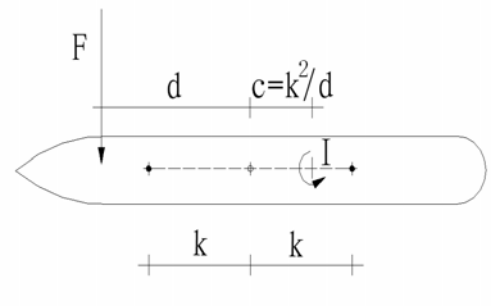

Figure 4.9. Rotation under a force applied far from the center of gravity.

Let us now consider what happens when a ship hits a fender. Let u_0 be the velocity of the translation of the ship and ω_0, its angular velocity at the instant the hull comes into contact with the berthing structure through a fender; *r* is the distance from the center of gravity of the ship to the fender; *a* is the distance from the fender to the vector representing the velocity of the center of gravity of the ship (Figure 4.10a).

As the ship's hull compresses the fender, a reaction force will develop at the contact point.

If the angle ρ of the reaction *R* with the normal at the surface of contact is larger than the angle of friction *m* between hull and fender, sliding will occur, and some energy will be consumed in the process. As berthing is usually intended to be done without sliding, and as it seems risky to rely on the energy consumed in such a process, it will be assumed hereafter that once the contact is established, the ship will rotate around the point of fender contact with an angular velocity ω_1 (Figure 4.10b).

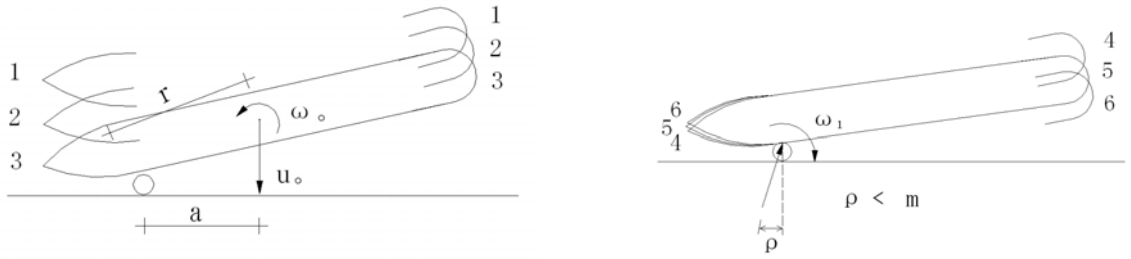

(a) (b)

Figure 4.10 (a) Ship with translation and a rotation while approaching a fender and (b) a rotation around the fender once the contact is made.

If the berthing maneuvre is not particularly smooth (and we are especially interested in the study of difficult maneuvers), the reaction of the fender on the ship will be a force much larger than any of the other forces which also affect the motion of the ship while it rotates around the point of contact. Such other forces are those caused by wind, currents, waves, cables and resistances opposed by the water. Let us assume, for the time being, that these forces can be ignored if compared with the reaction of the fender. As the reaction of the fender is by far the most important force that passes through the point of contact, it seems reasonable to admit that there will be no variation of the angular momentum about the point of fender contact while the ship rotates. By equating the angular momentum of the ship at the beginning of contact with the angular momentum during the rotation of the ship, and taking into account the energy conservation principle, it may be shown that the amount of energy W to be absorbed in the work done by the deflection of the fender can be evaluated by the expression.:

$$W = \frac{1}{2} m u_0^2 \left(1 - \frac{a^2}{k^2 + r^2}\right) + m u_0 \omega_0 \left(\frac{k^2 a}{k^2 + r^2}\right) + \frac{1}{2} m \omega_0^2 \left(\frac{k^2 r^2}{k^2 + r^2}\right) \tag{4.3}$$

The berthing maneuvre has to be oriented so as to reduce this amount of energy and thus render the berthing as smooth as possible.

2. Impact on berthing structure

If, when entering into contact with the fender, a ship is moving in a simple translation normal to the quay wall (Figure4.11), the amount of energy to be absorbed by the deflection of the fender and structure will be

$$W = \frac{1}{2} m u_0^2 \left(1 - \frac{a^2}{k^2 + r^2}\right) \tag{4.4}$$

If, when entering into contact with the fender, the ship is moving with a simple rotation (Figure 4.12), the energy to be absorbed will be

$$W = \frac{1}{2} m \omega_0^2 \frac{k^2 r^2}{k^2 + r^2} \tag{4.5}$$

In this case, the velocity of the point of the hull that hits the fender can be evaluated by

$$u_0 = \omega_0 r \tag{4.6}$$

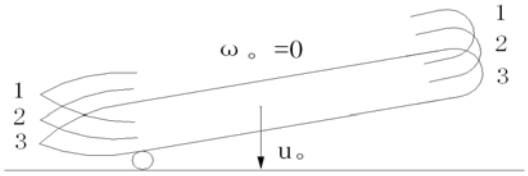

Figure 4.11 Impact on a fender of a ship with a simple translation

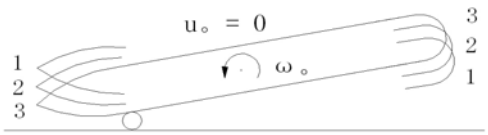

Figure 4.12. Impact on a fender of a ship with a simple rotation

By substituting this value into Equation (4.5) one obtains

$$W = \frac{1}{2} m u_0^2 (1 - \frac{r^2}{k^2 + r^2}) \tag{4.7}$$

Comparing Equation (4.4) with Equation (4.7) and comparing *a* with *r* in Figure 4.10a, one verifies that for equal velocities of the point of the ship which enters into contact with the fender the quantity of energy to be absorbed is smaller when the ship's motion consists of a simple rotation. Only when the velocity of translation is normal to the straight line connecting the point of contact to the mass center does *a* become equal to *r* and the amount of energy to be absorbed in an impact due to rotation is the same as that to be absorbed in an impact due to translation.

Therefore, it can be concluded that for equal velocities of the point of the hull which hits the fender, berthing made through a rotating motion are to be preferred to berthing made through simple translation motion.

Equations (4.4) and (4.7) show that for equal velocities of the point of the hull that hits the fender the amount of energy to be absorbed decreases when the distance from the mass center of the ship to the point of contact increases. To have a gentle berthing it is, therefore, desirable to orient the maneuvre so that the point which first makes contact with the structure is as far as possible from the center of gravity of the ship.

Since the fenders only adapt themselves well to the hull when contact is established in the "parallel" middle body of the ship, it is recommended that the first contact of the ship with the fender be made right at the end of the "parallel" body.

It must be pointed out that, in case of a simple rotation, although for a given velocity u_0 of the point that hits the fender, the further the point is from the center of gravity the smoother the impact (see Equation (4.7)), the fact remains that for a given angular velocity, ω_0 of the ship the further such point is from the center of gravity the harder will be the impact (see Equation (4.5)). However, as it is easier to think in terms of distances covered and velocities of the points of the hull than in terms of angular velocity of the ship and, furthermore, as a berthing operation always involves some translation, it seems advisable to choose the position of the point of contact as far as possible from the center of gravity.

3. Load simulation

Based on above-stated analysis, ship moored in dock is a typical problem of impact dynamics. Impact load tests of a free-falling body have validated that the impulse is basically an isosceles triangular impulse load，as shown in Equation (4.8)[11] (Figure 4.13).

$$P(t)=\begin{cases}2Ft/t_0 & 0\le t\le t_0/2\\ 2F(1-t/t_0) & t_0/2\le t\le t_0\\ 0 & t_0\le t\end{cases} \tag{4.8}$$

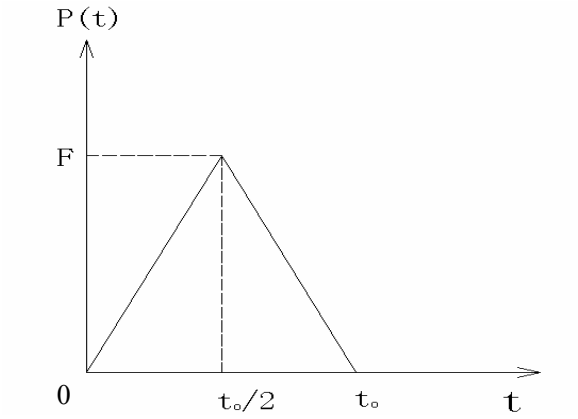

Figure 4.13 Triangular impulse load

We have now made the necessary preparation for carrying out a dynamical calculation. For any given time, the dynamical equations can be regarded as a series of balance equations in which inertia and damping forces are taken into consideration. Two methods have been used to find a solution of the dynamical equations, namely, the vibration superposition method and direct integration. In the calculation using the superposition method, the vibration type and the frequency of free vibrations should be found first. When there are relatively many degrees of freedom in the structural system, the problem of finding the characteristic values will become rather troublesome. For impulse load, there will be many aroused vibration types and, in an analysis using the superposition method, several vibration types are required to realize adequate precision. In addition, the superposition method is only applicable to linear systems. To find a solution in non-linear dynamics, only direct integration is usable. The common direct integration involves, as explained above, methods of central differences Wilson-θ method and Newmark-β method.

4.3.2.2. Damping coefficient

In the dynamic calculation, how to take the viscous damping into consideration is a key point for computing the vibration response of a multiple degrees of freedom system. For a

practical engineering system, it is impossible to compute and generate the damping matrix C, and at this stage, Rayleigh damping is mainly used. This is also termed scale damping.

In Rayleigh damping, it is assumed that the damping coefficient matrix C is a linear combination of the mass matrix and the stiffness matrix, i.e. $C = \alpha M + \beta K$

Here α and β are constants. According to the above mentioned assumption, let $\alpha = 0$. For the value of β, with reference to the values reported in [12] and [13], we assume $\beta = 10\ kN/s$ in this numerical computation process.

4.3.2.3. Procedure of the Newmark - β method

The calculation procedures of the Newmark - β method are the following:

(1) Initial calculation

① Form the stiffness matrix K, mass matrix M, and damping matrix C.

② Determine the initial values u_0, $\dot{u}_0$ and $\ddot{u}_0$.

③ Choose the time steps, the parameters δ and β, and set $\delta \geq 0.5$, $\beta = 0.25(0.5+\delta)^2$. We can then calculate the integration constants:

$$a_0 = \frac{1}{\beta \Delta t^2},\ a_1 = \frac{\delta}{\beta \Delta t},\ a_2 = \frac{1}{\beta \Delta t},\ a_3 = \frac{1}{2\beta} - 1,\ a_4 = \frac{\delta}{\beta} - 1, a_5 = \frac{\Delta t}{2}(\frac{\delta}{\beta} - 2)$$

$$a_6 = \Delta t(1-\delta),\ a_7 = \delta \Delta t$$

④ Form the effective stiffness matrix

$$K^* = K + a_0 M + a_1 C$$

⑤ Perform triangular factorization to K^*, i.e.

$$K^* = LDL^T$$

(2) Solve the response each time step

① Calculate the effective load at $t + \Delta t$

$$F_{i+1}^* = F_{i+1} + M(a_0 u_i + a_2 \dot{u}_i + a_3 \ddot{u}_i) + C(a_1 u_i + a_4 \dot{u}_i + a_5 \ddot{u}_i)$$

② Determine for the displacement at $t + \Delta t$ by solving the following equation

$$LDL^T u_{i+1} = F_{i+1}^*$$

③ Calculate the acceleration and velocity at $t + \Delta t$

$$\ddot{u}_{i+1} = a_0(u_{i+1} - u_i) - a_2 \dot{u}_i - a_3 \ddot{u}_i$$

$$\dot{u}_{i+1} = \dot{u}_i + a_6 \ddot{u}_i + a_7 \ddot{u}_{i+1}$$

4.3.3 Post-processing module

After the completion of all computations, the program enters the post-processing routines, mainly plotting and tabulating the results, including:

(1) Plotting deformation drawings: Plotting the results of deformation of the structural model under loads.

Take specimen no.1 as an example. Under ultimate load the deflection at mid-span is illustrated in Figure 4.14.

From the figure we may find the information such as the maximum deformation, the detailed location and the relation to the load, etc..

(2) Deformation animation: Using animation to simulate the deformation of the structure under loads.

(3) Stress contour map: The stress contour map method clearly describes the variation of a result in the whole model, and thus rapidly determines the "dangerous areas" in the model.

Take specimen no.1 as an example, the distribution of the longitudinal stresses under ultimate load is illustrated in Figure 4.15.

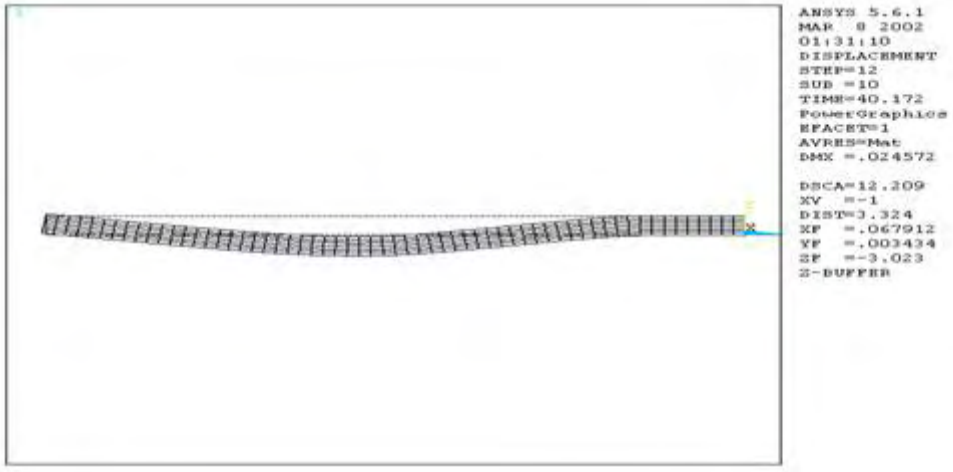

Figure 4.14 Deformation of specimen no.1

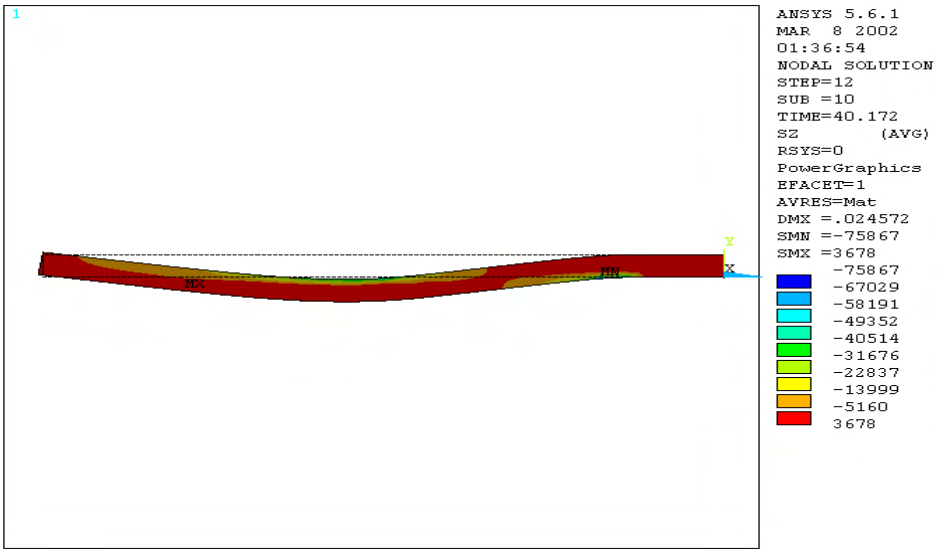

Figure 4.15 Distribution of longitudinal stresses on specimen no.1

4.4 Comparison between testing and theoretical computation results

In the following we shall compare theoretical results with the test results. Only statical tests have been carried out. However the statical results may be obtained using a dynamical method by choosing a proper damping.

Figure 4.16 shows the load-deflection curves obtained by test and by theoretical calculation for specimens no.2, no.3 and no.4. The figures show that the results of the non-linear computation and the dynamic computation have good consistency with the actually measured results.

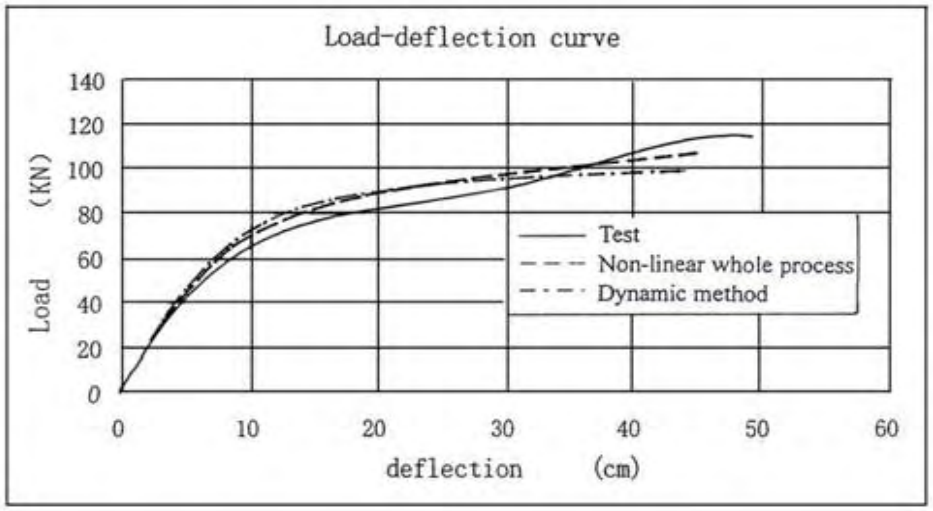

(a) Specimen no.2

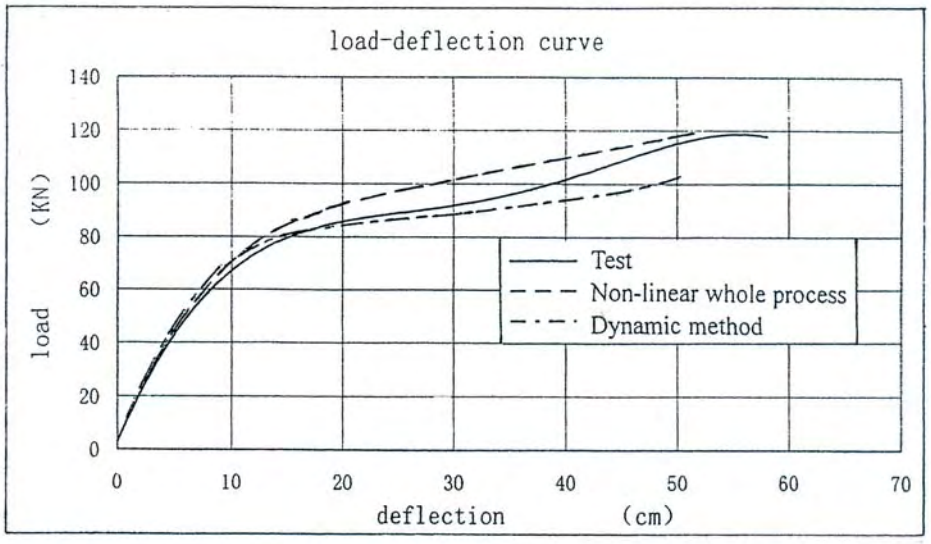

(b) Specimen no.3

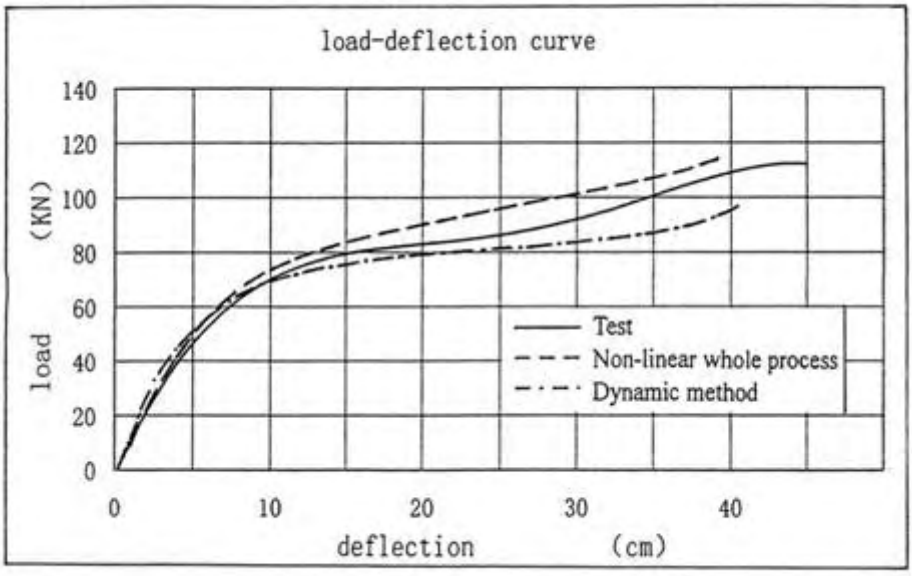

(c) Specimen no.4

Figure 4.16 Load-deflection curves of test and theoretical calculation

1. In the linear stage of the curve, there is some difference between the results from the theoretical computation and the actually measured results, in which the theoretical value of the slope of the curve is greater than the actually measured value. The reason is that the actually measured data in this figure are the results from the third loading cycle, i.e., several cracks have already appeared within the span, and therefore the bending stiffness of the section is smaller than that of the theoretical model without cracks and thus the deflection is relatively smaller; however, the difference is small.

2. In the non-linear stage, the deflections of the computation are all less than the actually measured values because the corrugated pipes occupy a relatively large proportion of the section compared with the sectional dimensions. During the loading process, the corrugated pipes have good bond to the concrete, which will give the member a better deformation performance under load. Further, since the concrete stress increases with the increase of the load, then when the concrete stress approaches the uniaxial strength, the lateral strain is getting bigger and thus the concrete is pressing the lateral steel bars in outward direction due to the continuous development of internal cracks. The lateral steel bar will produce a reaction force to the concrete, and this reaction force helps improving the ductility of the members.

3. The cracking load on specimen no.1 according to the non-linear computation is P=60kN, which is very much similar to the actually measured values. The first series of vertical cracks in computation occurs within the maximum positive bending moment area. These cracks are generally uniformly distributed, and their extension is restricted to the cover layer of the concrete. When increasing the loading, the vertical cracks according to

the computation extend upwards. The first inclined crack occurs within the shear span when the computed load P=78kN, and then this crack continuously extends upwards and downwards when increasing the load. At this time, the vertical cracks are basically stable. The number of cracks and the average crack spacing calculated by the non-linear method are, respectively, 15 and 15.5cm. For the dynamical computation, the form of the cracks and their distribution are similar to the results of the non-linear computation. However the computed cracking load of P=45kN is rather different from the actually measured value. Figure 4.17 shows the crack characteristics from the theoretical computations and the test.

Although the results of both the non-linear computation and the dynamical computation have good consistency with practical measured results, the non-linear computation is closer to the actually measured values; thus, it seems that simulation using this method can better model the actual performance of the structure.

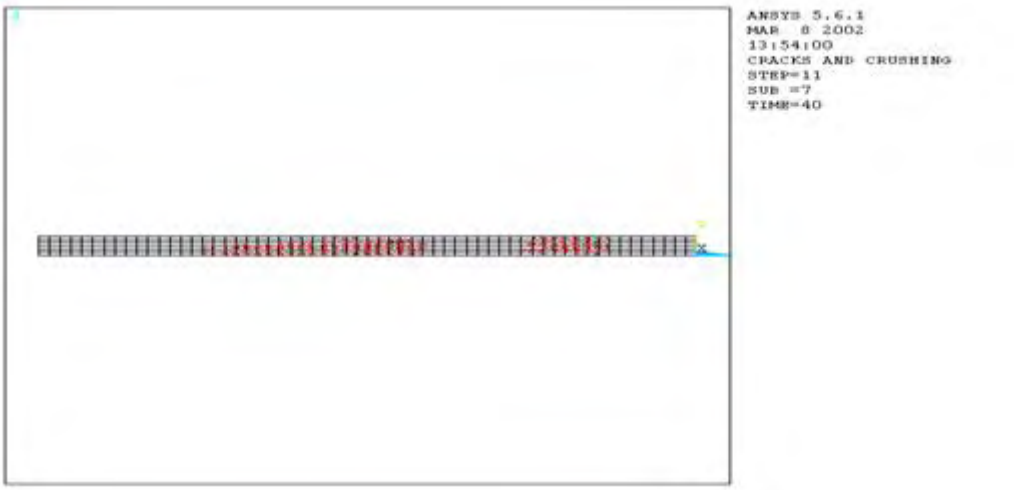

(a) Dynamic computation

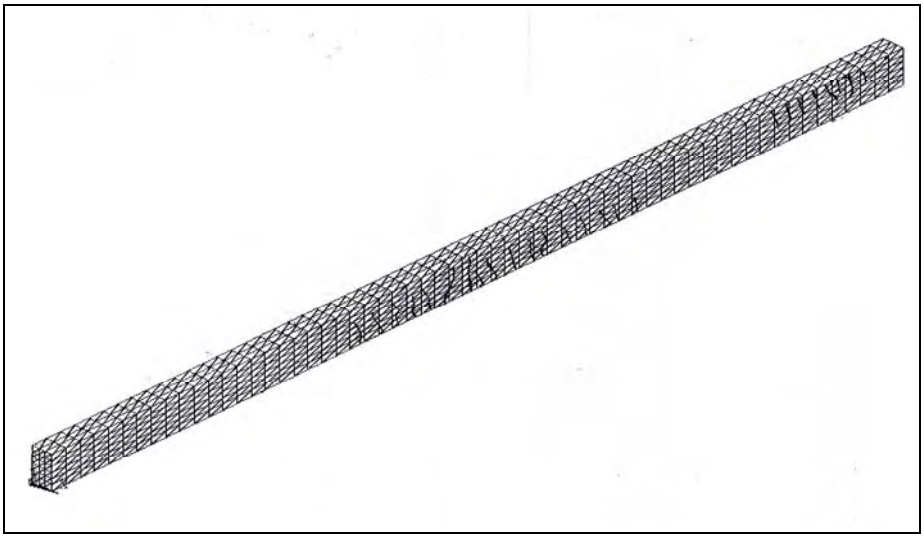

(b) Non-linear computation

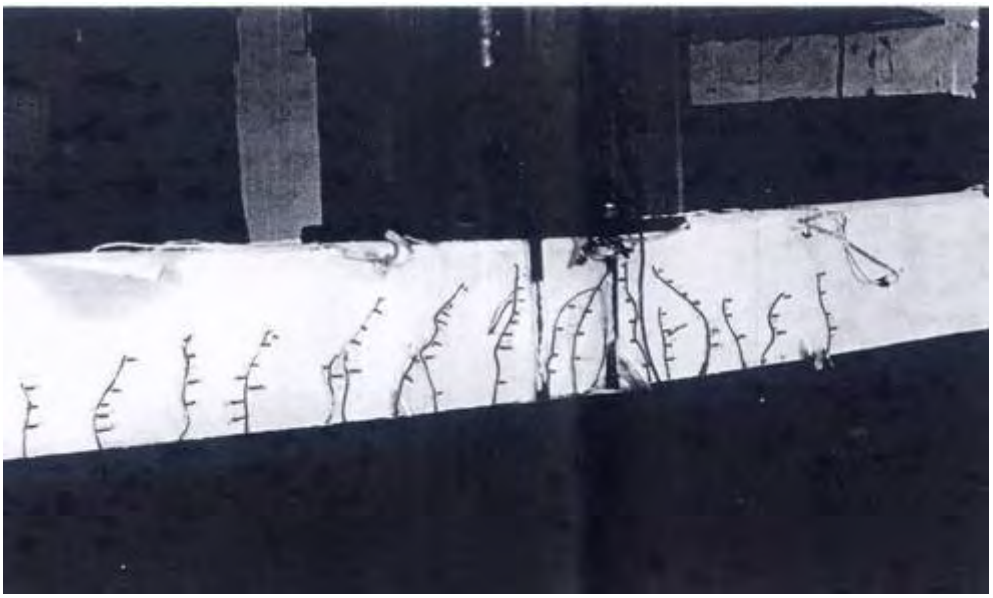

(c) Test result

Figure 4.17 Crack characteristics

4.5 Simulation computation of prestressed concrete berthing piles

4.5.1 Target of simulation analysis

Due to the restrictions in actual conditions, we can not prepare specimens for all the possible parameter combinations. In order to further study the performance of prestressed berthing piles, we analyze the performance of the prestressed berthing piles by changing some parameters based upon the above-mentioned conclusions of the computational model. The simulations are mainly used to analyze

1. The influence of concrete strength, and
2. The influence of the tensile strength and
3. The influence of the reinforcement ratio.

4.5.2 Influence of concrete strength

In the practical tests we used two concrete strengths. These are, respectively, C60 and C80. In theoretical computation, we give consideration to the variation of the concrete strength from C40 to C100. Tables 4.1, 4.2 and 4.3, respectively, indicate the influence of concrete strength keeping the pre-stressesing constant.

Table 4.1 Influence of concrete strength on deflection （cm）

(σ_k=0.5σ_u=930MPa)

Strength / Loads（kN）	C40	C50	C60	C70	C80	C90	C100

10	1.031	1.031	1.031	1.031	1.031	1.031	1.031
20	1.623	1.623	1.623	1.623	1.623	1.623	1.623
30	2.362	2.360	2.361	2.335	2.335	2.226	2.226
40	3.800	3.719	3.421	3.359	3.143	3.143	3.181
50	6.199	6.200	5.795	5.580	5.571	5.173	3.971
60	9.626	9.813	9.755	9.231	8.951	8.514	5.110
65		11.754	11.694	11.525	11.284	10.832	6.318
70		14.139	13.750	13.424	13.256	12.748	8.427
80			18.800	18.242	17.956	17.653	10.932
85			21.598	20.787	20.303	20.060	12.838
90			23.949	23.492	22.911	22.477	14.843
95			24.572	25.063	25.495	25.43	17.500
100				26.968	28.074	27.893	19.929
102					29.213	28.983	20.871
105					30.701	30.588	22.129
110					34.516	33.464	33.005
115					37.219	36.221	35.618
120					38.82	39.720	44.863
125						42.369	50.720

Table 4.2 Influence of concrete strength on deflection （cm）

(σ_k=0.6σ_u=1116MPa)

strength / loads（kN）	C40	C50	C60	C70	C80	C90	C100
10	1.034	1.034	1.034	1.034	1.034	1.034	1.034
20	1.625	1.625	1.625	1.625	1.625	1.625	1.625

30	2.355	2.355	2.332	2.332	2.332	2.228	2.228
40	3.625	3.526	3.455	3.133	3.137	3.143	3.015
50	6.033	5.705	5.555	5.445	5.208	5.319	3.917
60	9.668	9.353	9.144	8.938	8.341	7.931	4.512
65		11.112	10.816	10.742	10.573	10.428	4.888
70		13.594	13.171	13.117	12.794	12.595	6.918
80		16.365	17.857	17.765	17.688	17.305	10.167
85			20.530	20.162	19.897	19.756	12.205
90			22.554	22.691	22.646	22.130	17.032
95				25.521	25.166	24.716	18.136
100				26.968	27.890	27.212	19.457
102				30.796	28.899	28.528	10.654
105				34.231	30.634	29.954	21.851
110					33.064	32.680	24.121
115						35.833	37.527
120						38.494	40.763
122							46.697

Table 4.3 Influence of concrete strength on deflection（cm）

(σ_k=0.7σ_u=1302MPa)

Strength / Loads（kN）	C40	C50	C60	C70	C80	C90	C100
10	1.038	1.038	1.038	1.038	1.038	1.038	1.038
20	1.627	1.627	1.627	1.627	1.627	1.627	1.627
30	2.350	2.349	2.328	2.328	2.229	2.229	2.229
40	3.563	3.508	3.237	3.123	3.136	3.130	3.152

50	5.695	5.434	5.318	5.315	4.912	4.911	3.215
60	8.779	8.933	8.682	8.514	7.891	7.858	3.973
65		10.956	10.568	10.485	10.156	10.297	4.356
70		12.922	12.708	12.24	12.181	12.031	4.832
80		14.103	17.243	17.25	16.982	16.398	7.579
85			19.700	19.395	19.198	18.944	8.864
90			22.350	21.949	21.564	21.214	12.061
95			24.344	24.316	24.424	23.857	16.371
100				26.939	27.130	26.470	18.649
102				28.519	28.046	27.614	19.812
105				32.183	30.850	29.155	20.979
110					33.257	31.887	21.504
115						34.452	23.988
120						37.853	31.756
125						40.498	40.472
130						43.382	42.494
135						44.451	

Figure 4.18 shows the load-deflection curves for the relevant concrete strengths. From this figure we may see that under same pre-stressing conditions, although the load-deflection curve has quite similar rules of variation, there are obvious differences with respect to the crack resisting performance and deformation abilities:

1. Under the same pre-stressing conditions, the cracking load increases with the concrete strength, which indicate that the increase of the concrete strength will enhance the crack resisting performance of the berthing pile.

2. The computational results indicate that the higher concrete strength is, the smaller the deflection under the same load. In other words, for the same deflection, the required load increases with the concrete strength, which show that high-strength concrete members become more rigid with increasing stiffness. At the later stage of loading, however, the computational results show that under the same load the member with lower

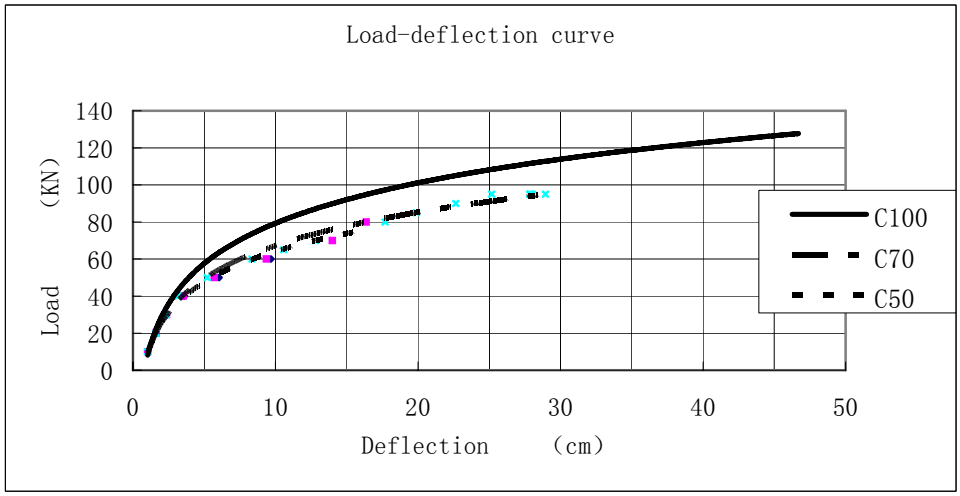

(a) $\sigma_K=0.5\sigma_u$

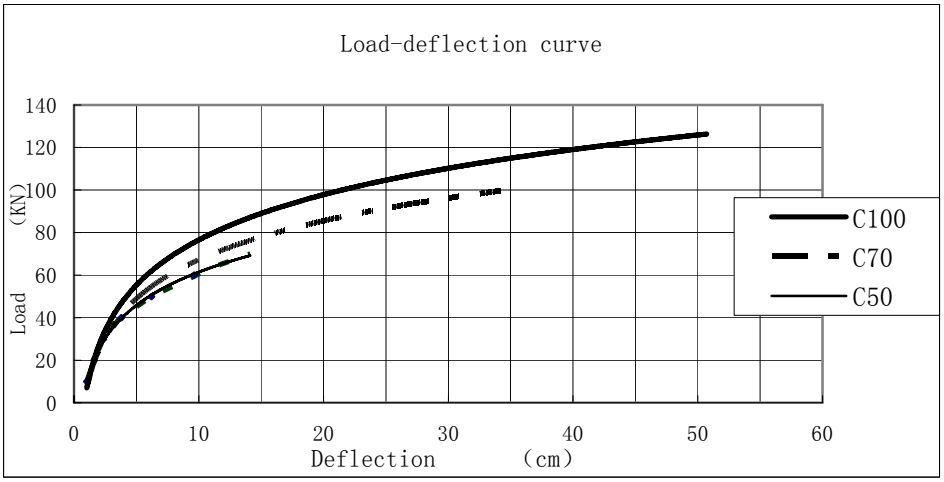

(b) $\sigma_K=0.6\sigma_u$

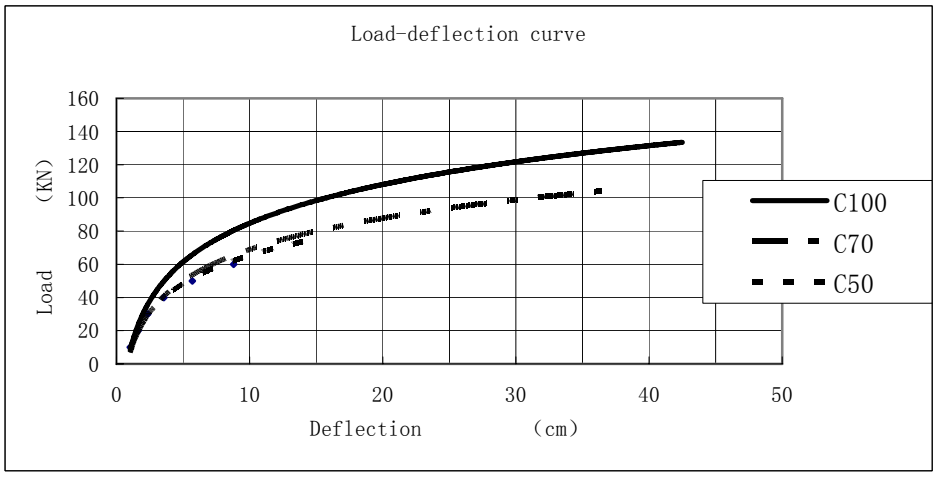

(c) $\sigma_K=0.7\sigma_u$

Figure 4.18 Load-deflection curve for different concrete strength

concrete strength has less deflection than the member with higher concrete strength. The reason is that at the later stage of loading, the cracks of the member with higher concrete strength are developed more effectively than for lower concrete strength because the member with lower concrete strength is near to its ultimate load.

3. Tables 4.1 to 4.3 and figure 4.18 show that there is a great difference in the ultimate deflection under the different concrete strengths. The higher the concrete strength is, the higher the limit deflection is. When the concrete strength is over C90, the absorbed energy is 105% of the absorbed energy of C80, but when the concrete strength is lower than C50, the absorbed energy is only 82.6% of C60.

4. Though the high-strength concrete prestressed berthing piles have relatively greater deformation ability, most of the deformation occurs in the later stage of loading. The higher the concrete strength is, the more obvious the later stage deformation is. However, in actual practice it is dangerous to use the deformation at the later stage of the berthing pile to absorb impact energy from ships. In addition, lower concrete strength not only absorbs less energy, but also it can not fully utilize high strength steel bars. Therefore, considering as a whole the crack resisting performance of the pile, its deformation ability and tensile strength, we suggest that the design strength for concrete berthing piles may be taken in the interval from C60 to C80.

4.5.3 Influence of pre- stress on performance of the berthing piles

Tables 4.1, 4.2 and 4.3 show the simultaneous calculations of the influence of pre-stress on deformation performance of the prestressed concrete berthing pile under the same concrete strength conditions. Under given concrete strength conditions, the influence of prestressing on the deformation performance of the concrete berthing pile is shown in Figure 4.19. This figure shows that under the same concrete strength conditions, the influence of the pre-stressing is not obvious regarding the general tendency of the deformation; moreover, the deformation ability is relatively different. For the specimens with smaller concrete strengths, such as C40 and C50, the pre-stressing has little influence on the ultimate deflection, because all specimens are damaged due to concrete crushing, and the strain in the steel bars are far lower than the ultimate strain. But for the specimens with a higher concrete strength, the influence of the pre-stressing on the ultimate load carrying capacity and ultimate deformation ability is relatively large. For the specimen of the concrete strength of C70, for example, the relative increment of the ultimate load between the low pre-stress and the high pre-stress is 9%, and the relative increment of ultimate deflection is 16.1%.

However, the ultimate bearing capacity and the ultimate deformation capacity do not always increase with the pre-stressing. When the strength of concrete reaches C100, not

only the ultimate deflection reduces by 16%, but also the ratio of the ultimate load to the cracking load reduces, which makes the specimen's brittleness increase and the ductility

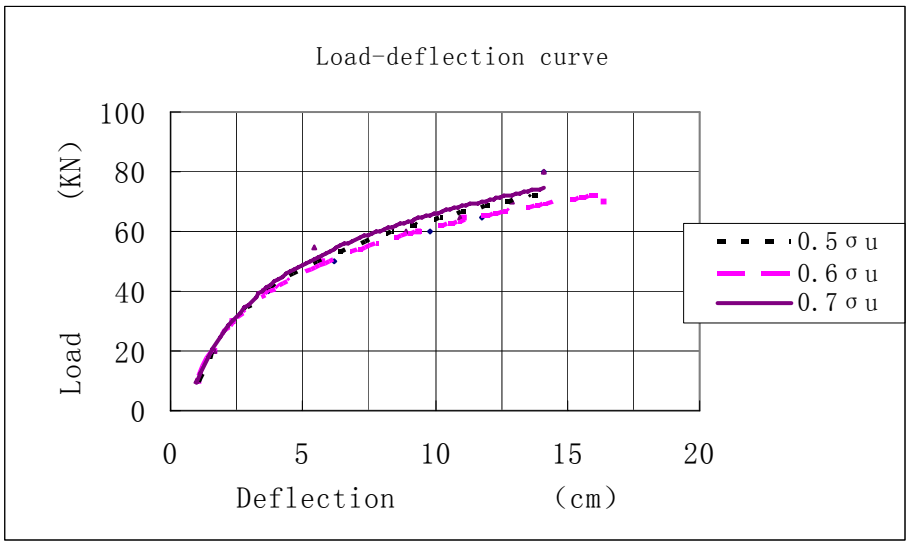

(a) Concrete strength of C50

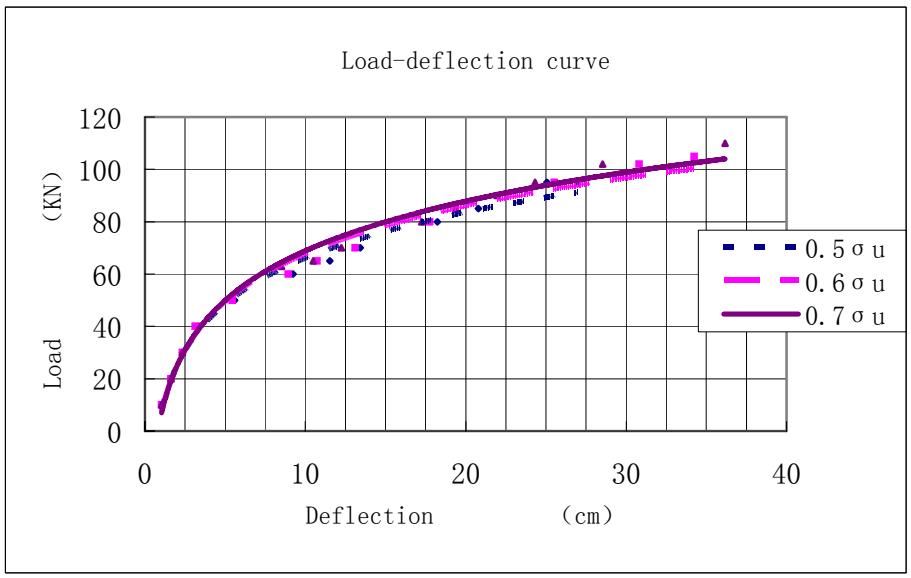

(b) Concrete strength of C70

Figure 4.19 Load-deflection curve related to different pre-stresses

decrease. The comparison studies have shown that a specimen with high pre-stressing has relatively higher strain energy, but the strain of the steel bar is far lower than the ultimate strain value before damage Thus, in order to make full use of the strength of the materials

and improve the damage form of the specimens, the pre-stressing of the berthing piles in practice does not have to be very high. We suggest that the pre-stressing should be controlled by the requirements for hoisting and piling during construction.

4.5.4 Mechanical properties of prestressed concrete berthing piles

The mechanical properties of the prestressed concrete berthing piles are defined by the deformation-reaction force-energy absorption curves.

Figure 4.20 shows the partly measured and partly computed deformation-reaction force-energy absorption curves. The reaction force is measured or calculated at the simple supported end. The design of an optimal prestressed concrete berthing pile should lead to relatively high energy absorption and smaller reaction force so as to provide the best protection to ships and hydraulic structures. The deformation-reaction force-energy absorption curves are not only mechanical property indexes of the berthing pile, but also of high practical value. Generally, the energy absorption is determined by the design value of the deformation, and then the size of ships related to this energy absorption is calculated. If the design requirements can not be met, redesigning is necessary.

From figure 4.20 we can see following characteristics:

1. All curves have similar shapes, and with the increase of deformation, both the reaction force and energy absorption are also increased. The absorption energy curve in Fig.20(e) is slightly different from the others because higher concrete strength of C100 is used. The steeper shape shows that most of deformation is produced in the later stage of loading.

2. In addition, increasing the concrete strength may increase the energy absorption of the member. However, when the concrete strength is over C80, the energy absorbed is mostly generated from the later stage of deformation of the member. From Figure 4.20(e) we may see that the later stage slope of the energy absorption curve is much greater than in other situations.

3. For the members with concrete strength lower than C60 and the members with circular spirals and eccentric reinforcement, the ratio of the reaction force to the energy absorption is greater than 1.0. These piles can be defined as rigid piles, e.g., the ratio of the reaction force to the energy absorption in figures 4.20(a) and (d) are respectively 1.44 and 1.83.

4. For the members with a relatively high concrete strength and high pre-stress, the ratio of the reaction force to the energy absorption is less than 1.0, e.g. the ratios in figures 4.20(b), (c) and (e) are 0.97, 0.86 and 0.95, respectively, and therefore they may be defined as flexible piles which are the optimal types of prestressed concrete berthing piles due to very good energy absorption properties.

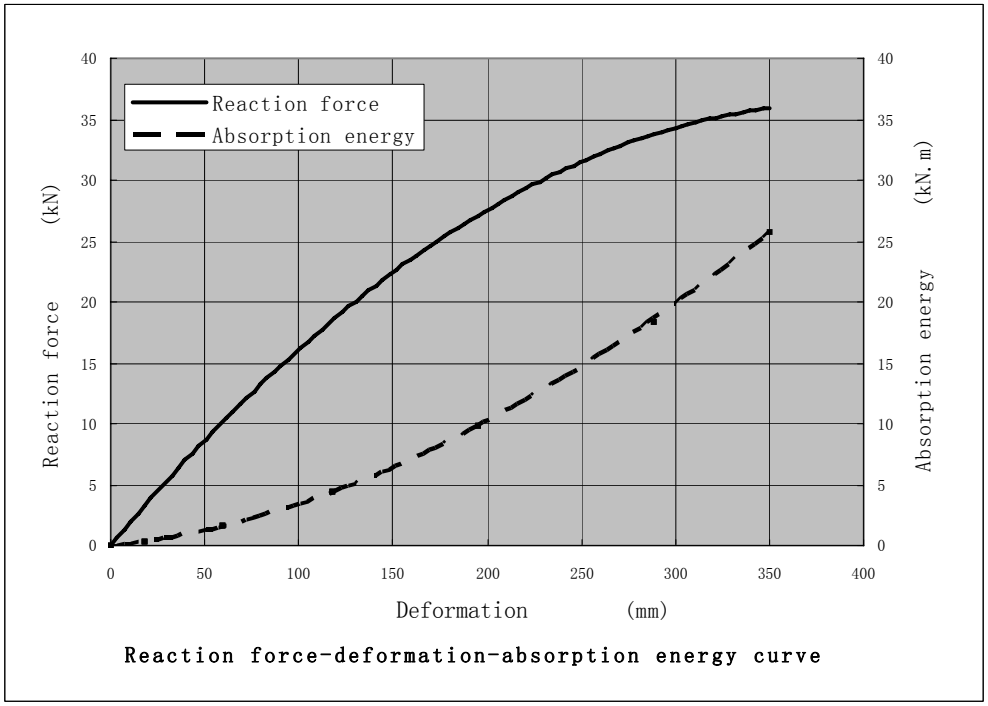

(a) Specimen no.1

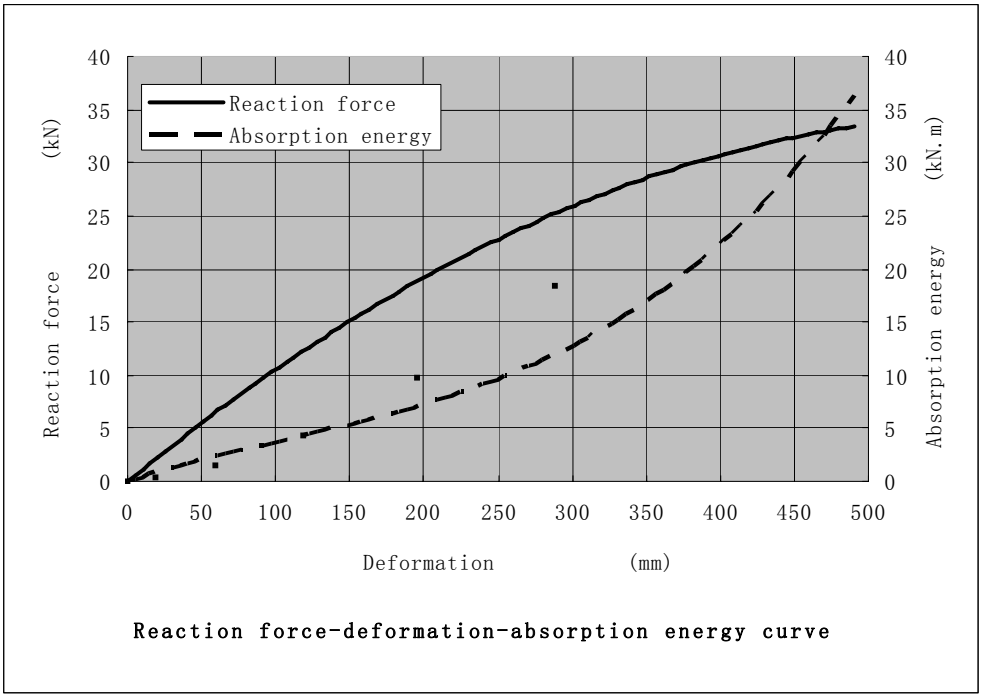

(b) Specimen no.2

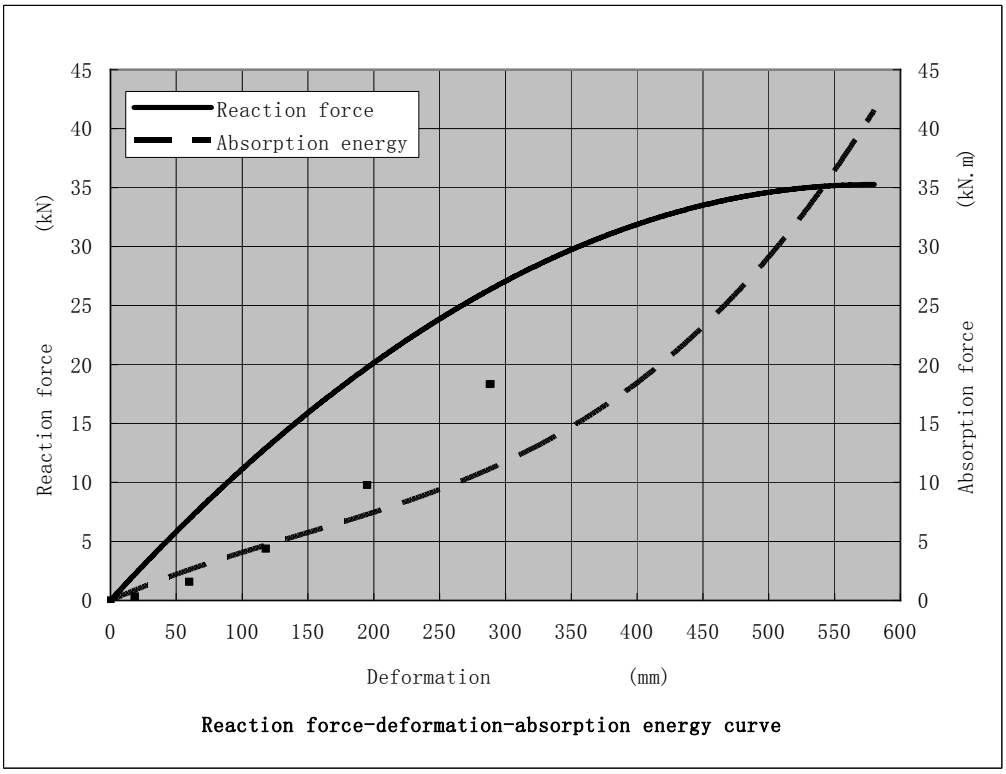

Reaction force-deformation-absorption energy curve

(c) Specimen no.3

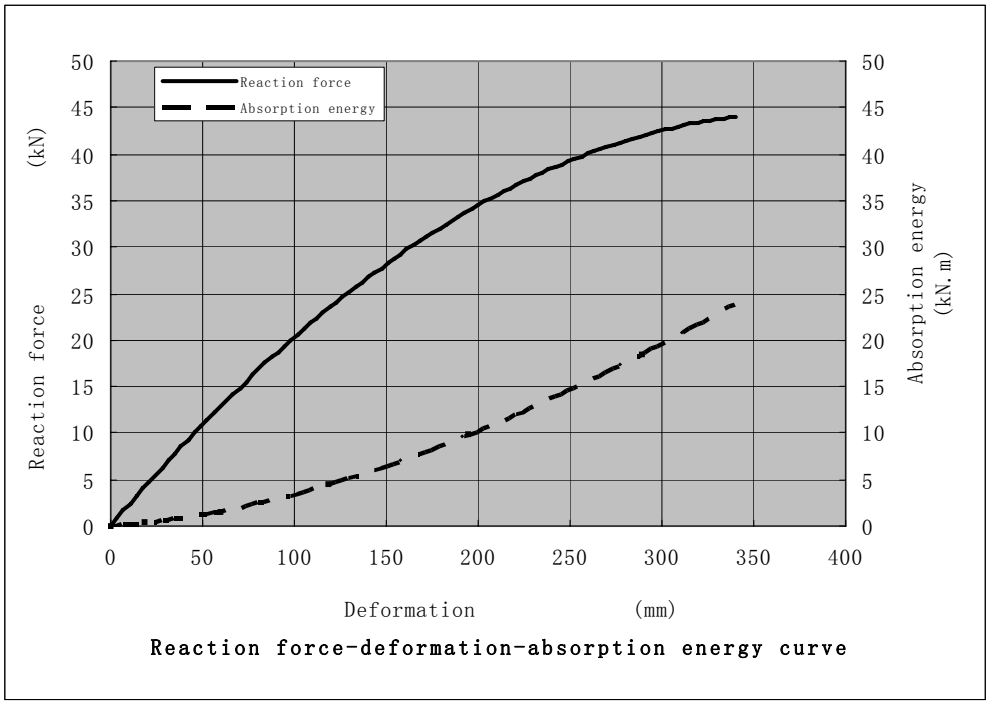

Reaction force-deformation-absorption energy curve

(d) Specimen no.5

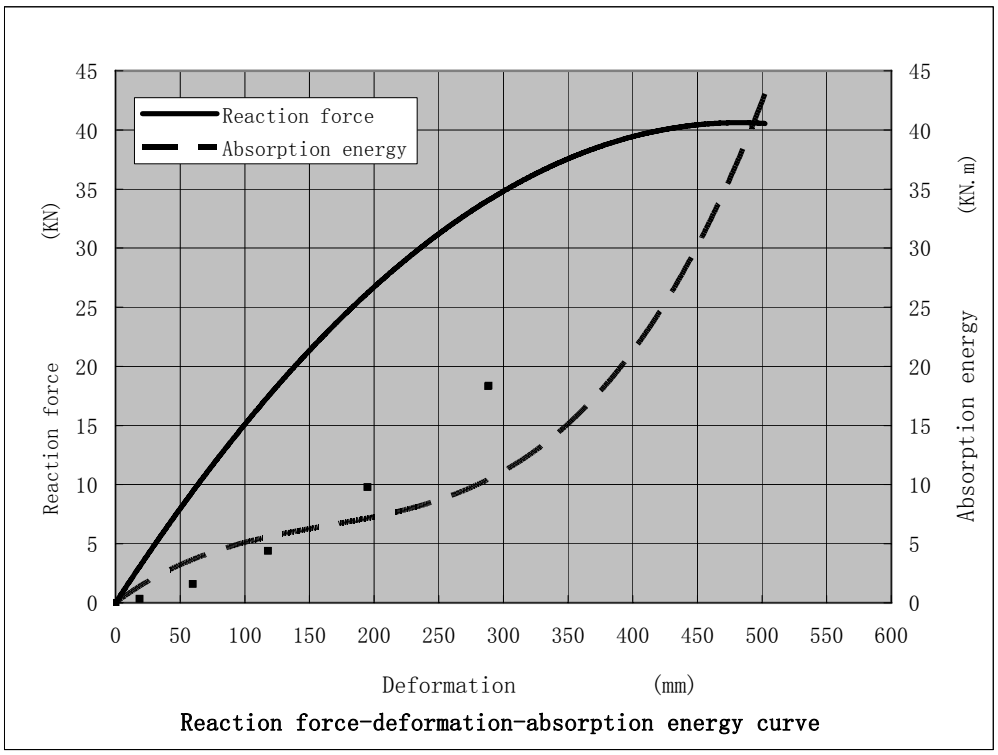

(e) Member of C100, 0.5 σ_u

Fig. 4.20 Reaction force-deformation-absorption energy curves

References

[1]. Translated by Qing Wenyu, Wang Zhenling, “Reinforced concrete structures”, Chongqing University Publishing House, 1985

[2]. Mong Dongming and Deng Bo, “Some problems on basic assumption of reinforced concrete structure calculation”, Journal of Port and Waterway Engineering Practice, 2002.3

[3]. Hehai University, “Hydraulic reinforced concrete”, the third edition, Publishing Press of Hydraulic Engineering, 1996

[4]. Xu Xibin and Zhen Jianhua, “Test research on bond performance of prestressed concrete slabs with new type of wires”, Journal of Chongqing Jiaotong University, 1999.12

[5].Liu Nanko, Zhang Binghue, “Theoretical analysis and calculation on the sectional moment-curvature of concrete continuous beam”, Journal of Hunan Technical University, 2001.2

[6]. Wu Dongqing and Liu Hong, “Materials and material performance”, Chongqing University Publishing House, 2000.3

[7]. D.E.Branson, “Deformation of reinforced concrete structures”, Mcgraw-Hill Book Company, New York, 1989

[8]. The Ministry of Communications, China, “Code of the port engineering”, the People’s Communications Publishing House, 1997

[9]. Per Bruun, “Port Engineering”, Translated by The First Design Institute of Navigation Engineering, The Ministry of Communications, China, The People’s Communications Publishing

House, 1996
[10]. Cheng Wanjia, “Hydraulic structures”, The People’s Communications Publishing House, 2000
[11]. Jin Waiting and Gong Shunfeng, Horizontal Dynamic Parameters of Nuclear Engineering Fractures under Funning Impact Load, Journal of Vibrating Engineering, Vol.15, no.4, Dec.2002
[12]. Zhou JingXiang, “Structural dynamics”,Ha Erbing Technical University Publishing House, 1996
[13]. Gu Wenwu, “Test researches on damping coefficient of materials”, Journal of Shi Jiazhuang Railway, Vol.12, no.12 Jun.1999

Chapter 5

Application of the research findings

5.1 Chongqing Cuntan Port

Chongqing is the largest port city located on the upper reaches of the Yangtze River and also a center city in South China. Having the advantage of a multi-layer transportation network consisting of waterway, roadway, railway and aviation, and possessing the Golden Waterway of the Yangtze River, Chongqing has the potential to become a logistics center in the upper reaches of the Yangtze River. As the leading port in the upper reaches of the Yangtze River, Chongqing port is acting as the hub of traffic in Southwest China, both in terms of waterway and land transportation, playing an important role in commodity circulation between Southwest China, Middle China and East China.

The research findings are applied in Stage Ⅱ of Chongqing Cuntan Port District. The Port is a comprehensive container port, the largest scale of construction in the upper reaches of the Yangtze River. Its construction overcomes the constraint of having to build a vertical dock imposed by large water level difference in the upper reaches of the Yangtze River, and accordingly it enriches the mode of dock structure in this area and greatly enhances the work efficiency of containers. Therefore guidance is very important to construct an inland river port wharf. Here, a brief introduction to the development of Cuntan Port District is given[1][2].

5.1.1 Current Status of Cuntan Port District

The Cuntan Port District, is located on the north bank of the Yangtze River, six km downstream from Chaotianmen , Chongqing City, as shown in Fig.5.1. It links to the Wu-Gui line, one of the City's Grade 1 main truck road, two km from the Renhe Freight Station in Chongqing Jiangbei District and 3.4 km from Tangjiatuo Railway Freight Station in Chongqing. It is close to the export processing zone of Chongqing's new northern district, which is located on the brink of urban city, and has easy access to a variety of transportation means such as railway, highway and airway. The water field where the Cuntan Port District is situated has advantageous conditions, a sufficient land field, and is proved to be a good site for building a port of the City.

5.1.2 General Planning of the Cuntan Port District

Fig.5.2 shows the general planning of the Cuntan Port District. The plan is to occupy an area of approximately two million square meters (one million square meters for construction of an infrastructure of the port, and one million square meters for building a logistics center), with a 1,500 m usable river bank. The function of the port is expected to be the western logistics center and an export-oriented hub port of the upper reaches of the

Fig. 5.1 Map of port district and transportation facilities

Yangtze River, offering transport of the containers, the commercial automobiles and service of logistics. It is estimated that transportations from the container of Cuntan Port District will reach 700,000 TEU, with a roll-load of 300,000 commercial automobiles in 2015. The construction scale of the Cuntan Port District includes two 3,000-ton berths for the automobile roll-load with an annual handling capacity of 300,000 sets, and seven 3,000-ton berths for containers with annual handling capacity of 700,000 sets. The planned anchor land will be controlled in the section from Cuntan Railway Bridge to Tangjiatuo, and the total investment is estimated at RMB1.5 - 2.0 billion. The project will be constructed in several stages.

5.1.3 Engineering survey of the Cuntan Port District

5.1.3.1 Scale of construction

According to the plan of the port area construction, Stage Ⅰ of the Cuntan Port District will occupy a land area of around 0.3 million square meters with a bank line of 950 m.

The scale of construction includes one 3,000-ton berth for automobile roll-load, with an annual handling capacity of 150,000 sets, and two 3,000-ton berths for containers, with an annual handling capacity of 200,000 TEU. The total investment of Stage Ⅰ is RMB700 million, which will be completed in 2006.

Stage Ⅱ has the same land area as Stage Ⅰ. Its scale of construction includes one 3,000-ton berth for automobile roll-load, with an annual handling capacity of 150,000 sets, and five 3,000-ton berths for containers, with an annual handling capacity of 500,000 TEU. The construction of Stage Ⅱ will be started in 2006 and completed in 2010.

Fig. 5.2 Map of general planning of the Cuntan Port District

5.1.3.2 Technique of loading-unloading

1. Berth for container

Each berth of container provides with two sets of 40.5 ton bank-side container loading-unloading bridge cranes in front of the berths, and the loading-unloading efficiency of a single bridge crane is 17 natural containers each hour. For work of the stockyard, a 30.5 - 40.5 m track type gantry crane will be used and a track-type gantry crane and traction type container trailer will be adopted to transport containers horizontally. The track-type gantry crane is arranged horizontally along the parallel bank, where each berth is provided with four track-type gantry cranes. The technological process is:

ship←→bank side container crane ←→traction trailer ←→track type container gantry crane ←→stockyard

2. Roll-load berth

Two berths are available where the commercial automobiles pass through the middle gangplank mounted on the side of a roll-load ship, and a pontoon and movable steel bridge approach is used to realize the roll working of loading and unloading. The technological process is:

roll-load ship ←→ pontoon ←→ movable steel bridge approach ←→ car storage yard

5.1.3.3 General plan layout

1. Container berth

The vertical dock arrangement and staged land field scheme will be adopted. To reduce the influence of the project on flood control and the conditions of water flow, an arrangement of the overhead platform will be used for the dock, and that of a bridge approach connection will be adopted for the land field. The platform of the two berths in Stage Ⅰ is 221 m length and 30 m wide. The width of the bridge approach is 16 m, and the average length is 90 m. The front line of the dock is laid near 159.0 m hydroisohypse, the distance of slope to the top line of the land field is 120 m, and the port pool is formed after removing the reefs using explosives. For the front-line design elevation of the dock, 191.50 m is taken according to the high water-level plus the super-high value, and the river bottom elevation is designed to be 153.60 m. The land field is arranged in a ladder shape, and a sloped bank revetment is adopted. In the range of a 450 m land field, a 3-stage container stack-up yard will be set up. The elevations for each stage are 190.6, 207.0 and 215.5 m, respectively. The road in the port area is arranged in a ring. The width of the main trunk road is 20 and 15 m respectively, and an in-situ concrete plate surface layer is adopted for structure of the road and the stockyard.

2. Roll-load berth

As far as the dock arrangement is concerned, the bent line bank-along slope dock is made, where a pontoon is arranged and, by means of a movable steel bridge approach, connected to an inclined slope. Horizontally, the length of the inclined slope is 400 m and the width is 9 m. The longitudinal ramp of the road consists of three sections, and in the middle is the transition section. The front line of the road is located 155.0 m from the hydroisohypse. The elevation of the designed river bottom is 155.0 m. The parking area is situated at the back of the planned no.1 and no.2 container berths, which is shaped like a ladder. The land field elevations are 196.0, 202.0 and 209.8 m respectively, and in-situ concrete slab surface layer is adopted for the road structure of the parking area and the stockyard.

5.1.3.4 Formation of land field and treatment of ground base

The land field is formed by excavation and backfilling, in which the amount of excavation and amount of fill are 3.1 million m^3 and 1.9 million m^3 respectively. The excess earth is transported to the logistics zone of the port area. The backfilled land field of the port area will be treated by means of rolling in layers. The port area will link up with the Wu-Gui road by setting up two level crossings.

5.1.4 Hydraulic structure

5.1.4.1 Container berth

There are two kinds of structural types to be considered. One is a slope wharf and another is a vertical structure. The slope structural type, as shown in Fig. 5.3[3], may well

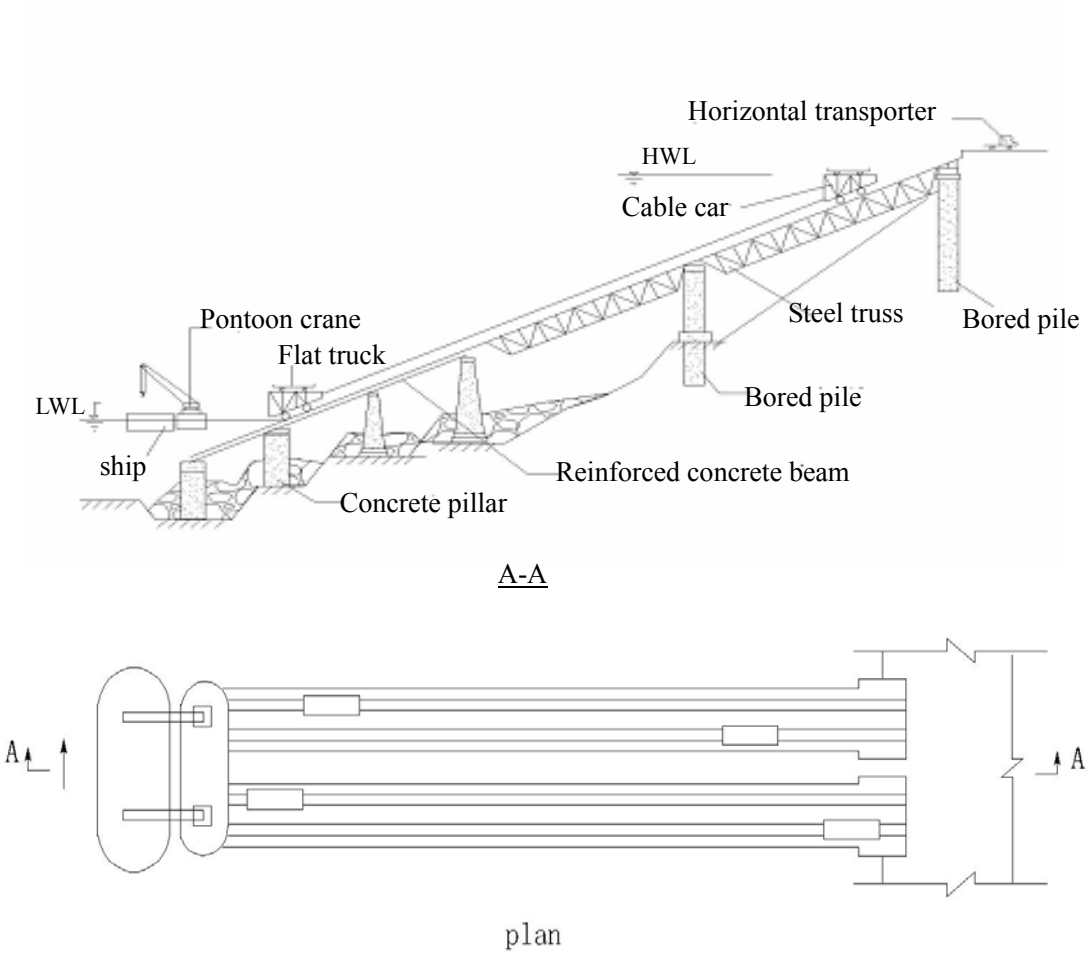

Fig. 5.3 Slope structure

Fig. 5.4 Hydraulic structure of container berth

be suitable for the large changing of the water level. For this kind of wharf, a pontoon concept is necessary for the berthing of the ship and handling of the cargo[4]. Comparing with the traditional vertical structural type, the main problem of a slope type is very low handling efficiency because of the slope transportation and the frequent movement of the pontoon with the changing of the water level. This problem is counteracting the advantages of simplicity, low investment costs and the suitability for the changing of the water levels. Then, the vertical type is used in the Cuntan Port**,** as shown in Fig.5.4.

The dock of container berths is structured as pile foundation, where the length of the dock platform is 221 m and the width is 30 m. The superstructure is composed of transverse girders, front beams, track beams, connection beams and plates. To meet the needs for mooring and berthing, there are mooring facilities at six different elevations in the front of the dock, as shown in Fig.5.4. For the structure of container berths of Stage Ⅱ, the post-prestressed concrete pile is used as the berthing pile to carry the lateral loads from the impact of berthing ships. The concrete strength of the pile is C80 and 26 stranded cables are arranged in symmetry. The pre-stress of the cable is $\sigma_K = 0.65\sigma_u$. As a fender system, the post-prestressed concrete berthing piles are arranged in the front of the dock to directly absorb the energy.

On the platform, three overhead bridge approaches are connected to the land field, each being 90 m long and 16 m wide. At both ends of the bridge approach, bell-mouths link up with the bank and the platform, respectively, with the longitudinal slope of 5%. The structure of the bridge approach is a pile foundation beam and a slab in bent frame. The bent frames are spaced at 13.5 m and 14.5 m, and each bent frame has three piles. The superstructure of the bridge consists of an in-situ concrete reinforced beam and in-situ reinforced T-shape girders.

Fig. 5.5 is the calculated curve of reaction force–deformation and absorption energy of the prestressed concrete berthing pile, which is calculated on the basis of the designed parameters. Under the condition of an ultimate deformation of the berthing pile, the maximum absorption energy is 39.5 kNm. For the considerations of safety, however, 50 percent or 60 percent of the absorption energy may be considered in design. Normally, the prestressed concrete berthing pile is used to be combined with other fender equipments[5][6]. Therefore it can fully satisfy the design requirements.

5.1.4.2 Bank revetment engineering

The 800 m long bank revetment mainly consists of a solid slope structure, which is formed by way of backfilling through rolling in layers and excavation of stones. The slope structure is composed of boulder strip revetments and crushed stone filtering layers. The block stones are fixed at the foot of the slope, and mortar-boned boulder strips are erected at the top of the slope to form a retaining wall.

5.2 Fujian Sandu port

Sandu Island, the largest island of Ningde City with an area of 24.9 square kilometers,

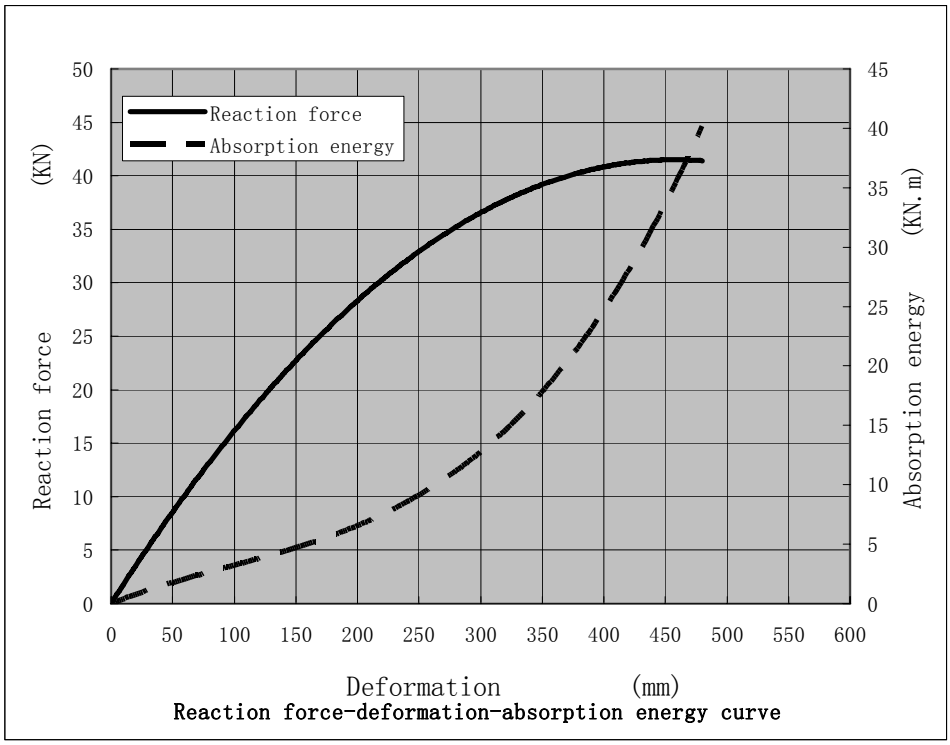

Fig. 5.5 The calculated reaction force-deformation and absorption energy curve

is located in Ningde City of Fujian Province. It is a passenger-cargo port with capacity of 1000 tons. The platform of the port is a jetty-shaped arrangement, as shown in Figure 5.6, and an open type structure is designed. The vertical and parallel shore lines are 60 m and 38 m, respectively. The slab is a pre-stressed reinforced concrete hollow core structure with thickness of 50 cm. The beam, with a height of 100 cm, is a cast-in-situ reinforced concrete structure, substructure of the port consists of 55 cm × 55cm pre-stressed reinforced concrete square piles where the pile length is 30 m and the pile toe is located in pebble layer. There are two straight piles and a pair of skew piles for each bent, as shown in Figure 5.7.

The berthing pile is a 60cm × 60cm prestressed reinforced concrete square pile. The concrete strength is C80 and 20 pieces of 7Φ4 stranded cable are used in a symmetric arrangement. In order to make the strain energy relatively high, a relatively lower effective pre-stress is adopted, which produces about 5.0 MPa pre-compressive stresses in the section so that the cracking during piling and swing delivering can be controlled. Fig.5.8 shows the calculated moment-curvature curve. The calculated maximum energy absorption of the prestressed concrete berthing pile is 31.55 kNm. This may meet the requirement of berthing for a ship of 1000-ton.

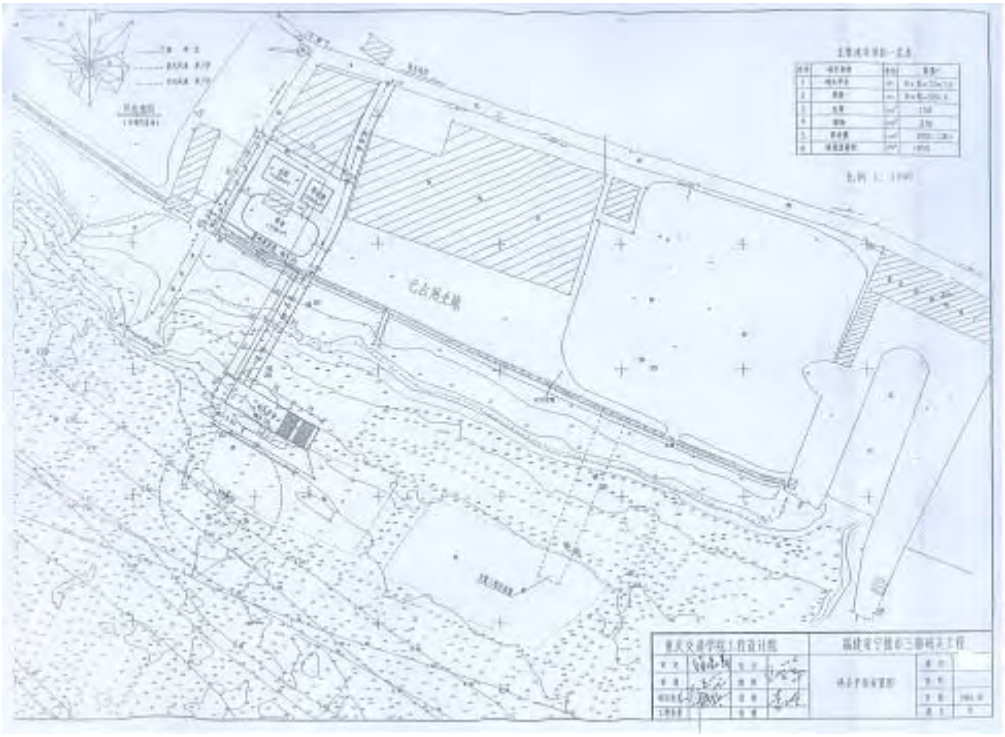

Fig.5.6 Layout of Sandu Port

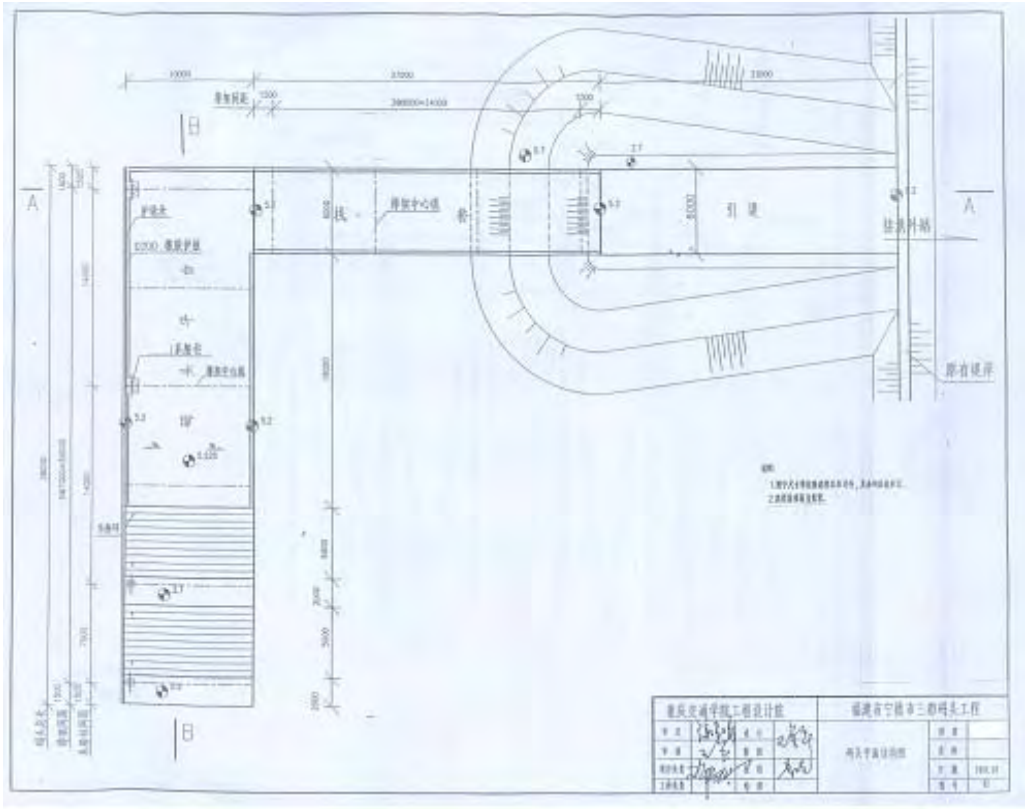

(a) Layout of structure

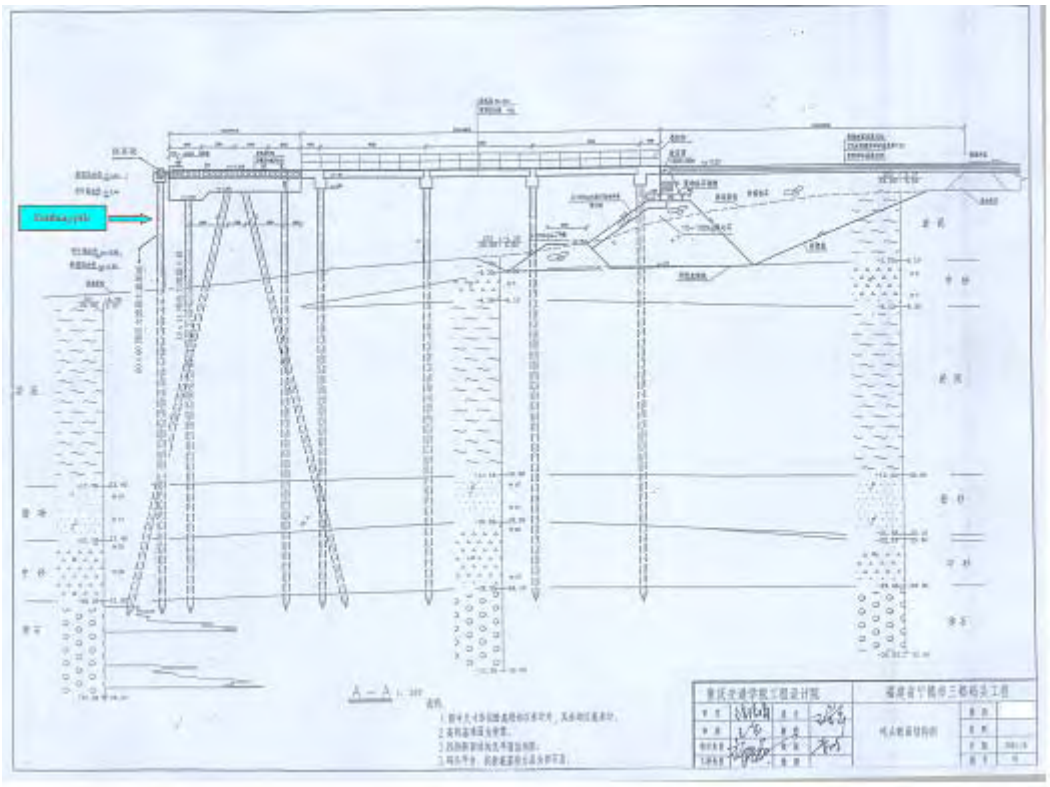

(b) A-A section

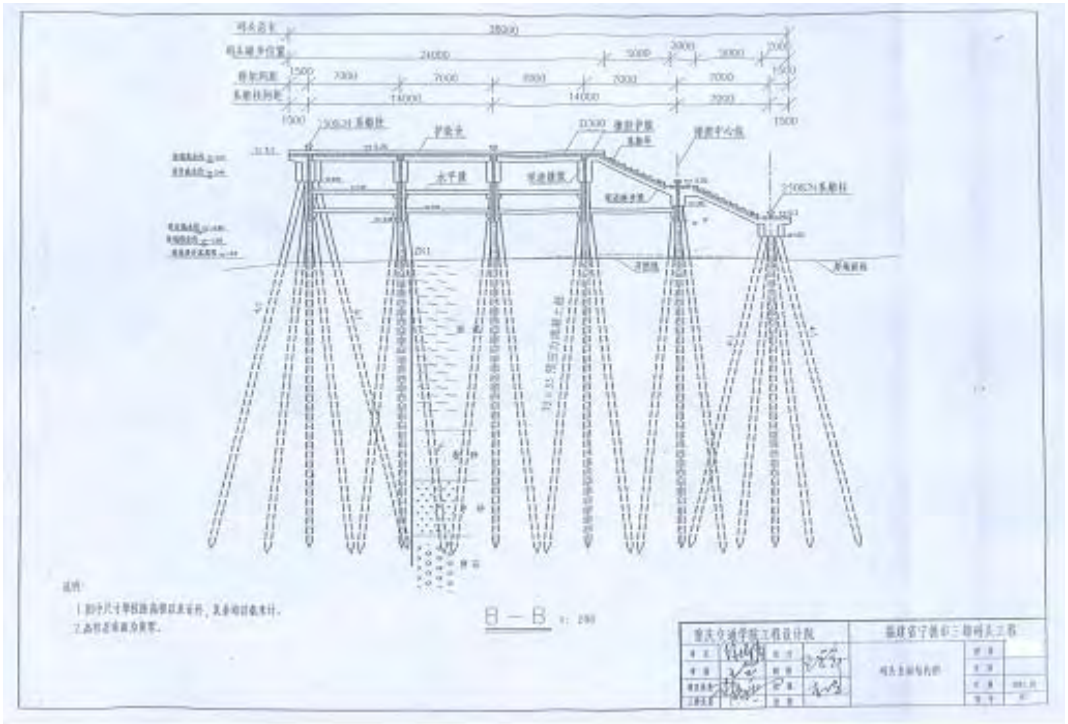

(c) B-B section a

Fig.5.7 Layout of structure and sections

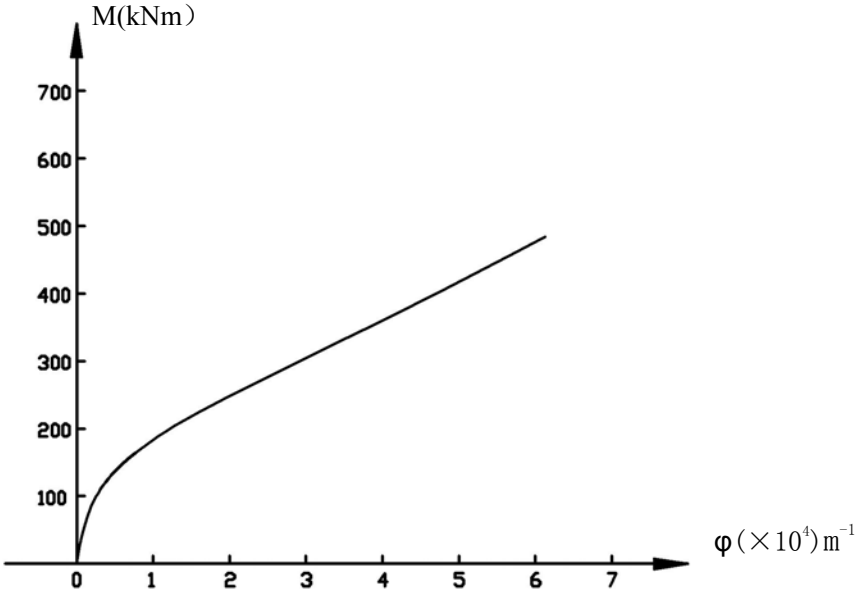

Fig.5.8 Moment –curvature curve

References

[1] Chongqing Harbor Company, Structural design of Phase 1 project Cuntan Port District, Structural design and analysis of Chongqing, 2004.10

[2] Liu Bingchuang and Kong Fanjun, Construction of Phase 1 project Cuntan Port Distric, Journal of Port and Waterway Engineering, 2004.3

[3] Cheng Wanjia, “Hydraulic structures”, The people’s communications publishing house, 2000

[4] “Handbook for design of sea harbors”, volume two, The first design institute of navigation engineering, The Ministry of Communications, China, The People’s communications publishing house, 1998

[5] Xu Xibin, “Research on structural types of wharf supported on piles”, Journal of port and waterway engineering, June 2000

[6] Jiang Xizhu and Lu Weiyu，”New Wharf Structural Types”，People’s publishing press, Beijing China,1999

Chapter 6

Conclusions

The prestressed concrete berthing piles differ greatly from the conventional piles under the action of a horizontal load. They absorb the impact force of a ship by their elasticity. Compared with the piles generally used under the action of a horizontal load, the prestressed concrete berthing piles are required to be made of high strength materials to adapt to the large displacement performance criteria. Further the foundation conditions should be good, otherwise after the berthing piles has received the impact forces of a ship, they may not return to the original position, and hence their capability of absorbing impact forces will gradually decrease. In addition to high requirements for materials and foundation, the berthing piles also need to be of a proper structural type so that the pile and fender structure is fully utilized to absorb a large impact energy from a ship while the pile itself carries relatively small external force.

Based on tests of six post-prestressed concrete berthing piles and theoretical analysis and computation to a large number of members with different parameters, this paper has described research on the work performance of prestressed concrete berthing piles. The research work focused on the factors affecting the service performance of the piles, such as the concrete strength, the pre-stress, the sectional reinforcement, cracking characteristics, ultimate bearing capacity and absorption of energy.

The conclusions are as follows:

1. The theoretical analysis and results of computation obtained for the members using different design parameters show that they are very close to the actually measured results both with repect to the overall deformation performance and to the local deformation performance, which indicates that the test scheme to simulate the fixed end condition is correct, and the theoretical model and computation results are reliable. Therefore, the calculations of prestressed concrete berthing piles with different parameters can be simulated by the theoretical calculations used in the paper.

2. Since a prestressed concrete berthing pile is located in a special working environment, the cracks cause steel corrosion, which consequently deteriorates the durability performance of the pile. The cyclic load tests have shown that when unloading after cracking, the cracks will be fully closed; the load applied to re-opening the crack will be similar to the cracking load in the former cycle. The good crack closure performance observed in the tests will, to a maximum degree, reduce the steel bar corrosion due to a crack formed under an occasional load, which will greatly help to improve the durability of prestressed concrete berthing piles.

3. It has been shown by the test results of the specimens no.1 and no.2 that large

pre-stress may improve the service performance of the prestressed concrete berthing pile, which is different from ordinary prestressed concrete members with low concrete strength. Both the ultimate load and deflection are increased with the increase of the pre-stress. From the view of improving the cracking resistance performance of the prestressed concrete berthing piles, the pre-stress should be relatively large. However, the pre-stress obviously influences the deformation capacity at the later stage of loading. For the members with a high concrete strength, the total deformation ability will be reduced when the pre-stress increases, but for the members with low concrete strength, the result is just the opposite. In practical design of prestressed concrete berthing piles, therefore, we suggest that the pre-stress of the berthing pile should be determined by the premises of guaranteeing a certain cracking resistance during the period of construction and service; by all means it must have a relatively large deformation capacity.

4. Usually, high strength-concrete has a higher elastic modulus than low-strength concrete, so that any losses of the prestressing force due to an elastic shortening of the concrete are reduced. Creep losses, which are roughly proportional to elastic losses, are lower as well. High bearing stresses in the vicinity of tendon anchorages for post-tensioned members are more easily accommodated, and high bond strength results in a reduction in the development length required for transferring the prestressing force from the cable to the concrete. In addition, concrete of higher compressive strength also has a higher tensile strength, so that the formation of flexural and diagonal tensile cracks is delayed. Within the range of concrete strengths which has been studied in this paper, the energy absorption ability of the prestressed concrete berthing piles increase with the concrete strength, because higher concrete strength members exhibit relatively greater deformation capacity in the later stage of loading. Since the utilization of the deformation capacity for the berthing pile, at the later stage of loading, is very limited in practical application, we suggest that the concrete strength of prestressed concrete berthing piles is selected between C60 and C80. A small value of the strength should be used when the pre-stress is high, and vice versa.

5. Generally, circular spirals confine concrete much more effectively than rectangular or square hoops. The reason is that circular spirals, because of their shape, are in axial hoop tension and provide a continuous confining pressure around the circumference, which at large transverse strains approximates fluid confinement. As a rule, however, square hoops can apply only confining reactions near the corners of the hoops because the pressure of the concrete against the sides of the hoops tends to bend the sides outwards. But the results of the theoretical analysis and computation show that the circular spirals can not improve the bearing capacity and energy absorption effectiveness of prestressed concrete berthing piles, which is absolutely different from prestressed concrete piles under only axial compressive loads. The symmetric reinforcement of the closed rectangular stirrups may provide large energy absorption, lower reaction force, and easy manufacturing, and therefore it is the optimal transverse reinforcement type.

6. The prestressed concrete berthing piles should be designed to minimize the ratio between reaction force and energy absorption, which keeps the elasticity of the pile within a certain range before concrete spalling. This is not only good for improving the strain energy of the prestressed concrete berthing piles and for obtaining optimal energy absorption effectiveness, but also to prevent the steel bars from corrosion by the effective closure of a crack after the removal of frequently applied loads.

7. As for the impact prevention devices used in hydraulic structures, the results of the tests and theoretical analysis have shown that, comparing to the steel berthing piles, the prestressed concrete berthing piles with high-strength materials are economic and feasible, and can provide a satisfactory deformation capacity before concrete spalling. Normally

prestressed concrete berthing piles are used together with other buffering materials, thus they will provide an economic and safe protection system. Therefore they offer better protection to the harbor and minimize the collision forces on hydraulic structures.

Report no R-139
ISSN 1601-2917
ISBN 87-7877-210-9